Gold N-heterocyclic carbene complexes as anti-cancer agents: Au-Se interactions and solubility

By

Sunel de Kock

Thesis presented in partial fulfilment of the requirements for the degree Master of Science in Chemistry at the University of Stellenbosch

Supervisor: Prof. Catharine Esterhuysen

Co-supervisor: Prof. Jan Dillen

Faculty of Science

Department of Chemistry & Polymer Science

December 2016

Stellenbosch University https://scholar.sun.ac.za

Declaration

By submitting this thesis/dissertation electronically, I declare that the entirety of the work contained therein is my own, original work, that I am the sole author thereof (save to the extent explicitly otherwise stated), that reproduction and publication thereof by Stellenbosch University will not infringe any third party rights and that I have not previously in its entirety or in part submitted it for obtaining any qualification.

December 2016

Copyright © 2016 Stellenbosch University

All rights reserved

Stellenbosch University https://scholar.sun.ac.za

Abstract

A theoretical study of a series of Au(I) complexes was performed in order to evaluate their suitability as anti-cancer prodrugs targeting the mitochondria and the TrxR enzyme. The complexes studied comprise a range of cationic Au(I) complexes bearing different N-heterocyclic carbene (NHC) and phosphine ligands, and form part of a class of compounds known as delocalised lipophilic cations (DLCs).

To reduce the complexity of calculations, two small model Se anions were chosen to represent the Se in the TrxR active site. In order to assess their appropriateness as models, these compounds were compared to compounds of larger size with greater resemblance to the enzyme active site. Optimised geometries of several of the Au complexes were compared to crystal structure data to evaluate the chosen model chemistry (PBE0-D3/TZVP). Good agreement was observed and a rationale for differences could be provided.

Lipophilicity has been identified as an important variable affecting the performance of Au(I) anti-cancer drugs, and the octanol-water partition coefficients (*Log P*) of a range of Au complexes were therefore calculated. The lipophilicities of NHC complexes were found to be very similar to that of phosphine complexes, confirming that NHCs can serve as a replacement for phosphine ligands in DLCs. A strong correlation between both molecular volume and average electrostatic potential with *Log P* was identified, indicating that these properties may be useful in the prediction of lipophilicity of similar compounds, and that the size of the N-substituent of an NHC can be varied to obtain Au complexes of predictable relative lipophilicity.

Ligand exchange reactions of Au(I) compounds are thought to occur via an associative mechanism in which a three-coordinate transition state is formed. The reactant van der Waals (vdW) complex may provide hints as to the ease of forming the transition state, which occurs subsequently along the reaction path. To estimate the propensity of a series of Au-NHC complexes to form vdW complexes with the TrxR active site Se, the geometries of vdW complexes of these coordination complexes and model Se fragments were optimised and the free energies of association were calculated. Complexes bearing benzimidazolylidene-type NHC ligands were found to interact more strongly than those bearing imidazolylidene NHC ligands, and more sterically demanding N-substituents on the NHC ligands were found to hinder the formation of close Au···Se contacts.

The energetics of ligand exchange of a variety of Au-NHC and Au-phosphine complexes were also investigated. The N-substituent of an NHC ligand was found not to meaningfully affect the strength of the Au-NHC bond, indicating that the N-substituent could be varied to tune the lipophilicity without affecting the lability of the ligand. NHC ligands were found to be more strongly bound to Au than phosphine ligands, suggesting that phosphine ligands are more suitable as exchangeable ligands than NHCs.

Stellenbosch University https://scholar.sun.ac.za

Uittreksel

‘n Teoretiese studie van ‘n reeks Au(I) komplekse is uitgevoer om hul bruikbaarheid as antikanker progeneesmiddels wat die mitochondrieë en TrxR ensiem teiken te evalueer. Die bestudeerde komplekse beslaan ‘n reeks kationiese Au(I) komplekse met verskillende N-heterosikliese karbeen (NHC) en fosfien-ligande, en vorm deel van ‘n groep chemiese stowwe wat bekend staan as gedelokaliseerde lipofiliese katione (DLCs).

Om die kompleksiteit van die berekeninge te verminder is twee klein model Se anione gekies om die Se in die aktiewe setel van TrxR te verteenwoordig. Hierdie chemiese verbindings is met groter verbindings met ‘n hoër ooreenkoms tot die ensiem se aktiewe setel vergelyk om hul toepaslikheid as modelle te evalueer. Om die teoretiese model (PBE0-D3/TZVP) te beoordeel is die geoptimiseerde structure vergelyk met kristalstruktuur data. ‘n Goeie ooreenkoms tussen die structure is waargeneem en ‘n rasionaal vir die verskille was gebied.

Lipofilisiteit is geïdentifiseer as ‘n belangrike veranderlike wat die prestasie van Au(I) antikankermiddele beïnvloed, dus was die oktanol-water verdelingskoëffisiënte (*Log P*) van ‘n reeks Au komplekse bereken. Dit is gevind dat die lipofilisiteit van NHC komplekse baie soortgelyk is aan die van fosfien komplekse, wat bevestig dat NHCs as vervangers van fosfien ligande in DLCs kan dien. ‘n Sterk korrelasie tussen beide molekulêre volume en die gemiddelde elektrostatiese potensiaal met *Log P* is geïdentifiseer, wat aandui dat die eienskap bruikbaar mag wees in die voorspelling van lipofilisiteit van soortgelyke komplekse, en dat die grootte van die N-substituent van ‘n NHC gewissel kan word om Au komplekse van voorspelbare relatiewe lipofilisiteit te verkry.

Ligand uitruilings reaksies van Au(I) verbindings gebeur vermoedelik via ‘n assosiatiewe meganisme waarin ‘n drie-koördinaat oorgangstoestand gevorm word. Die van der Waals (vdW) kompleks wat gevorm word voor die ontstaan van die oorgangstoestand kan leidrade bied oor die gemak van oorgangstoestandformasie. Om die geneigdheid waarmee ‘n reeks Au-NHC komplekse vdW komplekse met die TrxR aktiewe setel Se vorm te skat is die strukture van vdW komplekse tussen hierdie koördinasie komplekse en model Se fragmente geoptimiseer en die vrye energieë van assosiasie bereken. Dit is gevind dat komplekse met benzimidazolielideen ligande sterker interaksies vorm as komplekse met imidazolielideen ligande, terwyl steriesveeleisende N-substituente op die NHC ligande gevind is om die vorming van kort Au···Se kontakte te verhinder.

Die energetika van ligandverruilling van ‘n verskeidenheid Au-NHC en Au-fosfien komplekse is ook ondersoek. Die N-substituent van ‘n NHC ligand het nie ‘n betekenisvolle effek op die sterkte van die Au-NHC verbinding nie, wat aandui dat die N-substituent gewissel kan word om die lipofilisiteit te verstel sonder om die labiliteit van die ligand te beïnvloed. NHC ligande vorm sterker verbindings met Au as die fosfien ligande, wat daarop dui dat fosfien ligande meer gepas is as uitruilbare ligande as NHCs.

Stellenbosch University https://scholar.sun.ac.za

Acknowledgements

I would like to thank the following individuals for their support during my studies:

My supervisor, Prof. Esterhuysen, for her guidance and her help in staying grounded.

My co-supervisor, Prof. Dillen, for always providing wisdom even when he couldn't provide answers.

My colleagues in the De Beers building, for providing much needed distraction from work.

Charl Möller at the HPC, for maintaining the system upon which I performed most of my calculations.

My family and friends, for their patience and love.

The Wilhelm Frank Trust, without which none of this would have been possible.

Stellenbosch University https://scholar.sun.ac.za

Glossary

ADF	Amsterdam Density Functional
AIM	Atoms in Molecules
BD	Bond dissociation
BDE	Bond dissociation energy
BP	Becke-Perdew
CBS	Complete Basis Set
COSMO	COnductor-like Screening MOdel
COSMO-RS	COnductor-like Screening MOdel for Real Solvents
CSD	Cambridge Structural Database
CSM	Continuum solvation model
Cys	Cysteine
DFT	Density Functional Theory
DLC	Delocalised Lipophilic Cation
ECP	Effective Core Potential
EDA	Energy Decomposition Analysis
ESI	Electronic supplementary information
ESP	Electrostatic Potential
G09	Gaussian 09
GD3	Grimme's D3 dispersion correction with original damping function
GEA	Gradient Expansion Approximation
GGA	Generalised Gradient Approximation
GR	Glutathione reductase
GTO	Gaussian type orbital
H-bond	Hydrogen bond
LSDA	Local Spin Density Approximation
LSDA	Local spin density approximation
MMP	Mitochondrial membrane permeabilisation
MP	Mitochondrial membrane potential
MPT	Mitochondrial permeability transition
NHC	N-heterocyclic carbene
PBE	Perdew-Becke-Ernzerhof functional
PBE0	Perdew-Becke-Ernzerhof hybrid functional
ROS	Reactive oxygen species
SCF	Self-consistent field
SCRF	Self-consistent reaction field
Sec	Selenocysteine
STO	Slater type orbital
Trx	Thioredoxin
TrxR	Thioredoxin reductase
TZP	Core double zeta, valence triple zeta, polarised basis set of ADF
TZVP	The def2-TZVP basis set of Ahlrichs and coworkers
ZORA	Zeroth Order Regular Approximation
ZPVE	Zero-point vibrational energy

Stellenbosch University https://scholar.sun.ac.za

Table of Contents

Stellenbosch University https://scholar.sun.ac.za

Stellenbosch University https://scholar.sun.ac.za

1 Introduction

1.1 The mode of action of Au(I) anti-cancer drugs

The blockbuster success of cisplatin,[1,2] the first of the platinum-containing anti-tumour agents, stimulated the search for other metallodrugs[3] – not only because of cisplatin's efficacy, but also due to its undesirable side effects.[4,5] The platinum cancer drugs achieve their toxicity through DNA crosslinking, but do so with little selectivity for cancer cells. Systemic toxicity and the development of resistance by various mechanisms limit the use of platinum drugs.

The medicinal use of gold dates back to ancient China and gold compounds have been used in the treatment of rheumatoid arthritis since the 1920s.[6] The first orally active Au(I) anti-arthritic, auranofin (Figure 1-1), was approved for clinical use in 1985.[7] In 1979, years before clinical approval, it was shown to possess anti-tumour activity in addition to its anti-arthritic properties.[8] Studies performed on Au(I) complexes have indicated that they affect mitochondrial activity and that apoptosis induction may be attributed to thioredoxin reductase (TrxR) inhibition.[9–11] The design of Au(I) anti-cancer agents has therefore been focussed on targeting the mitochondria or the TrxR enzyme. Because these compounds do not target DNA, they may be useful in the treatment of patients who have developed resistance to Pt-based drugs.

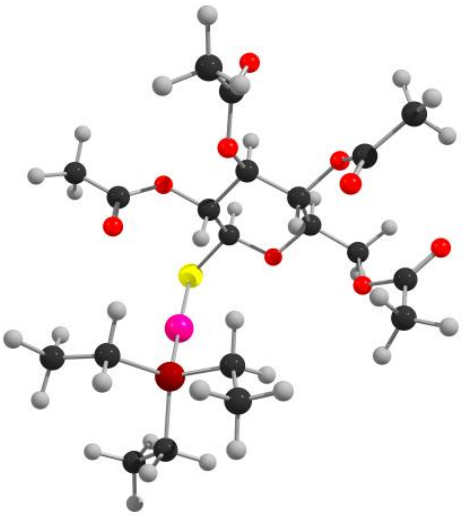

Figure 1-1: Auranofin

1.1.1 Mitochondria targeting

The mitochondria are described as the powerhouse of the cell, but these organelles are also responsible for triggering apoptosis, *i.e.* cellular suicide, if they detect that any of the myriad processes they regulate have gone awry.[12] This convergence of regulatory functions in the mitochondria makes them an attractive target for cancer treatment.[13]

Evidence suggests that Au(I) drugs may effect their anti-mitochondrial action by inducing mitochondrial permeability transition (MPT).[14] The permeability transition pore complex is a transmembrane protein found in mitochondria, thought to regulate the exchange of small molecules between the mitochondrial matrix and the cytosol. Usually it is in a low-conductance state, but can be stimulated to assume a high-conductance state, notably by an increase in the concentration of reactive oxygen species (ROS). When this permeability transition occurs,

Stellenbosch University https://scholar.sun.ac.za

the flow of small solutes into the mitochondrial matrix is deregulated, which results in the dissipation of the mitochondrial membrane potential (MP) and osmotic swelling of the mitochondrial matrix. When the swelling results in the rupture of the mitochondrial membranes, this is known as mitochondrial membrane permeabilisation (MMP). This leads to functional impairment of the mitochondria and the release of cytotoxic proteins into the cellular cytosol, and eventually results in cell death.

Furthermore, it has been found that the MTP – the chemical potential established across the mitochondrial membrane which is necessary for ATP production and Ca^{2+} sequestration – is elevated in many cancer cell lines.[15] A class of therapeutic agents known as delocalised lipophilic cations (DLCs) exploits this elevated membrane potential to preferentially target cancer cells.[16] Such species, among which are Au(I) complexes with phosphine and N-heterocyclic carbene (NHC) ligands, are able to partition through the mitochondrial membrane due to their lipophilic character, attracted to the mitochondria and accumulating inside them due to the relatively high pH environment of the mitochondrial matrix. Cytotoxicity may occur due to the interaction of the DLC with a specific target inside the mitochondria or the disturbance of the MP which can lead to apoptosis induction.

1.1.2 Thioredoxin reductase inhibition

TrxR is a ubiquitous selenoprotein, with three types being identified in humans: TrxR1 which occurs in the cytosol, TrxR2 which is found in the mitochondria, and TrxR3 which is specific to the testis. It is the only known enzyme to reduce thioredoxin (Trx),[17] and as such it has a pivotal role to fulfil in maintaining the cellular redox balance. Indeed, inhibition of this enzyme has been shown to affect tumour progression and development.[18]

TrxR is an attractive target in anti-cancer therapy for a number of reasons, in addition to the cytotoxic effects of its inhibition. To perform its duty of reducing Trx, the enzyme possesses (at least) two active sites, one of which contains neighbouring selenocysteine (Sec) and cysteine (Cys) amino acid residues. This active site is situated on the mobile and solvent-exposed C-terminal arm of the enzyme.[19–22] The exposed nature of this active site implies easy access for inhibiting agents. The Sec residue in TrxR has been found to be a target of many electrophilic drugs,[23] and the relative scarcity of this residue in proteins allows for selective targeting. Furthermore, elevated levels of TrxR have been found in several different human tumour cell lines, where TrxR is thought to aid tumour growth.[24–26] Since TrxR inhibition is pro-apoptotic, this suggests that selectivity for cancer cells may be achieved by TrxR-targeting therapies.

Although many compounds have been found to inhibit TrxR, Au(I) complexes are among the most effective, with IC_{50} values in the nanomolar to micromolar range.[10] These compounds

Stellenbosch University https://scholar.sun.ac.za

act as *prodrugs*, achieving inhibition of TrxR by protein metallation at Se after ligand dissociation from the Au(I) complex.

1.2 Aims of the study

Our theoretical study was focused on a small number of Au(I)-NHC and -phosphine complexes (Table 1-1) for which experimental results are available. We were interested in comparing these complexes in terms of their weak interaction with the Sec residue of the TrxR active site, the energetics of their ligand exchange reactions, and their lipophilicity, which is important for their ability to target the mitochondria.

The formation of a van der Waals (vdW) complex of reactants often precedes a chemical reaction, and a greater similarity of such a complex to the transition state may lead to the reaction occurring with greater ease[27]. The vdW complexation of the Au(I) prodrugs with the TrxR active site is also of interest considering that theoretical and experimental studies suggest that the ligand exchange reaction proceeds by an *associative mechanism*, that is, the Au(I) complex will coordinate with the active site first, forming a three-coordinate transition state before ligand dissociation takes place.[28–31] The effect of varying the substituent on the NHC nitrogen (hereafter referred to as the N-substituent) was investigated, as was the difference in vdW complex formation between the Au(I) complexes bearing imidazolylidene and benzimidazolylidene ligands.

The strength of the Au-ligand bond is important in determining how easily ligand exchange with the TrxR active site Se can take place, and also how easily unintended ligand exchanges, especially with other thiol-proteins, may take place. The different NHC ligands, a selection of phosphine ligands, the Cl^- anion, and two Se-bearing ligands were investigated in terms of their bonding in Au(I) complexes.

As mentioned, lipophilicity is an important attribute for mitochondria-targeting therapeutics. As such, the lipophilicity of a number of Au(I) complexes was calculated to determine the influence of the ligand types.

1.3 Investigated Au complexes

The ligands in Table 1-1 are numbered according to their volume (as defined by a 0.001 *e* $bohr^{-1}$ electron density isosurface). The majority of the complexes studied are of the Au-NHC variety, the NHC ligands containing examples of the imidazolylidene and benzimidazolylidene type (imidazolylidene = NHCx, benzimidazolylidene = NHCxb). Cationic complexes containing two identical NHC ligands (Au_2 NHCx and Au_2 NHCxb) were studied, as well as neutral complexes with one NHC ligand replaced by Cl^- (AuCl_NHCx and AuCl_ NHCxb). The lead compound Auranofin was included, along with a number of other

Stellenbosch University https://scholar.sun.ac.za

phosphine complexes (phosphine = Phos$x$). The ligand “Thio1” is the tetraacetylthioglucose ligand found in auranofin.

The Au_2NHCx complexes were chosen based on the work of Berners-Price *et al*.,[30,32] who evaluated these linear, two-coordinate cationic Au(I)-NHC complexes for their potential as anti-mitochondrial anti-tumour agents. A direct positive relation was identified between the lipophilicity (as estimated by the octanol-water partition coefficient) of the compounds and their ability to induce mitochondrial swelling and cyclosporine A-sensitive MMP.[32] The authors were also able to show that these compounds could effectively bond to Sec and Cys residues through ligand exchange, with high selectivity for Sec.[30]

Berners-Price *et al.* also investigated a number of neutral AuCl_NHCx complexes and noted that preliminary biological studies showed that their mitochondrial activity was correlated with their lipophilicity.[33] Two Au-NHC complexes bearing the auranofin phosphine and thiosugar ligands opposite the NHC were also included.

Ott *et al* studied a range of Au(I) complexes with the 1,3-diethylbenzylimidazol-2-ylidene (NHC3b) ligand.[34–36] They found that cationic lipophilic character was important for inducing anti-mitochondrial effects, and that the stability of the coordination bonds (as estimated with bond dissociation energies (BDE) calculated by density functional theory) was predictive of their affinity for the TrxR enzyme target, but also for serum albumin, the most common thioprotein in human plasma.[34] A lower BDE could thus be associated with stronger TrxR inhibition, but also with unwanted binding to serum albumin. They studied the interaction of the Au(I) complexes with a selenocysteine-containing peptide by mass spectrometry, and in all cases found molecular ions corresponding to an Au-NHC or Au cation bonded to the peptide. When examining a series of cationic Phos$x$-Au-NHC3b complexes they observed a correlation between bioactivity and the extent of cellular accumulation, as well as low IC_{50} values for TrxR inhibition.[35] The most efficient cellular uptake was observed for the complex bearing a triphenylphosphine ligand (Phos4), which was attributed to its higher lipophilicity relative to the complexes bearing trialkylphosphine ligands. Although the Phos4 ligand exhibited the lowest BDE, the smaller trialkylphosphine ligands were more effective inhibitors of TrxR. In a later mass spectrometry study they were able to show that the same Au compounds were able to metallate a dodecapeptide exactly resembling the C-terminal part of TrxR through direct coordination to Se.[36]

Stellenbosch University https://scholar.sun.ac.za

Table 1-1: Au complexes with CSD[37] REFCODE and citation. R = NHC nitrogen-substituents , X = phosphine-substituents

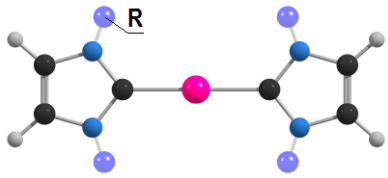

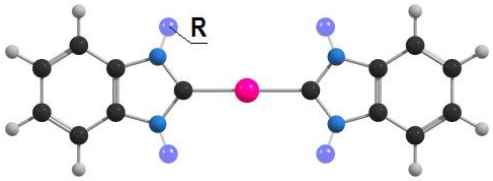

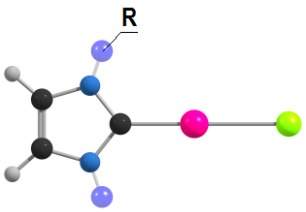

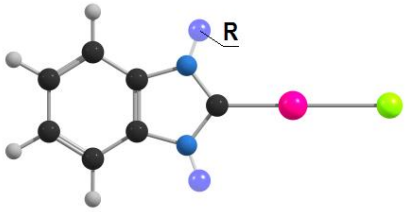

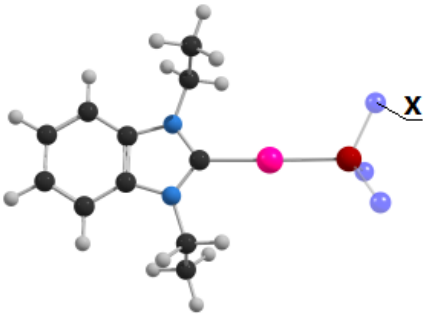

Complex	Charge	REFCODE	R	X	Ref.
Au_2NHC1	1	UMAGUL	H		
Au_2NHC2	1	YERFAD	Me		32
Au_2NHC3	1		Et		30
Au_2NHC4	1	YERFIL	i-Pr		32
Au_2NHC5	1	YERFUX	t-Bu		32
Au_2NHC6	1	YERFOR	n-Bu		32
Au_2NHC7	1	YERGAE	Cy		32
Au_2NHC1b	1		H		
Au_2NHC2b	1	KIZWEX	Me		
Au_2NHC3b	1	FIBYAR	Et		34
Au_2NHC4b	1	CIVMIE	i-Pr		
Au_2NHC5b	1		t-Bu		
Au_2NHC6b	1		n-Bu		
Au_2NHC7b	1		Cy		
AuCl_NHC1	0		H		
AuCl_NHC2	0		Me		33
AuCl_NHC3	0		Et		
AuCl_NHC4	0		i-Pr		33
AuCl_NHC5	0		t-Bu		33
AuCl_NHC6	0		n-Bu		
AuCl_NHC7	0		Cy		33
AuCl_NHC1b	0		H		
AuCl_NHC2b	0		Me		
AuCl_NHC3b	0		Et		34
AuCl_NHC4b	0		i-Pr		
AuCl_NHC5b	0		t-Bu		
AuCl_NHC6b	0		n-Bu		
AuCl_NHC7b	0		Cy		
Auranofin	0	AGLPAU		Et	
Phos1-Au-NHC3b	1		Et	Me	35
Phos2-Au-NHC3b	1		Et	Et	35
Phos3-Au-NHC3b	1		Et	i-Pr	35
Phos4-Au-NHC3b	1		Et	Ph	34
Phos4-Au-NHC5	1		t-Bu	Ph	33
Thio1-Au-NHC5	0		t-Bu		33

Stellenbosch University https://scholar.sun.ac.za

1.4 Thesis layout

The remainder of this thesis comprises eight chapters. Chapter 2 describes the theory behind the methods used in the study, while Chapter 3 describes the specific methodology followed.

Chapter 4 details the geometry optimisation and Atoms in Molecules (AIM) analysis of several Se-containing molecules and peptides, with the aim of assessing the appropriateness of using the small Se fragments, $SeCH_3^-$ and $SeCF_3^-$, as models for the TrxR active site Se. The small fragments are compared in terms of electrostatic potential (ESP) properties and atomic basin charge to larger Se-containing peptides, which are presumed to bear a greater similarity to the TrxR active site. The ESP maps of the two small Se fragments are also examined for clues to the most likely mode of coordination with Au(I) complexes.

In Chapter 5 the geometry optimisation and AIM analysis of the Au(I) complexes is recounted. Optimised geometries are compared to crystal structures to assess the accuracy of the chosen model chemistry and the effect of the ligands on the geometric parameters of the complexes is considered. The ESP is also investigated to see how the ligands affect the charge distribution, and for clues as to the likely mode of coordination with anionic species. The ESP will also become important when considering the solubility properties of these complexes.

Chapter 6 concerns the solubility of the Au complexes and ligands. The free energy of hydration and octanol-water partition coefficient (*Log P*) are related to other properties of the complexes. Calculated *Log P* values are compared with experimental results.

Chapter 7 concerns the vdW complexes formed between the small Se compounds and Au-NHC complexes. The strength of the interaction is assessed in the gas phase and in solution.

The energetics of ligand exchange reactions between the Au complexes and the small Se models is the subject of Chapter 8. Bond dissociation energies (and free energies) are evaluated and related to experimental findings.

The conclusion of the study and some possible implications for the design of Au(I) anti-cancer drugs are covered in Chapter 9.

Stellenbosch University https://scholar.sun.ac.za

References

(1) Rosenberg, B.; VanCamp, L.; Trosko, J.; Mansour, V. *Nature* **1969**, *222*, 385–386.

(2) Wiltshaw, E. *Platin. Met. Rev.* **1979**, *23*, 90–98.

(3) Barry, N. P. E.; Sadler, P. J. *Chem. Commun.* **2013**, *49*, 5106–5131.

(4) Donzelli, E.; Carfí, M.; Miloso, M.; Strada, A.; Galbiati, S.; Bayssas, M.; Griffon-Etienne, G.; Cavaletti, G.; Petruccioli, M. G.; Tredici, G. *J. Neurooncol.* **2004**, *67*, 65–73.

(5) Stordal, B.; Davey, M. *IUBMB Life* **2007**, *59*, 696–699.

(6) Higby, G. J. *Gold Bull.* **1982**, *15*, 130–140.

(7) Sutton, B. M. *Gold Bull.* **1986**, *19*, 15–16.

(8) Simon, T. M.; Kunishima, D. H.; Vibert, G. J.; Lorber, A. *Cancer* **1979**, *44*, 1965–1975.

(9) McKeage, M. J.; Maharaj, L.; Berners-Price, S. J. *Coord. Chem. Rev.* **2002**, *232*, 127–135.

(10) Bindoli, A.; Rigobello, M. P.; Scutari, G.; Gabbiani, C.; Casini, A.; Messori, L. *Coord. Chem. Rev.* **2009**, *253*, 1692–1707.

(11) Berners-Price, S. J.; Filipovska, A. *Metallomics* **2011**, *3*, 863–873.

(12) McBride, H. M.; Neuspiel, M.; Wasiak, S. *Curr. Biol.* **2006**, *16*, 551–560.

(13) Fulda, S.; Galluzzi, L.; Kroemer, G. *Nat. Rev. Drug Discov.* **2010**, *9*, 476–489.

(14) Ott, I. *Coord. Chem. Rev.* **2009**, *253*, 1670–1681.

(15) Chen, Lan, B. *Ann. Rev. Cell Biol.* **1988**, *4*, 155–181.

(16) Spreckelmeyer, S.; Orvig, C.; Casini, A. *Molecules* **2014**, *19*, 15584–15610.

(17) Mustacich, D.; Powis, G. *Biochem. J.* **2000**, *346*, 1–8.

(18) Urig, S.; Becker, K. *Semin. Cancer Biol.* **2006**, *16*, 452–465.

(19) Williams, C. H.; David Arscott, L.; Müller, S.; Lennon, B. W.; Ludwig, M. L.; Wang, P. F.; Veine, D. M.; Becker, K.; Heiner Schirmer, R. *Eur. J. Biochem.* **2000**, *267*, 6110–6117.

(20) Zhong, L.; Arnér, E. S.; Holmgren, A. *PNAS* **2000**, *97*, 5854–5859.

(21) Sandalova, T.; Zhong, L.; Lindqvist, Y.; Holmgren, A.; Schneider, G. *PNAS* **2001**, *98*, 9533–9538.

(22) Biterova, E. I.; Turanov, A. a; Gladyshev, V. N.; Barycki, J. J. *PNAS* **2005**, *102*,

Stellenbosch University https://scholar.sun.ac.za

15018–15023.

(23) Saccoccia, F.; Angelucci, F.; Boumis, G.; Carotti, D.; Desiato, G.; Miele, A. E.; Bellelli, A. *Curr. Protein Pept. Sci.* **2014**, *15*, 621–646.

(24) Gasdaska, P. Y.; Oblong, J. E.; Cotgreave, I. A.; Powis, G. **1994**.

(25) Nakamura, H.; Masutani, H.; Tagaya, Y.; Yamauchi, A.; Inamoto, T.; Nanbu, Y.; Fujii, S.; Ozawa, K.; Yodoi, J. *Cancer* **1992**, *69*, 2091–2097.

(26) Rundlöf, A.-K.; Arnér, E. S. *Antioxidants Redox Signal.* **2004**, *6*, 41–52.

(27) Young, D. C. *Computational Chemistry: A Practical Guide for Applying Techniques to Real-World Problems*; John Wiley & Sons, Inc.: New York, USA, **2001**.

(28) Howell, J. a S. *J. Organomet. Chem.* **2009**, *694*, 868–873.

(29) Dos Santos, H. F. *Comput. Theor. Chem.* **2014**, *1048*, 95–101.

(30) Hickey, J. L.; Ruhayel, R. A.; Barnard, P. J.; Baker, M. V.; Berners-Price, S. J.; Filipovska, A. *J. Am. Chem. Soc.* **2008**, *130*, 12570–12571.

(31) Pacheco, E. A.; Tiekienk, E. R. T.; Whitehouse, M. W. *Gold Chemistry: Applications and Future Directions in the Life Sciences*; Mohr, F., Ed.; Wiley-VCH: Weinheim, Germany, **2009**, 285.

(32) Baker, M. V; Barnard, P. J.; Berners-Price, S. J.; Brayshaw, S. K.; Hickey, J. L.; Skelton, B. W.; White, A. H. *Dalton Trans.* **2006**, *6*, 3708–3715.

(33) Baker, M. V; Barnard, P. J.; Berners-Price, S. J.; Brayshaw, S. K.; Hickey, J. L.; Skelton, B. W.; White, A. H. *J. Organomet. Chem.* **2005**, *690*, 5625–5635.

(34) Rubbiani, R.; Can, S.; Kitanovic, I.; Alborzinia, H.; Stefanopoulou, M.; Kokoschka, M.; Mo, S.; Sheldrick, W. S.; Wo, S.; Ott, I. *J. Med. Chem.* **2011**, *54*, 8646–8657.

(35) Rubbiani, R.; Salassa, L.; De Almeida, A.; Casini, A.; Ott, I. *ChemMedChem* **2014**, *9*, 1205–1210.

(36) Pratesi, A.; Gabbiani, C.; Michelucci, E.; Ginanneschi, M.; Papini, A. M.; Rubbiani, R.; Ott, I.; Messori, L. *J. Inorg. Biochem.* **2014**, *136*, 161–169.

(37) Allen, F. H. *Acta Cryst.* **2002**, B*58*, 380–388.

Stellenbosch University https://scholar.sun.ac.za

2 Theoretical methods

This section will provide some necessary background information on the theory underlying the methodologies used in this work. Sections 2.1 and 2.2.1 have been adapted from Koch,[1] section 2.5 from Cramer,[2] and section 2.6 contains highlights from Popelier.[3]

2.1 Solving the Schrödinger equation

Most quantum computational chemistry approaches involve the solution of the time-independent, non-relativistic Schrödinger equation

$$\hat{\mathrm{H}}\Psi_{\mathrm{i}}\left(\vec{\mathrm{x}}_1,\vec{\mathrm{x}}_2,\ldots\vec{\mathrm{x}}_{\mathrm{N}},\vec{\mathrm{R}}_1,\vec{\mathrm{R}}_2,\ldots\vec{\mathrm{R}}_{\mathrm{M}}\right)=\mathrm{E}\Psi_{\mathrm{i}}\left(\vec{\mathrm{x}}_1,\vec{\mathrm{x}}_2,\ldots\vec{\mathrm{x}}_{\mathrm{N}},\vec{\mathrm{R}}_1,\vec{\mathrm{R}}_2,\ldots\vec{\mathrm{R}}_{\mathrm{M}}\right) \tag{2-1}$$

where $\hat{\mathrm{H}}$ is the Hamiltonian operator, acting on the wave function Ψ_{i} and returning the total energy of a system of N electrons and M nuclei in a vacuum and in the absence of an external electric or magnetic field. The Hamiltonian is composed of terms for the kinetic and potential energy of the electrons and nuclei (given in atomic units for simplicity):

$$\hat{\mathrm{H}}=-\frac{1}{2}\sum_{i=1}^{\mathrm{N}}\nabla_i^2-\frac{1}{2}\sum_{\mathrm{A}=1}^{\mathrm{M}}\frac{1}{\mathrm{M_A}}\nabla_{\mathrm{A}}^2-\sum_{i=1}^{\mathrm{N}}\sum_{\mathrm{A}=1}^{\mathrm{M}}\frac{\mathrm{Z_A}}{\mathrm{r}_{i\mathrm{A}}}+\sum_{i=1}^{\mathrm{N}}\sum_{j>i}^{\mathrm{N}}\frac{1}{\mathrm{r}_{ij}}+\sum_{\mathrm{A}=1}^{\mathrm{M}}\sum_{\mathrm{B}>\mathrm{A}}^{\mathrm{N}}\frac{\mathrm{Z_A}\mathrm{Z_B}}{\mathrm{R_{AB}}} \tag{2-2}$$

The first two terms are the kinetic energy terms for the electrons and nuclei respectively, with the well-known Laplace operator denoted by ∇_{i}^2 and the mass of atom A denoted by $\mathrm{M_A}$. The potential energy is contained in the last three terms – first the electron-nucleus attraction, with Z_A denoting the nuclear charge and r_{iA} the distance between electron i and nucleus A, followed by the electron-electron repulsion, r_{ij} being the distance between electrons i and j, and lastly the repulsion between nuclei, with R_{AB} the distance between nuclei A and B.

Equation 2-2 can be simplified by exploiting the large differences in the masses of the electrons and nuclei. On the timescale of the movement of the electrons the nuclei can be viewed as fixed, therefore the nuclear kinetic energy term can be dropped while the repulsion between the nuclei becomes a constant. This is known as the *Born-Oppenheimer* approximation and leads to the electronic Hamiltonian,

$$\hat{H}_{elec}=-\frac{1}{2}\sum_{i=1}^{\mathrm{N}}\nabla_{\mathrm{i}}^2-\sum_{i=1}^{\mathrm{N}}\sum_{\mathrm{A}=1}^{\mathrm{M}}\frac{\mathrm{Z_A}}{\mathrm{r}_{i\mathrm{A}}}+\sum_{i=1}^{\mathrm{N}}\sum_{j>i}^{\mathrm{N}}\frac{1}{\mathrm{r}_{ij}}=\hat{T}+\hat{V}_{Ne}+\hat{V}_{ee} \tag{2-3}$$

and solution of the Schrödinger equation with $\hat{H}_{elec}$ gives

Stellenbosch University https://scholar.sun.ac.za

$$\hat{H}_{elec}\Psi_{elec} = E_{elec}\Psi_{elec} \tag{2-4}$$

Defining

$$E_{nuc} = \sum_{A=1}^{M}\sum_{B>A}^{N}\frac{Z_A Z_B}{R_{AB}}$$

leads to the following expression for the total energy:

$$E_{tot} = E_{elec} + E_{nuc} \tag{2-5}$$

It should be noted that the wave function itself is not an observable – only the square of Ψ has a physical interpretation, *i.e.* the probability density:

$$|\Psi(\vec{x}_1, \vec{x}_2, \ldots \vec{x}_N)|^2 d\vec{x}_1 d\vec{x}_2 \ldots d\vec{x}_N \tag{2-6}$$

The probability interpretation implies that the integral of Equation 2-7 over the full range of all variables must equal one,

$$\int \cdots \int |\Psi(\vec{x}_1, \vec{x}_2, \ldots \vec{x}_N)|^2 d\vec{x}_1 d\vec{x}_2 \ldots d\vec{x}_N = 1\,. \tag{2-7}$$

With the Hamiltonian in hand, its eigenfunctions, Ψ_i, and eigenvalues, E_i, remain to be determined. An analytical solution to this problem is impossible for all but the simplest of systems, however, the wave function of the ground state can be systematically approached by the use of the *variational principle*. According to this principle, when the expectation value of the energy is calculated using a suitable trial wave function, this expectation value will be an upper bound to the true ground state energy (in bracket notation):

$$\langle \Psi_{trial} | \hat{H} | \Psi_{trial} \rangle = E_{trial} \geq E_0 = \langle \Psi_0 | \hat{H} | \Psi_0 \rangle \tag{2-8}$$

To find the ground state energy and wave function $E[\Psi]$ is minimised by searching through all physically sound N-electron wave functions:

$$E_0 = \min_{\Psi \to N} E[\Psi] = \min_{\Psi \to N} \langle \Psi | \hat{T} + \hat{V}_{Ne} + \hat{V}_{ee} | \Psi \rangle \tag{2-9}$$

In practice the search will be limited to some subset of the allowed functions, implying that only an approximation to the true ground state wave function can be determined.

Stellenbosch University https://scholar.sun.ac.za

2.2 Density functional theory

2.2.1 The Hohenberg-Kohn theorems and the Kohn-Sham equations

In theory, if the wave function for some chemical system can be determined, all properties of interest can be determined with the proper quantum mechanical operator. However, the tractability of approximating a function that depends on 3N spatial and N spin variables decreases rapidly as the number of electrons is increased. Density functional theory (DFT) addresses this problem by attempting a solution of the Schrödinger equation by way of the electron density, an observable property of the system that depends only on three spatial variables.

The first challenge in the development of DFT was to show that the ground state density uniquely determines the Hamiltonian and all properties of the system. This was accomplished with the first theorem of Hohenberg and Kohn by way of *reductio ad absurdum*. The proof starts by considering two potentials, V_{ext} and V'_{ext}. These potentials differ by more than a constant (since adding a constant to the potential would not affect the wave function or the electron density) but result in the same electron density $\rho(\vec{r})$ associated with the corresponding ground states of N particles. The external potentials form parts of two different Hamiltonians that differ only in terms of the external potential, $\hat{H} = \hat{T} + \hat{V}_{ee} + \hat{V}_{ext}$ and $\hat{H}' = \hat{T} + \hat{V}_{ee} + \hat{V}'_{ext}$. These Hamiltonians are associated with two different ground state wave functions and their corresponding energies, which are not equal. The different external potentials, Hamiltonians, and wave functions are assumed to lead to the same electron density:

$$V_{ext} \Rightarrow \hat{H} \Rightarrow \Psi \Rightarrow \quad \rho(\vec{r}) \quad \Leftarrow \Psi' \Leftarrow \hat{H}' \Leftarrow V'_{ext} \tag{2-10}$$

Because the wave functions are different, Ψ' may be used as a trial wave function for $\hat{H}$:

$$E_0 < \langle \Psi' | \hat{H} | \Psi' \rangle = \langle \Psi' | \hat{H}' | \Psi' \rangle + \langle \Psi' | \hat{H} - \hat{H}' | \Psi' \rangle \tag{2-11}$$

or

$$E_0 < E'_0 + \langle \Psi' | \hat{T} + \hat{V}_{ee} + \hat{V}_{ext} - \hat{T} - \hat{V}_{ee} - \hat{V}'_{ext} | \Psi' \rangle$$

yielding

$$E_0 < E'_0 + \int \rho(\vec{r}) \{V_{ext} - V'_{ext}\} d\vec{r} \tag{2-12}$$

Stellenbosch University https://scholar.sun.ac.za

Repeating the above steps but swapping the primed and unprimed variables leads to

$$E_0' < E_0 - \int \rho(\vec{r})\{V_{ext} - V_{ext}'\}d\vec{r}\,. \tag{2-13}$$

Adding Equations 2-12 and 2-13 we arrive at the following contradiction

$$E_0 + E_0' < E_0' + E_0\,, \tag{2-14}$$

which implies that there cannot be two different external potentials leading to the same ground state density, and therefore the external potential is uniquely specified by the ground state density. The complete ground state energy is a *functional* (a function of a function) of the ground state electron density, as are its individual components:

$$E_0[\rho_0] = T[\rho_0] + E_{ee}[\rho_0] + E_{Ne}[\rho_0] \tag{2-15}$$

The kinetic energy and electron-electron repulsion energy terms, which are independent of the system, can be collected into the *Hohenberg-Kohn functional* $F_{HK}[\rho_0]$:

$$F_{HK}[\rho] = T[\rho] + E_{ee}[\rho] = \langle\Psi|\hat{T} + \hat{V}_{ee}|\Psi\rangle \tag{2-16}$$

If the explicit forms of $T[\rho]$ and $E_{ee}[\rho]$ were known this would provide a means to solve the Schrödinger equation *exactly*.

The second Hohenberg-Kohn theorem lays out the variational principle for DFT. The theorem shows that $F_{HK}[\rho]$ will deliver the lowest energy only when the input density is the true ground state density:

$$E_0 \leq E[\tilde{\rho}] = T[\tilde{\rho}] + E_{Ne}[\tilde{\rho}] + E_{ee}[\tilde{\rho}] \tag{2-17}$$

We start with a trial density $\tilde{\rho}(\vec{r})$ which satisfies the necessary boundary conditions, and is associated with some external potential $\tilde{V}_{ext}$. This trial density defines its own Hamiltonian and wave function, $\widetilde{\hat{H}}$ and $\tilde{\Psi}$. Taking this wave function as a trial wave function for the Hamiltonian generated by the true external potential we have

$$\langle\tilde{\Psi}|\hat{H}|\tilde{\Psi}\rangle = T[\tilde{\rho}] + V_{ee}[\tilde{\rho}] + \int \tilde{\rho}(\vec{r})V_{ext}d\vec{r} = E[\tilde{\rho}] \geq E_0[\rho_0] = \langle\Psi_0|\hat{H}|\Psi_0\rangle\,. \tag{2-18}$$

While the Hohenberg-Kohn theorems laid the theoretical groundwork for DFT, Kohn and Sham devised a practical approach that could be applied to chemical problems. Realising that the

Stellenbosch University https://scholar.sun.ac.za

calculation of the kinetic energy term was behind the inaccuracy of direct density functionals, and that orbital-based methods show much better performance, they introduced the concept of a non-interacting reference system composed of one electron functions.

The Hartree-Fock (HF) approach uses a single Slater determinant made up of N spin orbitals to represent the wave function. Electron-electron repulsion is approximated by regarding the electrons as non-interacting fermions moving in an effective potential. The kinetic energy for this kind of wave function is

$$T_{HF} = -\frac{1}{2}\sum_{i}^{N}\langle\chi_i|\nabla^2|\chi_i\rangle\,, \tag{2-19}$$

where the χ_i functions represent the HF spin orbitals. The χ_i are chosen such that the expectation value of the energy is minimised while the orbitals remain orthonormal:

$$E_{HF} = \min_{\Phi_{SD}\to N}\langle\Phi_{\mathrm{SD}}|\hat{T} + \hat{V}_{Ne} + \hat{V}_{ee}|\Phi_{SD}\rangle\,. \tag{2-20}$$

A non-interacting reference system can be set up with a Hamiltonian containing an effective, local potential $V_S(\vec{r})$, with "local" here referring to the fact that the potential is dependent on the coordinate at which the function is evaluated only:

$$\hat{H}_S = -\frac{1}{2}\sum_{i}^{N}\nabla_i^2 + \sum_{i}^{N}V_S(\vec{r}_i)\,. \tag{2-21}$$

This Hamiltonian contains no electron-electron interactions and its ground state wave function can therefore be represented by a Slater determinant, with the χ and Φ symbols replaced by φ and Θ to distinguish the following wave function from that obtained with HF:

$$\Theta_S = \frac{1}{\sqrt{N!}}\begin{vmatrix} \varphi_1(\vec{x}_1) & \varphi_2(\vec{x}_1) & \cdots & \varphi_N(\vec{x}_1) \\ \varphi_1(\vec{x}_2) & \varphi_2(\vec{x}_2) & \cdots & \varphi_N(\vec{x}_2) \\ \vdots & \vdots & & \vdots \\ \varphi_1(\vec{x}_N) & \varphi_2(\vec{x}_N) & \cdots & \varphi_N(\vec{x}_N) \end{vmatrix} \tag{2-22}$$

The one-electron Kohn-Sham operator $\hat{f}^{KS}$ is defined as

$$\hat{f}^{KS} = -\frac{1}{2}\nabla^2 + V_S(\vec{r}), \tag{2-23}$$

Stellenbosch University https://scholar.sun.ac.za

with the Kohn-Sham orbitals determined by

$$\hat{f}^{KS}\varphi_i = \epsilon_i\varphi_i \,. \tag{2-24}$$

The effective potential is chosen such that the density resulting from the summation of the moduli of the squared orbitals is exactly equal to the true ground state density of the real system of interacting electrons,

$$\rho_S(\vec{r}) = \sum_i^N \sum_s |\varphi_i(\vec{r}, s)|^2 = \rho_0(\vec{r}) \,. \tag{2-25}$$

The exact kinetic energy of the non-interacting reference system is given by

$$T_S = -\frac{1}{2}\sum_i^N \langle\varphi_i|\nabla^2|\varphi_i\rangle \,. \tag{2-26}$$

The energy T_S is not equal to the true kinetic energy of the interacting system, which led Kohn and Sham to divide the functional $F[\rho]$ as follows:

$$F[\rho(\vec{r})] = T_S[\rho(\vec{r})] + J[\rho(\vec{r})] + E_{XC}[\rho(\vec{r})] \tag{2-27}$$

The term E_{XC} is known as the *exchange-correlation energy*. This term contains the residual kinetic energy (T_C), as well as the non-classical electrostatic contribution (E_{ncl}), i.e. exchange, Coulomb correlation, and the self-interaction correction,

$$E_{XC}[\rho] \equiv (T[\rho] - T_S[\rho]) + (E_{ee}[\rho] - J[\rho]) = T_C[\rho] + E_{ncl}[\rho] \,. \tag{2-28}$$

The kinetic energy T_S and the classical electron-electron repulsion J can be calculated accurately while all the unknown terms are collected in E_{XC}, which is much smaller in magnitude. However, a method to uniquely determine the orbitals of the non-interacting reference system is still required before this can be useful or, in other words: how can V_S be defined so as to give the Slater determinant for the non-interacting system that is associated with the same density as the real system?

The energy of the real system expressed in terms of the separation described above is

Stellenbosch University https://scholar.sun.ac.za

$$
\begin{aligned}
E[\rho(\vec{r})] &= T_S[\rho] + J[\rho] + E_{XC}[\rho] + E_{Ne}[\rho] \\
&= T_S[\rho] + \frac{1}{2}\int\int \frac{\rho(\vec{r}_1)\rho(\vec{r}_2)}{r_{12}} d\vec{r}_1 d\vec{r}_2 + E_{XC}[\rho] + \int V_{Ne}\rho(\vec{r}) d\vec{r} \\
&= -\frac{1}{2}\sum_i^N \langle\varphi_i|\nabla^2|\varphi_i\rangle + \frac{1}{2}\sum_i^N\sum_j^N |\varphi_i\vec{r}_1|^2 \frac{1}{r_{12}} \left|\varphi_j(\vec{r}_2)\right|^2 d\vec{r}_1 d\vec{r}_2 + E_{XC}[\rho(\vec{r})] \\
&\quad -\sum_i^N \int \sum_A^M \frac{Z_A}{r_{1A}} |\varphi_i(\vec{r}_1)|^2 d\vec{r}_1 \,. \qquad (2\text{-}29)
\end{aligned}
$$

Imposing the necessary constraints on the orbitals, it can be shown that

$$
\begin{aligned}
\left(-\frac{1}{2}\nabla^2 + \left[\int \frac{\rho(\vec{r}_2)}{r_{12}} d\vec{r}_2 + V_{XC}(\vec{r}_1) - \sum_A^M \frac{Z_A}{r_{1A}}\right]\right)\varphi_i &= \left(-\frac{1}{2}\nabla^2 + V_{eff}(\vec{r}_1)\right)\varphi_i \qquad (2\text{-}30) \\
&= \epsilon_i \varphi_i \,,
\end{aligned}
$$

with V_{eff} exactly equal to V_S (Equation 1-23)

$$
V_S(\vec{r}) \equiv V_{eff}(\vec{r}) = \int \frac{\rho(\vec{r}_2)}{r_{12}} d\vec{r}_2 + V_{XC}(\vec{r}_1) - \sum_A^M \frac{Z_A}{r_{1A}} . \qquad (2\text{-}31)
$$

The recipe for determining the ground state energy is thus as follows

$$
V_S \Rightarrow \varphi \Rightarrow \rho \Rightarrow E
$$

The only problem remaining is V_{XC}, the exchange-correlation potential. If this were known exactly, the Kohn-Sham equations would provide the exact ground state energy. Unfortunately the form of V_{XC} is unknown and this quantity must be approximated. This point is further discussed in the following sections.

2.2.2 Jacob's ladder of density functional theory

Since the formulation of DFT chemists have sought new and improved exchange-correlation functionals to yield greater accuracy and satisfy more fundamental constraints. To describe a hierarchy of ever more sophisticated approximations John Perdew put forth the concept of a "Jacob's ladder" of density functional approximations.[4] He identifies five levels of sophistication between "Hartree World" and "Chemical Accuracy" (Figure 2-1). At the lowest rung of the ladder is the local spin density approximation (LSDA). In this approximation the

Stellenbosch University https://scholar.sun.ac.za

exchange-correlation energy is equivalent to that of a hypothetical *uniform electron gas*. The approximation is *local* in the sense that it depends only on the electron density value at each point in space. While this may at first seem like a poor approximation for atoms and molecules, systems where the electron density is typically far from homogeneous, the LSDA provides surprisingly good results. This can be attributed to the exact properties which this approximation takes from the uniform electron gas – the only system for which the form of the exchange and correlation functionals are known nearly exactly.

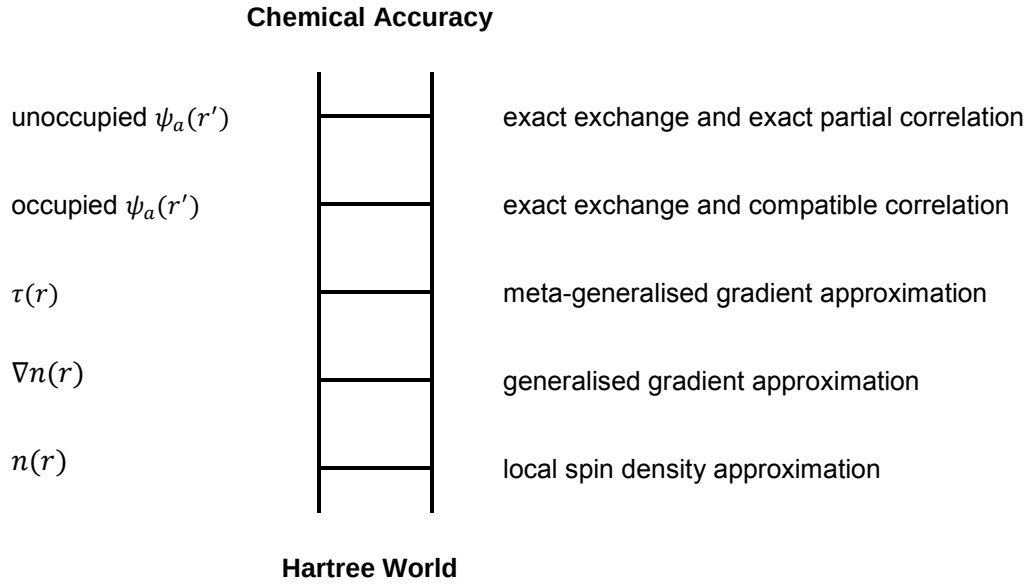

Figure 2-1: Perdew's "Jacob's ladder" of DFT.

While the LSDA provides reasonable molecular geometries and vibrational frequencies, atomisation energies are often grossly overestimated.[5] This led physicists to develop functionals also utilising the *gradient* of the electron density. If the LSDA is viewed as the first term in a Taylor expansion of the uniform electron gas, adding the next term brings us to the gradient expansion approximation (GEA). The GEA, however, does not yield superior accuracy to the LSDA – in going beyond the LSDA, the GEA loses many of the physically meaningful properties of the simpler approximation. The exact properties referred to here are those of the *exchange-correlation hole*, which describes the local depletion of electron density around an electron due to Pauli repulsion and the correlated movement of electrons. The pragmatic solution to the GEA problem was to simply truncate the holes in order to satisfy the restrictions for the true holes. Functionals of this type are known as generalised gradient approximation (GGA) functionals, and they lie at the second rung of the ladder. The greater accuracy of the GGA functionals spurred computational chemists to adopt DFT, where formerly it was mainly utilised by solid state physicists.

Stellenbosch University https://scholar.sun.ac.za

At the third rung lies the meta-generalised gradient approximation (meta-GGA) functionals. This is the last level where the calculation of computationally expensive second integrals can be avoided. The exchange-correlation energy in these functionals now also depends on the kinetic energy density (and potentially on higher order terms in the Taylor expansion of the electron density). Functionals of this type can generally not be constructed without resorting to extensive parameterisation.

The next rung of the ladder is occupied by the hybrid functionals. Since the exchange energy of a Slater determinant can be calculated exactly, and the exchange energy makes the greater contribution to the exchange-correlation energy than correlation, the logical next step in advancing DFT was to design functionals including some Hartree-Fock exchange. The exchange hole function is no longer local, and the correlation functionals for hybrids had to be adapted accordingly. The most famous of these hybrid functionals is B3LYP, which achieves an unsigned error close to 2 kcal mol^{-1} with respect to the G2 test set, coming very close to chemical accuracy (generally taken to be ~1 kcal mol^{-1}).

The relatively new, double hybrid functionals are found on the fifth rung. These functionals go beyond the single hybrids by including second order perturbation theory correlation. The functionals represent the state of the art, and exhibit accuracy beyond that of the single hybrid functionals,[6] albeit at a greatly increased cost.

2.2.3 The BP and PBE0 functionals

Two functionals were used in this work – the Becke-Perdew GGA functional and the PBE0 hybrid functional. The BP functional (also known as BP86) is the combination of Becke's 1988 exchange functional[7] with Perdew's 1986 correlation functional.[8] This functional was used in the parameterisation of COSMO-RS within the Amsterdam Density Functional (ADF) program[9] and was applied in all calculations of solubility properties in this work.

The PBE0 functional[10] was used in all geometry optimisations, frequency calculations, and energy decomposition analyses performed in this investigation. It is composed of the Perdew-Burke-Ernzerhof (PBE) functional[11] and an amount of exact exchange. Both functionals have been constructed avoiding parameterisation while seeking the satisfaction of fundamental constraints, an approach that has been shown to deliver accuracy and results that are easier to interpret in terms of the underlying model.[12]

PBE0 has been extensively benchmarked and shows good performance in describing transition metal complex geometries, thermochemistry and dispersion interactions when combined with Grimme's dispersion correction.[6,13–15] Furthermore, the method produces results in good agreement with high level coupled cluster calculations for the description of

Stellenbosch University https://scholar.sun.ac.za

complexes of Au(I) and Au(III) with unsaturated hydrocarbons,[16] and has recently been used to study Au(I) NHC complexes with phosphane ligands.[17]

2.2.4 Grimme's D3 dispersion correction

The problem of dispersion in DFT has led to the development of a number of methods to account for this phenomenon,[18,19] the most popular of which are the atom-pairwise dispersion corrections of Grimme.[20–22] The correction takes the following form:

$$E_{disp} = -s_6 \sum_{i=1}^{N-1} \sum_{j=i+1}^{N} \frac{C_6^{ij}}{R_{ij}^6} f_{dmp}(R_{ij}), \tag{2-30}$$

where N is the number of atoms, C_6^{ij} is the dispersion coefficient for the atom pair ij, s_6 is a global scaling factor and R_{ij} is the distance separating i and j. The dispersion energy is simply added to the self-consistent field energy to arrive at the dispersion-corrected energy. The damping function, $f_{dmp}(R) = \frac{1}{1+e^{-\alpha(R/R_0-1)}}$, prevents near-singularities at small R, and effectively removes the correction for atoms at covalent distances. The C_6 coefficients for the first of Grimme's DFT-D correction schemes were determined from the dipole-oscillator strength distributions for 44 molecule pairs,[23] averaged over the possible hybridisation states of the atoms. In order to cover a larger part of the periodic table in a consistent manner, the DFT-D2 dispersion coefficients were based on DFT/PBE0 calculations of atomic ionisation potentials and static dipole polarisabilities. Grimme noted the shortcoming of the method for atoms in a molecule with properties very different from the free atom in the ground state.[21] With the next iteration, pairwise-specific coefficients are calculated from first principles, thereby taking into account the effect of "hybridisation" on dispersion interactions. This version also allows for the calculation of analytical gradients and shows vastly improved results for transition metals.[22]

2.3 Basis sets and effective core potentials

In quantum chemistry calculations the unknown molecular orbital function is typically approximated using linear combinations of a set of basis functions.[24] This is known as the basis set approximation. In the limit where the basis set size is infinite, it is said to be complete and is no longer an approximation. Increasing the size of the basis set provides a way to systematically improve the accuracy of self-consistent field calculations.

Two types of basis functions are in general use – Slater type orbitals (STOs) and Gaussian type orbitals (GTOs). The advantages of the STO include rapid convergence to the complete basis set limit with increasing number of functions, and a more accurate representation of electronic behaviour close to the nuclei. Their major disadvantage is that they cannot be used

Stellenbosch University https://scholar.sun.ac.za

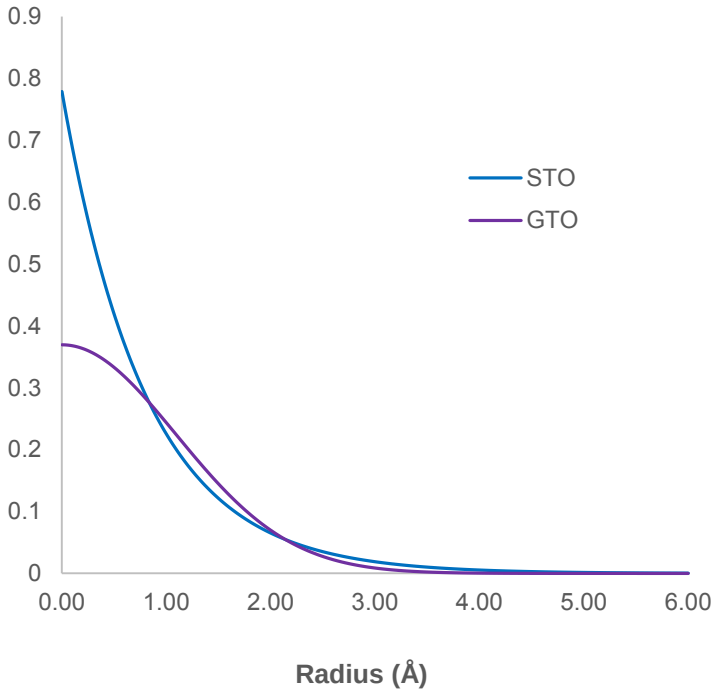

Figure 2-2: Shapes of the Slater and Gaussian type orbitals for an arbitrary system.

in the analytical calculation of three- and four-centre two-electron integrals. GTOs do not suffer from this drawback, but more of them are needed to reach a desired level of accuracy. This is a consequence of the form of the function – at the nuclei the GTOs possess a zero slope instead of a cusp, and the function dies off too quickly with increasing distance from the nucleus (Figure 2-2).

Basis sets can be characterised by their size and their composition in terms of polarisation and diffuse functions. A minimum basis set contains only enough functions to contain all the electrons, which usually results in a poor approximation. Doubling the number of basis functions per atomic orbital (tripling, quadrupling, …) results in a double (triple, quadruple, …) zeta basis set. At the triple zeta level, most density functionals can be presumed to be close to convergence with regards to the basis set limit.[25] For the description of the charge polarisation that occurs during chemical bonding, it is useful to add higher angular momentum functions, called polarisation functions. For the description of weak interactions occurring far from the nuclei, diffuse functions are added.

For elements from the lower reaches of the periodic table, the number of functions needed for an all-electron basis set may become prohibitively expensive. One approach to reduce the cost of calculations on heavy atoms is to replace the core electrons (which do not significantly contribute to bonding) with an effective core potential (ECP). These ECPs are constructed by parameterising a pseudopotential against high level of theory all-electron results. The added benefit of an ECP is that relativistic effects which come into play for heavier elements can be efficiently incorporated into a calculation. The use of an ECP reduces the resources necessary for a calculation, as the core electrons are now just represented by a potential which the valence electrons react to. In addition, costly relativistic calculations can be avoided by combining a relativistic ECP with a conventional SCF calculation.[24]

Stellenbosch University https://scholar.sun.ac.za

2.3.1 Def2-TZVP-PP and TZP/ZORA

The basis sets used in this work are both of triple zeta quality with polarisation functions. The def2-TZVP basis set[26] is composed of GTOs and has been optimised for DFT calculations. It has been designed for use with the Stuttgart ECPs.[27] TZP/ZORA is composed of STOs and is one of the basis sets designed for use in the Amsterdam Density Functional program with the Zeroth Order Regular Approximation (ZORA).[28]

2.4 Relativistic effects and the Zeroth Order Regular Approximation

The importance of relativistic effects in chemistry was not realised until great strides had been made in developing more accurate models for quantum chemical calculations.[29] These effects arise when electrons travelling close to the speed of light experience relativistic mass increase, and become important for the lower elements of the periodic table. As noted above, these effects can be incorporated into calculations by the use of ECPs, but scalar relativistic approximations like ZORA[30] are considered to give superior results. This accuracy comes at a price – all-electron calculations can take far longer when the system contains many heavy atoms, and linear dependence in the basis set may become a problem, especially when adding diffuse functions.

2.5 Continuum solvation

The chemistry occurring in a condensed phase can be dramatically different to that occurring in the gas phase. To model the behaviour of a solute in a solvent accurately and with minimal approximation would require the inclusion of perhaps thousands of solvent molecules. Besides making the calculation far too complex for a quantum mechanical treatment, to truly arrive at meaningful results would additionally require a statistical thermodynamics treatment.

The stabilisation of the solute-solvent interaction derives mainly from reorientation/polarisation of the solvent molecules in the presence of the solute. Continuum solvation models (CSMs) provide a useful approximation of the solvent environment by representing the solvent charge distribution as a continuous electric field. The most common variety of CSM used in quantum mechanical calculations is the self-consistent reaction field (SCRF) type. These models calculate the polarisation experienced by the solute and continuum in a self-consistent manner. The solute charge density induces polarisation in the continuum, which in turn further polarises the solute, *etc*. The work required to create the charge distribution is given by

$$G = -\frac{1}{2}\int \rho(\vec{r})\phi(\vec{r})d\vec{r}\,, \tag{2-31}$$

with ρ being the solute charge density and ϕ the gradient of the electrostatic potential (ESP).

Stellenbosch University https://scholar.sun.ac.za

The Poisson equation from classical electrostatics expresses the electrostatic potential as a function of the charge density and the dielectric constant:

$$\nabla^2\phi(\vec{r}) = -\frac{4\pi\rho(\vec{r})}{\epsilon}. \tag{2-32}$$

The dielectric constant, ϵ, is a medium-dependent property and is related to its electric susceptibility. The solute is placed within a cavity which displaces the dielectric medium. Outside the cavity for conditions of zero ionic strength the Poisson equation is properly written as

$$\nabla\epsilon(\vec{r}) \cdot \nabla\phi(\vec{r}) = -4\pi\rho(\vec{r}). \tag{2-33}$$

For systems with non-zero ionic strength the far more complicated Poisson-Boltzmann (PB) equation applies, but it can be simplified for systems of low ionic strength to

$$\nabla\epsilon(\vec{r}) \cdot \nabla\phi - \epsilon(\vec{r})\lambda(\vec{r})\kappa^2\left(\frac{k_BT}{q}\right)\sinh\left[\frac{q\phi(\vec{r})}{k_BT}\right] = -4\pi\rho(\vec{r}). \tag{2-34}$$

Here q is the magnitude of the charge of the electrolyte ions, λ is a switching function which equals one or zero according to the electrolyte accessibility of a region, and κ is the Debye-Hückel parameter.

Analytical solutions to the PB equations are possible for some ideal cavity shapes, but these poorly approximate the shape of most molecules. For arbitrary cavity shapes much higher accuracy can be achieved, but the equations must be solved numerically. Most continuum solvent models construct the cavity from a set of atom-centred spheres, the radii of which are most often parameterised values. The typical procedure to solve the PB equations is as follows: First, divide space into a 3D grid. Then define the molecular cavity and assign grid points a dielectric constant based on their position within or outside the cavity. Finally, discretise the solute charge distribution onto interior grid points by some means and determine the ESP at each point by solving the PB equations. The solution of the PB equations can be much simplified by representing the potential as a charge density spread over the surface of the molecule, eliminating the need for a 3D grid and improving the numerical quality. The COnductor-like Screening MOdel (COSMO) is one such *apparent surface charge* dielectric continuum model.

2.5.1 COSMO-RS

With COSMO the Poisson equations are solved using a boundary element approach, but the solution is simplified further by treating the continuum as having an *infinite* dielectric constant

Stellenbosch University https://scholar.sun.ac.za

and simply scaling the conductor-polarisation free energy after the calculation. Fortuitously, this results in a reduction in the size of the outlying charge error, but an outlying charge correction has also been implemented in the model to further reduce said error.[31]

The Conductor-like screening model for Real Solvents, COSMO-RS, goes beyond COSMO to treat some aspects of solvation by a statistical thermodynamics approach. The screening charge density on the cavity, the $\boldsymbol{\sigma}$ profile, is assumed to uniquely define the molecule in solution. This surface is divided into a number of fragments each with a characteristic charge density and an assigned chemical potential. This chemical potential is based on the matching of solute fragments with solvent surface fragments bearing complementary charges. Mixtures of different solutes and solvents are also easily handled by this scheme. Within this framework the strength of van der Waals interactions as well as hydrogen bonding between the solute and solvent can be estimated, in addition to a range of thermodynamic properties.[32]

2.6 Atoms in Molecules

The Quantum Theory of Atoms in Molecules (AIM) attempts to recover from the electron density topology the fundamental objects of chemistry – atoms and bonds.

The most conspicuous feature of the electron density is the large concentration it exhibits near the nuclei. By studying the *gradient* of ρ, or $\nabla\rho$, more features emerge that can be correlated to chemical concepts. In Figure 2-3 the *molecular graph* of AuCl_NHC1 is shown. Contour lines of differing ρ have been indicated on the figure. The atom-coloured lines terminating at the Cl and Au atoms are known as *gradient paths*. These lines are everywhere orthogonal to surfaces of constant ρ, and never cross unless $\nabla\rho = 0$. The gradient paths displayed here start at a minimum ρ, but really originate at infinity, pointing in the direction of steepest increase in the electron density. There are also gradient paths which do not terminate at the nuclei, but rather at points between them. These gradient paths define interatomic surfaces (IASs) dividing the atoms into

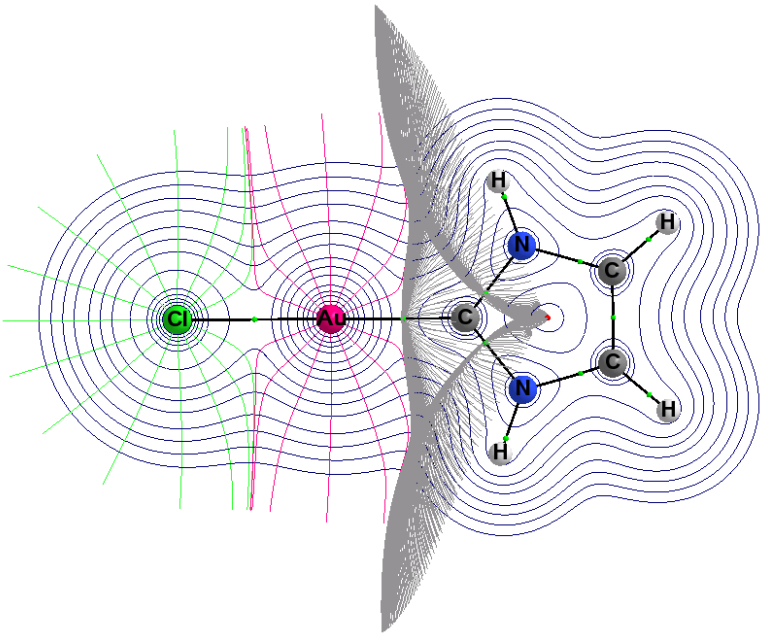

Figure 2-3: Molecular graph of AuCl_NHC1, with illustrated electron density contours and gradient paths.

Stellenbosch University https://scholar.sun.ac.za

individual *atomic basins* (illustrated for the carbene). The points where these gradient paths terminate, indicated in green, are known as *bond critical points* (BCPs). The BCP is the point on the IAS of highest ρ on the two dimensional surface, and lowest ρ in the dimension orthogonal to the IAS. The thick black lines joining the atoms are also gradient paths, starting at the BCP and terminating at the nuclei. When the molecular geometry is at a minimum on the potential energy surface, the lines joining the atoms are known as *bond paths*, and are indicative of a stabilising interaction between the two atoms. Higher order critical points are also known, *e.g.* ring critical points and cage critical points.

Taking the scalar derivative of the gradient vector field of ρ, we derive the Laplacian of the electron density, $\nabla^2\rho(\vec{r})$. This function provides information on local concentrations or depletions of electron density. It is possible to characterise bonds as open or closed shell based on the values of $\nabla\rho(\vec{r})$ and $\nabla^2\rho(\vec{r})$ at the BCPs. The Laplacian also provides a means of determining the *kinetic energy density*. Through the virial theorem one may obtain the potential energy density as well, which allows for more complex BCP analysis.[34,35]

2.7 Energy decomposition analysis

With the method of energy decomposition analysis (EDA) it is possible to decompose the total energy of an interaction, ΔE_{int}, into the following constituents: electrostatic energy - ΔE_{elst}, Pauli exchange repulsion - ΔE_{Pauli}, and orbital interaction - ΔE_{oi}. These techniques were developed by Morokuma and Ziegler[36–39] for HF and extended to Kohn-Sham DFT within ADF.[40,41]

The decomposition is performed in a stepwise fashion. First, self-consistent field calculations are performed for the fragments in their geometry-optimised form, in isolation. These prepared fragments are then brought together into their molecular arrangement, yielding a superposition of electron densities and thus ΔE_{elst}. The Pauli repulsion is then determined by orthonormalisation of the occupied fragment orbitals. The wave function is then allowed to relax to the final SCF-converged form, which gives ΔE_{oi}. When using a dispersion correction such as Grimme's D3 it is also possible to determine the dispersion component of the interaction.

Stellenbosch University https://scholar.sun.ac.za

References

(1) Koch, W.; Holthausen, M. C. *A Chemist ' s Guide to Density Functional Theory*, 2nd ed.; Wiley-VCH Verlag GmbH: Weinheim, Germany, **2001**.

(2) Cramer, C. J. *Essentials of Computational Chemistry*, 2nd ed.; John Wiley & Sons Ltd.: Chichester, England, **2004**.

(3) Popelier, P. *Atoms in Molecules: An Introduction*; Pearson Education Limited: Harlow, England, **2000**.

(4) Perdew, J. P.; Schmidt, K. *AIP Conf. Proc.* **2001**, *577* (Density Functional Theory and Its Application to Materials), 1–20.

(5) Jones, R. O.; Gunnarsson, O. *Rev. Mod. Phys.* **1989**, *61*, 689–746.

(6) Goerigk, L.; Grimme, S. *Phys. Chem. Chem. Phys.* **2011**, *13*, 6670–6688.

(7) Becke, A. D. *Phys. Rev. A* **1988**, *38*, 3098–3100.

(8) Perdew, J. P. *Phys. Rev. B* **1986**, *33*, 8822–8824.

(9) Pye, C. C.; Ziegler, T.; van Lenthe, E.; Louwen, J. N. *Can. J. Chem.* **2009**, *87*, 790–797.

(10) Adamo, C.; Barone, V. *J. Chem. Phys.* **1999**, *110*, 6158.

(11) Perdew, J. P.; Burke, K.; Ernzerhof, M. *Phys. Rev. Lett.* **1996**, *77*, 3865–3868.

(12) Perdew, J. P.; Ruzsinszky, A.; Tao, J.; Staroverov, V. N.; Scuseria, G. E.; Csonka, G. I. *J. Chem. Phys.* **2005**, *123*, 062201.

(13) Bühl, M.; Reimann, C.; Pantazis, D. a.; Bredow, T.; Neese, F. *J. Chem. Theory Comput.* **2008**, *4*, 1449–1459.

(14) Karton, A.; Tarnopolsky, A.; Lamère, J. F.; Schatz, G. C.; Martin, J. M. L. *J. Phys. Chem. A* **2008**, *112*, 12868–12886.

(15) Hansen, A.; Bannwarth, C.; Grimme, S.; Petrović, P.; Werlé, C.; Djukic, J.-P. *ChemistryOpen* **2014**, *3*, 177–189.

(16) Kang, R.; Chen, H.; Shaik, S.; Yao, J. *J. Chem. Theory Comput.* **2011**, *7*, 4002–4011.

(17) Rubbiani, R.; Salassa, L.; De Almeida, A.; Casini, A.; Ott, I. *ChemMedChem* **2014**, *9*, 1205–1210.

(18) Grimme, S. *Wiley Interdiscip. Rev. Comput. Mol. Sci.* **2011**, *1*, 211–228.

(19) Klimeš, J.; Michaelides, A. *J. Chem. Phys.* **2012**, *137*.

Stellenbosch University https://scholar.sun.ac.za

(20) Grimme, S. *J. Comput. Chem.* **2004**, *25*, 1463–1473.

(21) Grimme, S. *J. Comput. Chem.* **2006**, *27*, 1787–1799.

(22) Grimme, S.; Antony, J.; Ehrlich, S.; Krieg, H. *J. Chem. Phys.* **2010**, *132*.

(23) Wu, Q.; Yang, W. *J. Chem. Phys.* **2002**, *116*, 515–524.

(24) Jensen, F. *Introduction to Computational Chemistry*, 2nd ed.; John Wiley & Sons Ltd.: West Sussex, England, **2007**.

(25) Xu, X.; Truhlar, D. G. *J. Chem. Theory Comput.* **2011**, *7*, 2766–2779.

(26) Weigend, F.; Ahlrichs, R. *Phys. Chem. Chem. Phys.* **2005**, *7*, 3297–3305.

(27) Andrae, D.; Häußermann, U.; Dolg, M.; Stoll, H.; Preuß, H. *Theor. Chim. Acta* **1990**, *77*, 123–141.

(28) Van Lenthe, E.; Baerends, E. J. *J. Comput. Chem.* **2003**, *24*, 1142–1156.

(29) Pyykkö, P. *Chem. Rev.* **1988**, *88*, 563–594.

(30) van Lenthe, E.; Baerends, E. J.; Snijders, J. G. *J. Chem. Phys.* **1993**, *99*, 4597.

(31) Klamt, A.; Jonas, V. *J. Chem. Phys.* **1996**, *105*, 9972–9981.

(32) Klamt, A. *Wiley Interdiscip. Rev. Comput. Mol. Sci.* **2011**, *1*, 699–709.

(33) Bader, R. F. W. *Chem. Rev.* **1991**, *91*, 893–928.

(34) Nakanishi, W.; Hayashi, S.; Narahara, K. *J. Phys. Chem. A* **2008**, *112*, 13593–13599.

(35) Nakanishi, W.; Hayashi, S. *J. Phys. Chem. A* **2013**, *117*, 1795–1803.

(36) Morokuma, K. *J. Chem. Phys.* **1971**, *55*, 1236–1244.

(37) Kitaura, K.; Morokuma, K. *Int. J. Quantum Chem.* **1976**, *10*, 325–340.

(38) Ziegler, T.; Rauk, A. *Inorg. Chem.* **1979**, *18*, 1558–1565.

(39) Ziegler, T.; Rauk, A. *Inorg. Chem.* **1979**, *18*, 1755–1759.

(40) Bickelhaupt, F. M.; Baerends, E. J. *Kohn-Sham Density Functional Theory: Predicting and Understanding Chemistry*; Lipkowitz, K. B., Boyd, D. B., Eds.; Wiley-VCH: New York, USA, **2000**; Vol. 15.

(41) te Velde, G.; Bickelhaupt, F. M.; Baerends, E. J.; Fonseca Guerra, C.; van Gisbergen, S. J. A.; Snijders, J. G.; Ziegler, T. *J. Comput. Chem.* **2001**, *22*, 931–967.

Stellenbosch University https://scholar.sun.ac.za

3 Methodology

This chapter details the research methodologies used in this study. Most of the calculations described below were performed using the resources of the University of Stellenbosch's Rhasatsha high performance cluster and the CSIR's Centre for High Performance Computing. Visualisation of the electron density topology and related properties was done using AIMStudio graphical user interface to the AIMAll software package.[1] Other images were produced with the 3D chemistry visualisation software, Chemcraft.[2]

3.1 Geometry optimisation

Geometry optimisations were performed with the Gaussian 09, Revision D.01, computational chemistry software package (G09).[3] Structures were optimised using the PBE0 density functional[4] and the def2-TZVP basis set,[5] with a relativistic effective core potential (ECP) for gold (this combination of basis set and ECP hereafter referred to as TZVP).[6] The above basis set and ECP were downloaded from the EMSL basis set exchange.[7,8] Grimme's D3 dispersion correction with the original damping function was applied in all of the optimisations.[9] Stationary points were characterised by harmonic vibrational analysis (T = 310.15 K) to ensure that they represent minima on the potential energy surface. Tight optimisation criteria and an ultrafine integration grid were used for all optimisations unless noted otherwise. The log files of these calculations have been included in the electronic supplementary information (ESI).

3.2 Conformational search

Conformational searches were performed with the Discovery Studio program suite.[10] The molecules were constructed in Discovery Studio using the fragment builder, and conformational searches were performed using the BEST method with an energy threshold of 10 kcal mol^{-1}. The Smart minimiser was employed with a convergence criterion of a root mean squared gradient of 0.01 kcal mol^{-1}, using the default CHARMm force field and Momany-Rone partial charges. Discovery Studio also provides a means whereby the root mean square deviation of a structure from a reference structure may be calculated. This feature was used to identify the number of unique conformations and eliminate structurally similar conformations which were likely to reach the same minimum energy structure during geometry optimisation at the DFT level of theory.

3.3 Atoms in Molecules

Atoms in Molecules calculations were performed on our local machines using the AIMAll quantum chemistry software package and our in-house AIM program, eDensity.[1,11] and Wave function files for input into AIMAll were generated with G09. The WFX file format was used for wave functions with ECPs, which includes information on the missing core. For all-electron

Stellenbosch University https://scholar.sun.ac.za

calculations the WFN format was used. Bond critical points were identified by inspection in AIMAll's 3D visualisation component, AIMStudio. The default value of 0.04 a.u. for the weak critical point threshold was used to differentiate between strong and weak bonding.

3.4 Electrostatic potential

The AIMAll software package was used for the calculation of ESP properties. By default AIMAll calculates the electrostatic potential (ESP) at an electron density of 0.001 *e* bohr^{-1}. This setting was used throughout when calculating ESP properties, and when mapping the function to an isosurface to produce an ESP map (Figure 3-1) unless specified otherwise. It should be noted that the ranges of the colour scales of the ESP maps have been chosen to convey the variation of the ESP across the molecular isosurface, therefore ESP maps of different molecules should not be compared directly, but rather the numeric information from which the maps were generated should be consulted when attempting a comparison.

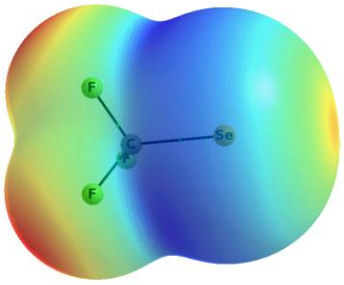

Figure 3-1: ESP map of trifluoromethaneselenolate.

3.5 Energy decomposition analysis

Energy decomposition analysis was performed on the coordination complexes as well as the van der Waals (vdW) complexes using an adaptation of the Morokuma bond energy decomposition scheme[12–14] implemented in the Amsterdam Density Functional (ADF) quantum chemistry software package.[15–17] G09-optimised geometries were used without further optimisation within ADF, retaining the PBE0 functional to ensure consistency in the energies calculated with G09 and ADF. Relativistic effects were taken into account with the zeroth order regular approximation (ZORA)[18–22] in combination with the ZORA/TZP all electron basis set (hereafter referred to as TZP).[23] Some care must be taken when applying hybrid functionals within ADF, as numerical problems may arise during the self-consistent field calculation, especially when using basis sets of triple zeta quality and higher. The numerical problems can be alleviated by adding diffuse fit functions (for a description of the density fitting procedure followed in ADF, see reference[24]), and also by checking for linear dependence in the basis set and removing linear combinations, both of which were done for all ADF calculations with the PBE0 functional. Grimme's D3 dispersion correction was also applied in these calculations. The parameters for the PBE0 functional are not available in ADF, but can be obtained from the University of Bonn's website[25] and specified manually.

3.6 Free energy of hydration and octanol/water partition coefficient

The free energy of hydration and the octanol/water partition coefficient were calculated using the COSMO-RS continuum solvation model as implemented in ADF.[26] Optimised structures

Stellenbosch University https://scholar.sun.ac.za

Table 3-1: COSMO-RS and Bondi radii.

Element	Radii (Å)		Ratio
	COSMO-RS	Bondi	
H	1.30	1.20	1.08
C	2.00	1.70	1.18
N	1.83	1.55	1.18
O	1.72	1.52	1.13
F	1.72	1.47	1.17
P	2.13	1.80	1.18
S	2.16	1.80	1.20
Cl	2.05	1.75	1.17
Se	2.22	1.90	1.17
Br	2.16	1.85	1.17
I	2.32	1.98	1.17
Au	1.94	1.66	1.17

from gas phase G09 calculations were used without further optimisation in the continuum solvation environment. This was done due to time constraints and also because the parameterisation of the COSMO-RS model in ADF was done on gas phase structures only. The COSMO-RS parameterisation within ADF was done using the Becke-Perdew exchange correlation functional, with the ZORA approximation for relativistic effects and the TZP small core basis set. These same settings were used for all COSMO-RS calculations described in this work, with a TZ2P basis set for Au, as recommended for heavy atoms. Default options were used as far as possible, but Se and Au were not included in the parameterisation and some quantities had to be estimated for these atoms, i.e. the solvent radii and the element specific dispersion constants. The radii of the spheres which surround the solute atoms within the continuum are parameterised values and not directly derived from fundamentals, nevertheless these radii correlate well with Bondi radii.[27,28] A comparison is shown in Table 3-1. The average of the ratios between the COSMO-RS and Bondi radii is ~1.16, but since the ratio for heavier atoms tends to be closer to 1.17, we opted to select this ratio for Se and Au, multiplying their Bondi radii by this amount to arrive at the solvent radii used for COSMO-RS calculations.

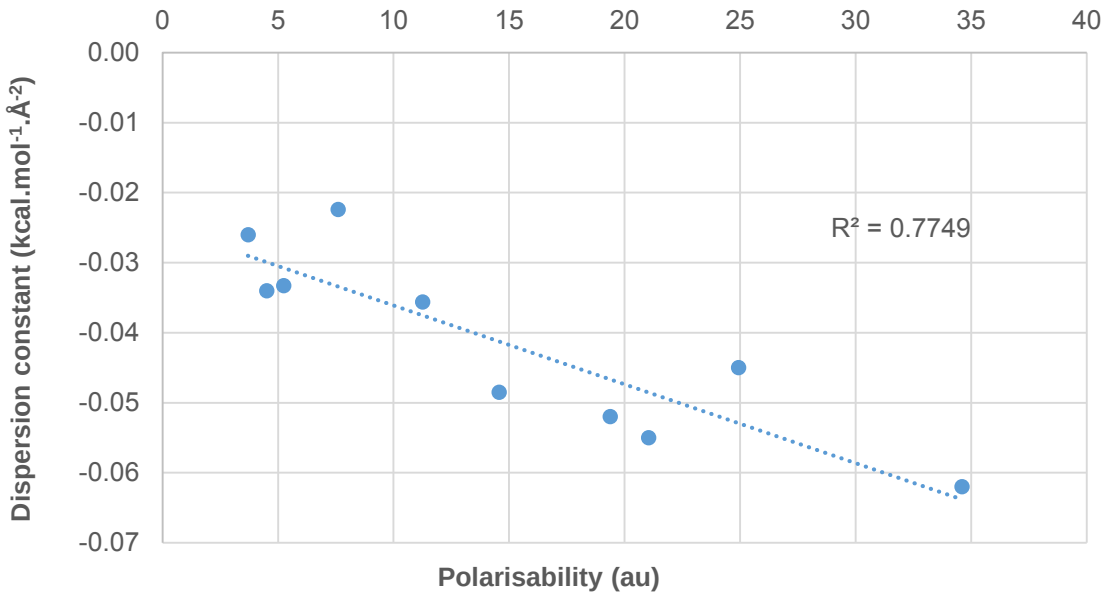

Figure 3-2: COSMO-RS dispersion constants as a function of atomic polarisability.

Stellenbosch University https://scholar.sun.ac.za

The dispersion constants are also fitted values, deriving mainly from the dispersion energy gain of the solute making the transition from the gas to the condensed phase. However, other free energy contributions related to molecular size may be involved as well, which is problematic for an approach in determining such a constant without parameterisation. Due to the lack of appropriate experimental data and the considerable computational expense of such an activity, we opted instead to estimate dispersion constants for Se and Au from their atomic polarisabilities.[29] The atomic polarisabilities of the atoms included in the COSMO-RS parameterisation were plotted with their dispersion constants, presuming a linear relationship (Figure 3-2). The value for nitrogen is particularly low, as noted by Klamt,[30] and so it was not included. The coefficient of determination indicates a reasonable fit of the data. Inserting the polarisabilities of Se and Au into the fit equation yields dispersion constants of -0.0537 and -0.0555 kcal mol^{-1} Å^{-2} for Se and Au, respectively.

3.7 Bond dissociation free energies

Similarly to other continuum solvation models, COSMO-RS has been parameterised against solvation free energies, and at a modest level of theory. This implies that performing such

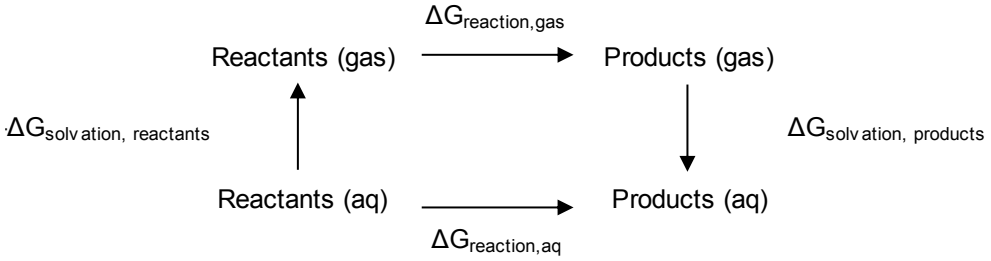

Figure 3-3: Thermodynamic cycle for reaction taking place in aqueous solution.

calculations at a higher level of theory cannot be expected to yield a systematic improvement in the quality of results. Continuum solvation models are also known to yield poor results for charged systems.[31] It is therefore suggested by Klamt that the correct way to use a continuum solvation model is to calculate solvation free energies in a manner consistent with their parameterisation, and combine this result with the results from high level gas phase calculations.[32] The general approach for calculating binding and bond dissociation (free) energies in solution involves a thermodynamic cycle (Figure 3-4).

In this scheme, the free energy of a species in solution is given by the following:

$$G_{aq}(X) = E_{gas}(X) + G_{gas,RRHO}(X) + \Delta G_{solvation}(X)\,, \qquad (3\text{-}1)$$

where E_{gas} is the electronic energy of the species in the gas phase, $G_{gas,RRHO}$ is the rigid rotor-harmonic oscillator energy, and $\Delta G_{solvation}$ is the solvation free energy. In this work E_{gas} was

Stellenbosch University https://scholar.sun.ac.za

calculated with G09 as described above, and $\Delta G_{solvation}$ is directly calculated by COSMO-RS. The remaining term presents a challenge when working with large systems, especially when the components are loosely bound, as in a vdW complex. Low-lying vibrational frequencies are known to be unreliable in the harmonic approximation, making an accurate estimation of entropy difficult. Grimme addresses this problem[33–35] by replacing the contribution of low-lying modes with a rotational entropy:

$$S_R = R\left[\frac{1}{2} + \ln\left(\left(\frac{8\pi^3 \mu' kT}{h^2}\right)^{\frac{1}{2}}\right)\right], \tag{3-2}$$

where R is the gas constant, μ' the effective moment of inertia, k the Boltzmann constant, T the absolute temperature, and h is Planck's constant. The procedure calls for an interpolation between the rotational and harmonic vibrational approximation wherein the vibrational and rotational entropies are combined using a weighting function of ω:

$$S = w(\omega)S_V + [1 - w(\omega)]S_R\,, \tag{3-3}$$

where $w(\omega)$ is given by the Head-Gordon damping function.[36] A wavenumber of 100 cm^{-1} was selected as the cut-off value – for all vibrational modes with a frequency below this value the vibrational entropy was effectively replaced with a free-rotor entropy.

Stellenbosch University https://scholar.sun.ac.za

References

(1) Keith, T. A. AIMAll (Version 15.05.18) TK Gristmill Software: Overland Park KS, USA **2015**.

(2) Chemcraft, http://chemcraftprog.com

(3) Frisch, M. J.; Trucks, G. W.; Schlegel, H. B.; Scuseria, G. E.; Robb, M. A.; Cheeseman, J. R.; Scalmani, G.; Barone, V.; Mennucci, G.; Petersson, A.; Nakatsuji, H.; Caricato, M.; Li, X.; Hratchian, H. P.; Izmaylov, A. F.; Bloino, J.; Zheng, G.; Sonnenberg, J. L.; Hada, M.; Ehara, M.; Toyota, K.; Fukuda, R.; Hasegawa, J.; Ishida, M.; Nakajima, T.; Honda, Y.; Kitao, O.; Nakai, H.; Vreven, T.; Jr., J. A. M.; Peralta, J. E.; Ogliaro, F.; Bearpark, M.; Heyd, J. J.; Brothers, E.; Kudin, K. N.; Staroverov, V. N.; Keith, T.; Kobayashi, R.; Normand, J.; Raghavachari, K.; Rendell, A.; Burant, J. C.; Iyengar, S. S.; Tomasi, J.; Cossi, M.; Rega, N.; Millam, J. M.; Klene, M.; Knox, J. E.; Cross, J. B.; Bakken, V.; Adamo, C.; Jaramillo, J.; Gomperts, R.; Stratmann, R. E.; Yazyev, O.; Austin, A. J.; Cammi, R.; Pomelli, C.; Ochterski, J. W.; Martin, R. L.; Morokuma, K.; Zakrzewski, V. G.; Voth, G. A.; Salvador, P.; Dannenberg, J. J.; Dapprich, S.; Daniels, A. D.; Farkas, O.; Foresman, J. B.; Ortiz, J. V.; Cioslowski, J.; Fox, D. J. Gaussian, Inc.: Wallingford CT **2013**.

(4) Adamo, C.; Barone, V. *J. Chem. Phys.* **1999**, *110*, 6158.

(5) Weigend, F.; Ahlrichs, R. *Phys. Chem. Chem. Phys.* **2005**, *7*, 3297–3305.

(6) Andrae, D.; Häußermann, U.; Dolg, M.; Stoll, H.; Preuß, H. *Theor. Chim. Acta* **1990**, *77*, 123–141.

(7) Feller, D. *J. Comput. Chem.* **1996**, *17*, 1571–1586.

(8) Schuchardt, K. L.; Didier, B. T.; Elsethagen, T.; Sun, L.; Gurumoorthi, V.; Chase, J.; Li, J.; Windus, T. L. *J. Chem. Inf. Model.* **2007**, *47*, 1045–1052.

(9) Grimme, S.; Antony, J.; Ehrlich, S.; Krieg, H. *J. Chem. Phys.* **2010**, *132*.

(10) *Dassault Systèmes BIOVIA, Discovery Studio Modeling Environment, Release 4.5, San Diego: Dassault Systèmes*. San Diego **2015**.

(11) eDensity, Dillen, J. Unpublished: Stellenbosch University.

(12) Morokuma, K. *J. Chem. Phys.* **1971**, *55*, 1236–1244.

(13) Kitaura, K.; Morokuma, K. *Int. J. Quantum Chem.* **1976**, *10*, 325–340.

(14) Ziegler, T.; Rauk, A. *Theor. Chim. Acta* **1977**, *46*, 1–10.

(15) te Velde, G.; Bickelhaupt, F. M.; Baerends, E. J.; Fonseca Guerra, C.; van Gisbergen, S. J. A.; Snijders, J. G.; Ziegler, T. *J. Comput. Chem.* **2001**, *22*, 931–967.

Stellenbosch University https://scholar.sun.ac.za

(16) Fonseca Guerra, C.; Snijders, J. G.; Te Velde, G.; Baerends, E. J. *Theor. Chem. Acc.* **1998**, *99*, 391–403.

(17) ADF2014, SCM, Theoretical Chemistry, Vrije Universiteit: Amsterdam, The Netherlands **2014**.

(18) van Lenthe, E.; Ehlers, A.; Baerends, E.-J. *J. Chem. Phys.* **1999**, *110*, 8943–8953.

(19) van Lenthe, E.; Baerends, E. J.; Snijders, J. G. *J. Chem. Phys.* **1993**, *99*, 4597.

(20) van Lenthe, E.; Baerends, E. J.; Snijders, J. G. *J. Chem. Phys.* **1994**, *101*, 9783.

(21) van Lenthe, E.; Snijders, J. G.; Baerends, E. J. *J. Chem. Phys.* **1996**, *105*, 6505–6516.

(22) van Lenthe, E.; van Leeuwen, R.; Baerends, E. J.; Snijders, J. G. **1996**, *57*, 281–293.

(23) Van Lenthe, E.; Baerends, E. J. *J. Comput. Chem.* **2003**, *24*, 1142–1156.

(24) Franchini, M.; Philipsen, P. H. T.; Van Lenthe, E.; Visscher, L. *J. Chem. Theory Comput.* **2014**, *10*, 1994–2004.

(25) http://www.thch.uni-bonn.de/tc/downloads/DFT-D3/functionals.html

(26) Pye, C. C.; Ziegler, T.; van Lenthe, E.; Louwen, J. N. *Can. J. Chem.* **2009**, *87*, 790–797.

(27) Klamt, A.; Jonas, V.; Bürger, T.; Lohrenz, J. C. W. *J. Phys. Chem. A* **1998**, *102*, 5074–5085.

(28) Klamt, A.; Eckert, F. *Fluid Phase Equilib.* **2000**, *172*, 43–72.

(29) Schwerdtfeger, P. *Table of experimental and calculated static dipole polarizabilities for the electronic ground states of the neutral elements,* http://ctcp.massey.ac.nz/dipole-polarizabilities (accessed 10 October 2015).

(30) Klamt, A. *COSMO-RS: From quantum Chemistry to Fluid Phase Thermodynamics and Drug Design*; Elsevier: Amsterdam, The Netherlands, **2005**.

(31) Cramer, C. J. *Essentials of Computational Chemistry: Theories and Models*, 2nd ed.; John Wiley & Sons Ltd.: Chichester, England, **2004**.

(32) Ho, J.; Klamt, A.; Coote, M. L. *J. Phys. Chem. A* **2010**, *114*, 13442–13444.

(33) Grimme, S. *Chem. - Eur. J.* **2012**, *18*, 9955–9964.

(34) Sure, R.; Antony, J.; Grimme, S. *J. Phys. Chem. B* **2014**, *118*, 3431–3440.

(35) Antony, J.; Sure, R.; Grimme, S. *Chem. Commun.* **2015**, *51*, 1764–1774.

(36) Chai, J.-D.; Head-Gordon, M. *Phys. Chem. Chem. Phys.* **2008**, *10*, 6615–6620.

Stellenbosch University https://scholar.sun.ac.za

4 Small Se fragments and peptides

The class of thioredoxin reductase (TrxR) found in humans has a molecular weight of approximately 55 kDa.[1] Treating such a large molecule quantum mechanically would be prohibitively expensive in terms of computational time, so we opted to use simple Se fragments to investigate the interaction of the Au complexes with the selenocysteine-containing active site. Since the active site is exposed, this is not as bad an approximation as would be the case if it were in the interior of the protein. Methaneselenolate ($SeCH_3^-$) and trifluoromethaneselenolate ($SeCF_3^-$) were selected as representative fragments, with the intent to compare them in terms of their ESP properties to the amino acid selenocysteine (Sec) (Figure 4-1), the cysteine-selenocysteine dipeptide (CysSec), and the glycine-cysteine-selenocysteine-glycine tetrapeptide (GCSG); the tetrapeptide presumably being the best mimic of the TrxR active site. With a C atom attached to Se, its electronic properties should be, to an extent, similar to the active site Se properties. Adding electron-donating H atoms or electronegative F atoms to the SeC fragment gives two species that should represent extremes in terms of Se nucleophilicity.

The Sec amino acid residue is mostly found with Se deprotonated at physiological pH (pK_a ~5.2),[2] and all the initial guess geometries of the above molecules were set up accordingly, with the amino acids and peptides in the zwitterionic form. With increasing molecular size comes greater flexibility, and the C-terminal end of the protein containing the active site is free floating, making it unlikely that a single molecular structure will provide an adequate description of the dynamic molecule. Sec, CysSec, and GCSG were therefore subjected to a conformational search before optimisation at the DFT level of theory. This was then followed by Atoms in Molecules (AIM) analysis.

4.1 Geometry optimisation

Following the protocol detailed in section 2.2 of the Methodology chapter, 8 conformations of Sec, 17 of CysSec and 32 of GCSG were generated using Discovery Studio.[3] Selecting the lowest energy conformer as a reference structure and evaluating the root mean square deviations of the other conformers we were able to discard a number of them, reducing the number of unique confirmations to 3 of Sec, 7 of CysSec, and 17 of GCSG. Using G09[4] these conformations were optimised at the PBE0-D3/TZVP level of theory, along with $SeCH_3^-$, $SeCF_3^-$, $SeCH_2CH_3^-$,and $SeC(CH_3)_3^-$ as smaller model compounds (log files are provided in the ESI).

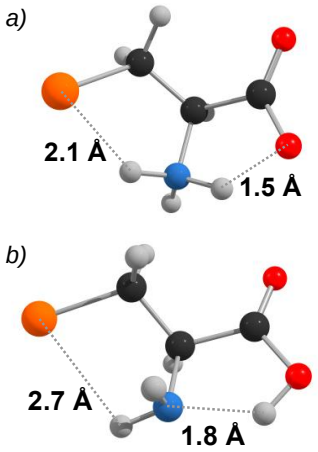

Figure 4-1: a) Sec-6, anionic zwitterionic form, b) Sec-8, anionic canonical form.

Stellenbosch University https://scholar.sun.ac.za

The energy difference between the most and least stable Sec conformations, Sec-8 (Figure 4-1b) and Sec-6 (Figure 4-1a), is approximately 5 kcal mol^{-1}. Some of this energy difference is due to a proton transfer from the amine group to the carboxylate group occurring during the Sec-8 geometry optimisation. Although the zwitterionic forms of amino acids and peptides are known to predominate in aqueous solution, experimental and theoretical studies have found that this is not the case in the gas phase.[5] The higher energy conformers, Sec-1 and Sec-6, remain in the zwitterionic form, with close contacts between amine hydrogens and the Se and O atoms.

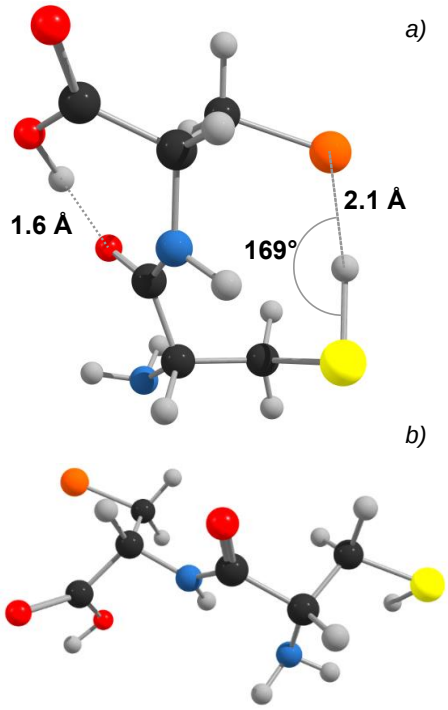

Figure 4-2: Optimised geometries of a)CysSec-17 and b) CysSec-8.

Geometry optimisation of the seven CysSec conformers yielded 6 unique conformations, 2 of the CysSec conformations (CysSec-3 and CysSec-5) having reached the same local minimum on the potential energy surface. The lowest energy conformer, CysSec-17 (Figure 4-2a), was found to be approximately 21 kcal mol^{-1} more stable than the highest energy conformer, CysSec-8 (Figure 4-2b). Proton transfer occurred in each of the six conformers, transforming the dipeptide from the zwitterionic to the canonical form. Short Se-H contacts are observed in all the conformers besides CysSec-8. In the case of CysSec-17 and CysSec-15, the thiol H has established a short contact with Se, putting the S and Se atoms at a distance to each other shorter than the sum of their vdW radii with a S-H-Se angle close to linear.

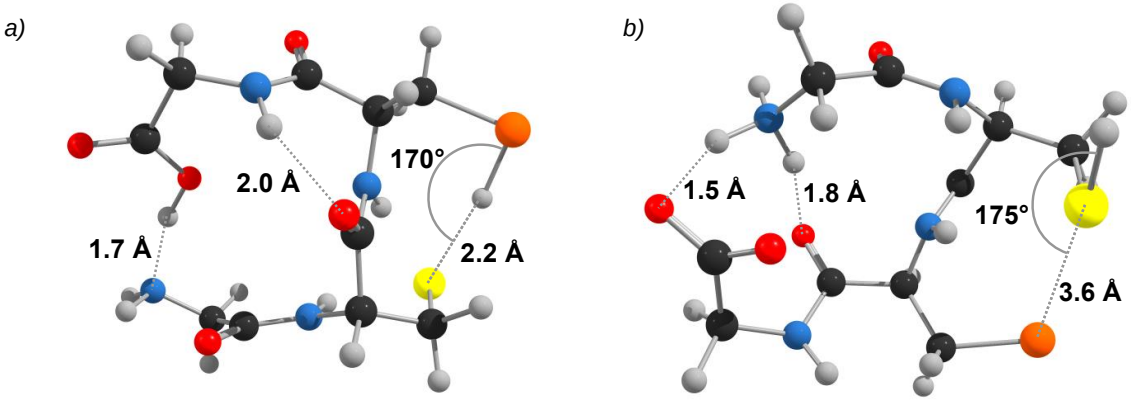

Figure 4-3: Optimised geometry of a) GCSG-11 and b) GCSG-3.

Stellenbosch University https://scholar.sun.ac.za

The tetrapeptide (GCSG) conformations span an even larger energy range of 29 kcal mol^{-1}. After geometry optimisation, only three of the conformations remain in the zwitterionic form, while the other conformers have undergone a proton transfer, usually between the two glycine amino acid residues at the C- and N-terminal ends. The lowest energy conformer, GCSG-11 (Figure 4-3a), is unusual in that it is the only Se species studied in which proton transfer occurred between the S and Se atoms. That GCSG-11 is the only species with an optimised structure with a protonated Se atom provides validation for our choice of anionic Se fragments as models for the TrxR active site Se. The GCSG-11 S and Se atoms remain close to each other (~3.6 Å separation) with the H atom between them in an almost linear orientation (170° S-H-Se angle). Short S···H distances are observed for this conformer, while the other conformers, in which Se is deprotonated, all exhibit a number of short Se-H contacts. GCSG-15 also has a short thiol H-Se contact, with a S-H-Se angle of 164°. The highest energy conformer, GCSG-3 (Figure 4-3b), has S and Se in close proximity to each other, but without an interceding H atom. The S and Se atoms are approximately 3.6 Å apart, a distance close to the sum of their vdW radii, with the thiol H pointing away from Se (175° Se-S-H angle).

Table 4-1: ESP on, atomic charge of, and weak bonds to Se atom.

Fragment	ESP (kcal mol^{-1})			q (*e*)	Weak bonds to Se
	Max	Min	Avg		
$SeCH_3$	-0.19	-0.21	-0.21	-0.72	0
$SeCF_3$	-0.16	-0.20	-0.19	-0.46	0
$SeCH_2CH_3$	-0.19	-0.21	-0.20	-0.70	0
$SeCC_3H_9$	-0.18	-0.20	-0.20	-0.69	0
Sec-8	-0.14	-0.19	-0.18	-0.66	0
Sec-1	-0.12	-0.18	-0.16	-0.62	1
Sec-6	-0.12	-0.19	-0.17	-0.59	1
CysSec-3	-0.13	-0.18	-0.17	-0.62	2
CysSec-8	-0.17	-0.20	-0.19	-0.61	0
CysSec-1	-0.12	-0.17	-0.16	-0.58	2
CysSec-6	-0.13	-0.17	-0.15	-0.58	3
CysSec-15	-0.12	-0.17	-0.16	-0.54	2
CysSec-17	-0.12	-0.17	-0.15	-0.48	1
GCSG-1	-0.14	-0.19	-0.18	-0.63	0
GCSG-14	-0.11	-0.17	-0.16	-0.62	2
GCSG-23	-0.13	-0.18	-0.17	-0.61	1
GCSG-31	-0.14	-0.19	-0.18	-0.61	0
GCSG-19	-0.12	-0.17	-0.16	-0.60	1
GCSG-22	-0.10	-0.17	-0.15	-0.60	3
GCSG-7	-0.11	-0.17	-0.15	-0.60	1
GCSG-4	-0.12	-0.17	-0.16	-0.60	1
GCSG-29	-0.13	-0.17	-0.16	-0.59	1
GCSG-16	-0.13	-0.17	-0.16	-0.59	1
GCSG-30	-0.10	-0.18	-0.15	-0.59	2
GCSG-2	-0.12	-0.17	-0.16	-0.58	1
GCSG-9	-0.12	-0.17	-0.15	-0.58	1
GCSG-20	-0.12	-0.17	-0.15	-0.58	1
GCSG-3	-0.13	-0.19	-0.17	-0.55	1
GCSG-15	-0.13	-0.18	-0.16	-0.52	2
GCSG-11	-0.09	-0.14	-0.12	-0.07	0

Stellenbosch University https://scholar.sun.ac.za

4.2 Atoms in Molecules and electrostatic potential

Wavefunction files were generated for the Se fragments and subjected to AIM analysis. Many of the short contacts identified in the molecular geometries were confirmed as stabilising interactions by the identification of bond paths with associated BCPs on the molecular graphs, including the short S-Se contact in GCSG-3 (Figure 4-4). The electron density (ρ) at the latter BCP is 0.012 *e* bohr^{-3} and the Laplacian of ρ ($\nabla^2\rho$) is positive, suggesting that it may be a strong vdW interaction.[6] Studies on chalcogen bonds, which are described as non-covalent chalcogen-chalcogen interactions in which one chalcogen acts as an acceptor of electron density, indicate that charge transfer may be involved.[7] Such S···Se interactions where Se acts as an electron donor would reduce the effective nucleophilicity of Se, making it less attractive to cationic species.

We were particularly interested in the ESP on the Se portion of the molecular surface and its atomic basin charge. By comparing these properties across the various Se species we hoped to gauge how the small model Se fragments would perform. The maximum, minimum and average ESP on the Se atom portion of the isodensity surface were compared, as well as the charge contained in the Se atomic basin, q(*e*), and the number of weak bonds to Se (Table 4-1).

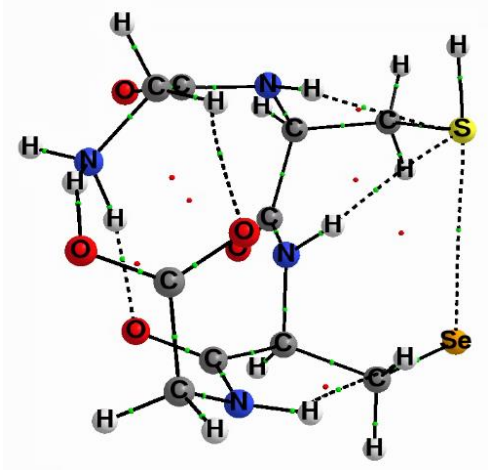

Figure 4-4: GCSG-3 molecular graph, showing weak S···Se interaction and extensive H-bonding.

In terms of q(*e*), $SeCH_3^-$ and $SeCF_3^-$ are found to represent the lower and upper bound, respectively (when disregarding GCSG-11). This is due to the greater electron-withdrawing power of the fluorine atoms relative to hydrogen. There is no discernible trend with respect to the Sec, CysSec, and GCSG groups of compounds, although in general, the atomic charge on Se decreases as the size of the molecular fragment increases, since the negative charge can be more effectively stabilised by a greater number of atoms (especially the oxygen atoms). This can also be seen in the ESP parameters, which become slightly less negative for the larger anions. There also appears to be a tenuous link between the number of hydrogen bonds (H-bonds) the Se participates in (identified on the AIM molecular graphs) and the ESP parameters. When the Se is involved in a weak interaction, the ESP tends to become less negative as electron density is shared in the interaction. In solution, the anionic Se species are expected to take part in extensive H-bonding with the solvent in addition to any potential intramolecular interactions, which may result in reduced negativity of the surface charge on

Stellenbosch University https://scholar.sun.ac.za

Se. In this sense, $SeCH_3^-$, $SeCF_3^-$ may not be similar to the Se in the TrxR active site. This difference is expected to have a larger impact when these fragments participate in weak intermolecular interactions, where the monomers interact across a distance and less charge polarisation takes place. When forming a coordination bond, q(*e*) may provide a better indication of the electron density available for bond formation.

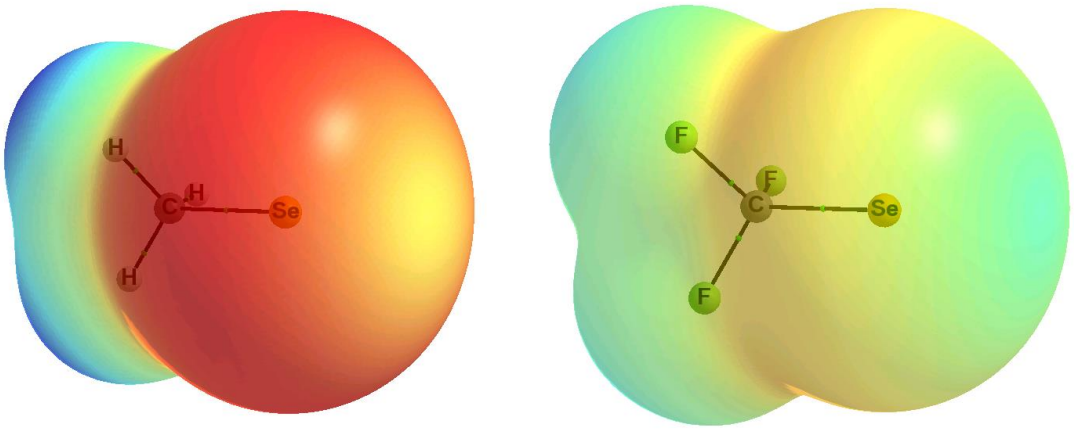

Figure 4-5: Electrostatic potential maps of $SeCH_3^-$ and $SeCF_3^-$. Red = -134 kcal mol^{-1}, Blue = -80 kcal mol^{-1}.

By generating ESP maps it is possible to visualise the areas of charge concentration and depletion on a molecular surface. Weakly interacting monomers generally orient themselves in such a way that an area of charge concentration on one is directed toward an area of charge depletion on the other. In this way the ESP map of a molecule can provide hints as to its most likely manner of coordination in a vdW complex. The ESP maps of $SeCH_3^-$ and $SeCF_3^-$ are shown in Figure 4-5 (extensive numerical information can be found in the ESI). Both ESP maps have the same colour scale, but the $SeCH_3^-$ map reflects the extremes of the scale while $SeCF_3^-$ exhibits little variation. It should be noted that even the areas of greatest charge depletion remain negatively charged. In $SeCH_3^-$ the part of the isosurface corresponding to the H atoms appears blue, indicative of the relative charge depletion in that part of the molecule. The Se surface is red, showing charge concentration, with a yellow area of relative charge depletion opposite to Se along the axis of the Se-C bond. In $SeCF_3^-$ the electronegative F atoms do not allow for as much charge polarisation towards Se, and most of the molecular surface appears green. A yellow band around Se and orthogonal to the axis of the Se-C bond is again observed. This band of relative charge accumulation will most likely be oriented toward a positively charged interaction partner, such as the Au(I) complexes studied in this work.

Stellenbosch University https://scholar.sun.ac.za

4.3 Conclusions

The ESP parameters of the two smaller model Se compounds are in general more negative than those of the larger Se compounds. This may imply that a Coulombic interaction between one of the compounds and a cationic interaction partner at medium distances may be more stabilising than a similar interaction with the Se in the TrxR active site. However, the Se atomic basin charges of the two smaller compounds bracket those of the larger anions, which may indicate that the active site Se would behave similarly to something intermediate between $SeCH_3^-$ and $SeCF_3^-$. These compounds can therefore be used to estimate extremes in behaviour between the Se in the TrxR active site and the Au complexes under study.

The S···Se interactions observed suggest that at least some of the time the S and Se of the Cys and Sec amino acid residues in the TrxR active site will be in close proximity to each other. Simulation of the dynamical evolution of the system would be required to confirm this, but the result is interesting considering that a crystal structure has been obtained of the TrxR-related protein glutathione reductase (GR) with an Au atom coordinated in a linear fashion between the two Cys residues in its active site.[8] Similar results have not been found for TrxR, but the optimised tetrapeptide conformations suggest that the Sec and Cys residues can orient themselves in a linear manner favourable for Au coordination. This is encouraging for a rational drug design approach aiming to block the TrxR active site by coordination bonding of Au to both the Sec and Cys residues.

Stellenbosch University https://scholar.sun.ac.za

References

(1) Mustacich, D.; Powis, G. *Biochem. J.* **2000**, *346*, 1–8.

(2) Berners-Price, S. J.; *Bioinorganic Medicinal Chemistry*; Alessio, E., Ed.; Wiley-VCH Verlag & Co. KGaA: Weinheim, Germany, **2011**, 201.

(3) *Dassault Systèmes BIOVIA, Discovery Studio Modeling Environment, Release 4.5, San Diego: Dassault Systèmes*. San Diego **2015**.

(4) Frisch, M. J.; Trucks, G. W.; Schlegel, H. B.; Scuseria, G. E.; Robb, M. A.; Cheeseman, J. R.; Scalmani, G.; Barone, V.; Mennucci, G.; Petersson, A.; Nakatsuji, H.; Caricato, M.; Li, X.; Hratchian, H. P.; Izmaylov, A. F.; Bloino, J.; Zheng, G.; Sonnenberg, J. L.; Hada, M.; Ehara, M.; Toyota, K.; Fukuda, R.; Hasegawa, J.; Ishida, M.; Nakajima, T.; Honda, Y.; Kitao, O.; Nakai, H.; Vreven, T.; Jr., J. A. M.; Peralta, J. E.; Ogliaro, F.; Bearpark, M.; Heyd, J. J.; Brothers, E.; Kudin, K. N.; Staroverov, V. N.; Keith, T.; Kobayashi, R.; Normand, J.; Raghavachari, K.; Rendell, A.; Burant, J. C.; Iyengar, S. S.; Tomasi, J.; Cossi, M.; Rega, N.; Millam, J. M.; Klene, M.; Knox, J. E.; Cross, J. B.; Bakken, V.; Adamo, C.; Jaramillo, J.; Gomperts, R.; Stratmann, R. E.; Yazyev, O.; Austin, A. J.; Cammi, R.; Pomelli, C.; Ochterski, J. W.; Martin, R. L.; Morokuma, K.; Zakrzewski, V. G.; Voth, G. A.; Salvador, P.; Dannenberg, J. J.; Dapprich, S.; Daniels, A. D.; Farkas, O.; Foresman, J. B.; Ortiz, J. V.; Cioslowski, J.; Fox, D. J. Gaussian, Inc.: Wallingford CT **2013**.

(5) Kim, J.-Y.; Ahn, D.-S.; Park, S.-W.; Lee, S. *RSC Adv.* **2014**, *4* , 16352–16361.

(6) Nakanishi, W.; Hayashi, S.; Narahara, K. *J. Phys. Chem. A* **2008**, *112* , 13593–13599.

(7) Wang, W.; Ji, B.; Zhang, Y. *J. Phys. Chem. A* **2009**, *113* , 8132–8135.

(8) Urig, S.; Fritz-Wolf, K.; Réau, R.; Herold-Mende, C.; Tóth, K.; Davioud-Charvet, E.; Becker, K. *Angew. Chem. Int. Ed.* **2006**, *45*, 1881–1886.

Stellenbosch University https://scholar.sun.ac.za

5 Au(I) coordination complexes

Crystal structure data is available for many of the complexes studied in this work. This provided us with a means to validate our model chemistry. Optimised geometries of the complexes enumerated in Table 1-1 were compared to available crystal structures from the Cambridge Structural Database (CSD).[1] These optimised structures provided a starting point for many of our calculations. The ESP of the complexes was examined, as this could provide insight into the most likely mode of coordination with anionic species, such as the model Se fragments, $SeCH_3^-$ and $SeCF_3^-$. The ESP can also reveal aspects of how a chemical species will be affected by solvation in a (polar) solvent

5.1 Geometry optimisation

The structures of a number of Au(I) complexes containing NHC and phosphine ligands (specified in section 1.3 of the Introduction chapter) were optimised at the PBE0-D3/TZVP level of theory. The starting structures for geometry optimisation were based on CSD crystal structures, omitting counterions and solvent molecules. For those complexes where a crystal structure was not available, an initial geometry was constructed using the bond lengths and angles found in similar complexes available in the CSD.

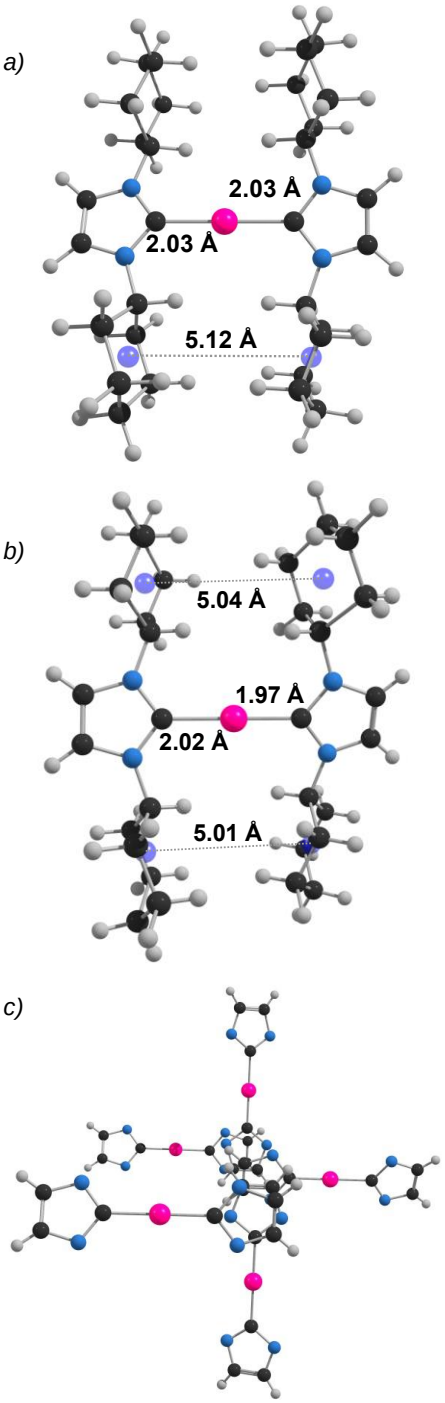

Figure 5-1: a)Au_2NHC7 optimised structure, b) Au_2NHC7 as found in YERGAE crystal structure, c) Packing of Au_2NHC7 in YERGAE crystal structure with counterions and N-substituents removed for clarity. Note the five stacked NHC rings.

Selected geometric parameters of the minimised Au_2NHCx and Au_2NHCxb complexes are shown in Table 5-1, along with available crystal structure parameters. The Au-C bond lengths show good agreement between the optimised and crystal structures, with two exceptions: Firstly, the Au-C bond distances in the crystal structure of Au_2NHC7 are 2.02 and 1.97 Å (Figure 5-1b) as opposed to 2.03 Å in the optimised structure (Figure 5-1a). This may be a packing effect, as the NHC ligands bound at a shorter distance to Au are stacked on top of

Stellenbosch University https://scholar.sun.ac.za

Table 5-1: Geometric parameters of Au_2NHCx and Au_2NHCxb complexes.

Complex	Optimised geometry			CSD REF	Crystal structure		
	Au-C (Å)	C-Au-C (°)	N-C--C-N (°)		Au-C (Å)	C-Au-C (°)	N-C--C-N (°)
Au_2NHC1	2.03	180	90	UMAGUL	2.02	178	163/176
					2.01/2.02	177	161/169
Au_2NHC2	2.04	180	90	YERFAD	2.02	180	180
Au_2NHC3	2.03	180	126				
Au_2NHC4	2.04	180	90	YERFIL	2.03	180	180
Au_2NHC5	2.06	180	95	YERFUX	2.03/2.04	176	86/101
Au_2NHC6	2.03/2.04	179	154/155	YERFOR	2.05	180	180
					2.03	180	180
					2.01/2.04	178	3/6
Au_2NHC7	2.03	180	15	YERGAE	1.97/2.02	180	17
Au_2NHC1b	2.03	180	90				
Au_2NHC2b	2.04	180	90	KIZWEX	2.10	180	180
Au_2NHC3b	2.03	180	60	FIBYAR	2.02/2.03	175	129/130
Au_2NHC4b	2.04	180	127	CIVMIE	2.02/2.03	176	20/27
Au_2NHC5b	2.06	173	77/121				
Au_2NHC6b	2.03	178	139/148				
Au_2NHC7b	2.04	180	115/119				

one another, a distance of 4.3 Å separating the NHC-ring centroids (Figure 5-1c). In both the crystal structure and optimised geometry the cyclohexane (Cy) rings on the N-substituents are facing each other, and their centroids are separated by a distance of ~5.0 Å (Figure 5-1). This alignment may be indicative of dispersion interactions between the Cy rings. The N-C···(Au)···C-N dihedral angles found in both the crystal structure and optimised geometry are equivalent (17° and 15°) and put the facing Cy rings into a near-eclipsed orientation.

The second deviation in bond length is found for the Au_2NHC2b complex and the crystal structure of KIZWEX. Consulting the CSD, we found three other crystal structures containing Au_2NHC2b with different counterions. The REFCODES and Au-C bond lengths are: FIBXUK – 2.05 Å, KIZWAT – 2.02 Å, and XIRMUI – 2.01 Å. We suspect that the variation in bond length is related to solvent effects.

The C-Au-C bond angles in both the crystal structures and optimised geometries show little deviation from linearity, as is typical of Au in the +1 oxidation state.[2] The optimised geometries typically have N-C···(Au)···C-N dihedral angles closer to orthogonal, while in the crystal structures the NHC rings are more likely to be coplanar. The coplanar arrangement may be preferred in the crystal structures to facilitate ring stacking, while the ligands have more

Stellenbosch University https://scholar.sun.ac.za

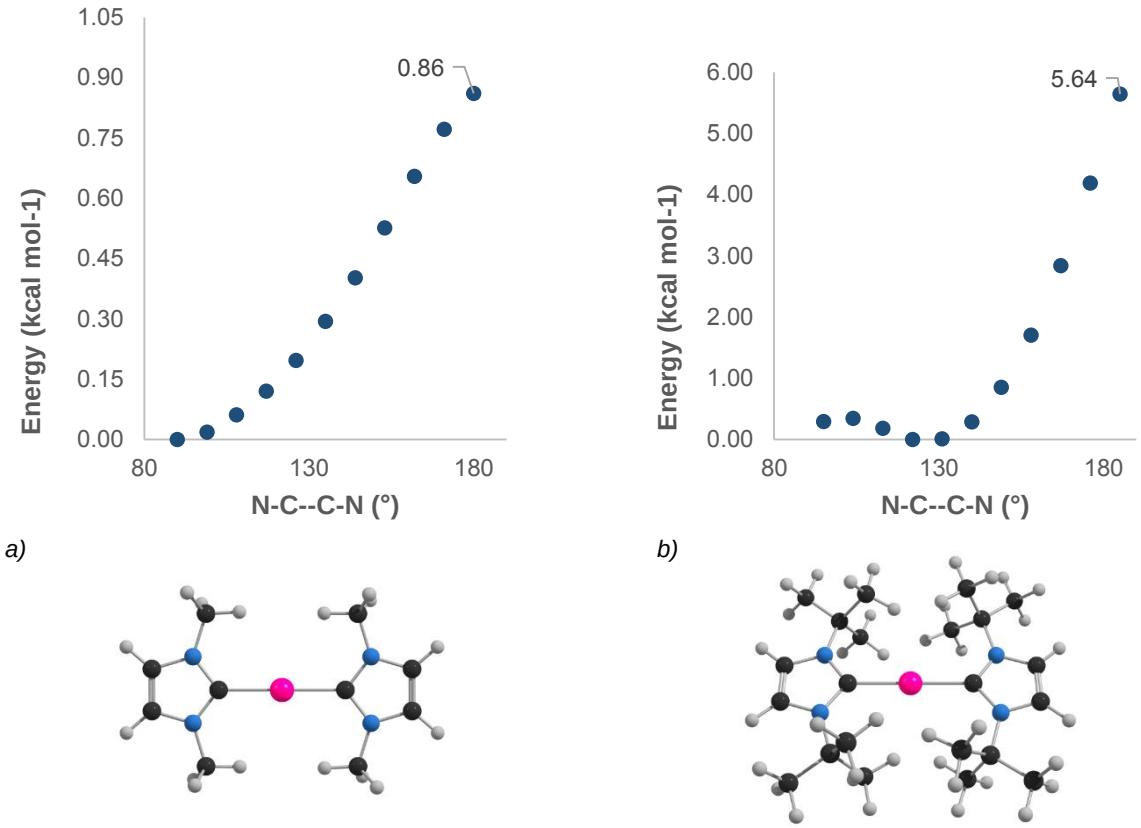

Figure 5-2: N-C···(Au)···C-N dihedral angle scan graphs for a) Au_2NHC2 and b) Au_2NHC5.

freedom to orient themselves during geometry optimisation in the absence of the periodic system. Relaxed scans (where a parameter is stepped through a range and geometry optimisation performed at each value) of the N-C···(Au)···C-N dihedral angle in Au_2NHC2 (little congestion at centre of complex) and Au_2NHC5 (congested centre – N-substituent = t-Bu) were performed to investigate the energetic barrier to rotation of the NHC rings (Figure 5-2a and b). The dihedral angle was increased from approximately 90° to 180° in steps of 9°. The highest energy conformation in both cases has a dihedral angle of ~180°, where the N-substituents on opposing rings are forced into close proximity to each other. For Au_2NHC2 the difference in energy between the minimum and maximum energy conformations is 0.86 kcal mol^{-1}, which implies a very low barrier to rotation. As expected for the more sterically congested Au_2NHC5, the energy difference is higher, but still not large at 5.6 kcal mol^{-1}.

The Au-C bond lengths do not appear to be affected by the presence of the extended ring system in the Au_2NHCxb complexes, and for the most part the other parameters are similar. Differences in the N-C···(Au)···C-N dihedral angle are observed for the Au_2NHC4(b) and Au_2NHC7(b) pairs, most likely due to an unfavourable steric interaction between the N-substituents and benzenoid ring H atoms occurring for the NHCxb variety of complexes (Figure 5-3 a and b). Differences in bond angles are observed between the Au_2NHCx and

Stellenbosch University https://scholar.sun.ac.za

Au_2NHCxb species – the N-substituents in the Au_2NHCxb species are bent slightly more towards the metal centre, increasing the H···H distance between N-substituent and benzenoid ring H atoms. This increases congestion at the metal centre, which affects the preferred N-C···(Au)···C-N dihedral angle.

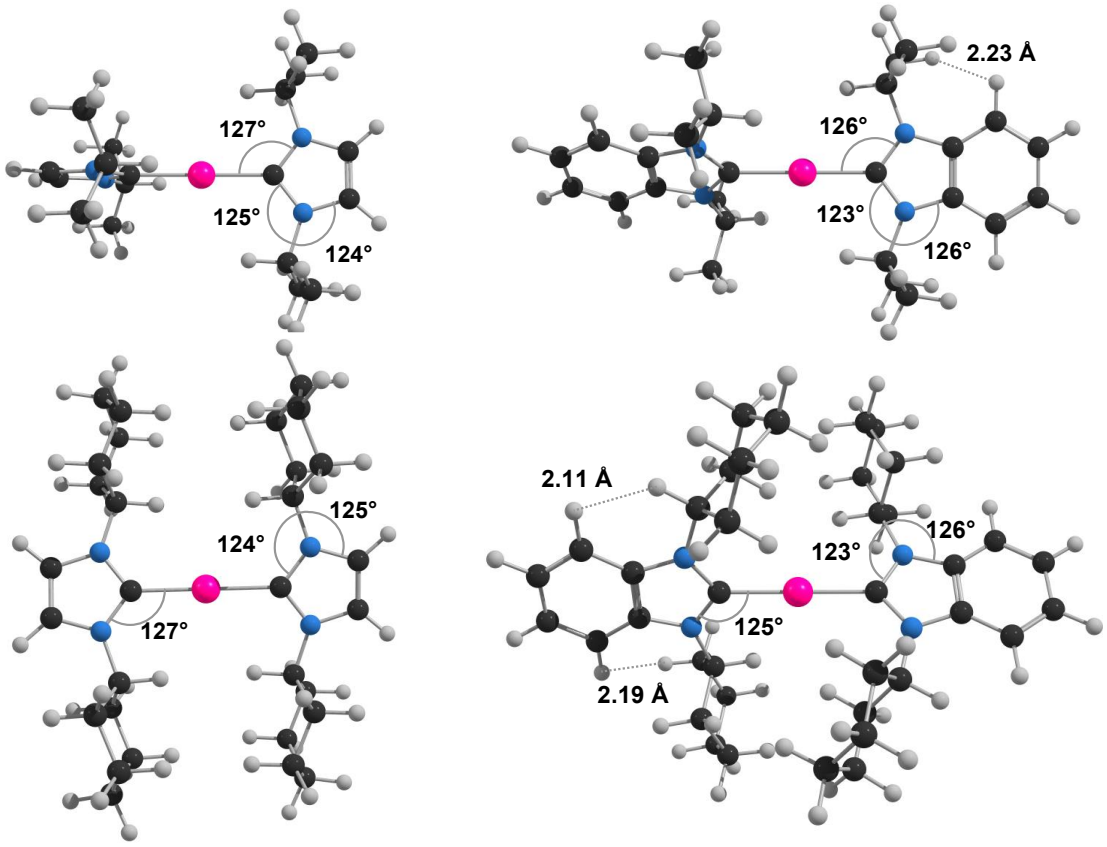

Figure 5-3: a) Au_2NHC4, b) Au_2NHC4b, c) Au_2NHC7 and d) Au_2NHC7b optimised structures with bond angles and short H···H distances indicated.

Table 5-2: Geometric parameters of the neutral AuCl_NHCx and AuCl_NHCxb complexes.

Complex	Optimised geometry			CSD REF	Crystal structure		
	Au-C (Å)	Au-Cl (Å)	C-Au-Cl (°)		Au-C (Å)	Au-Cl (Å)	C-Au-Cl (°)
AuCl_NHC1	1.98	2.26	180				
AuCl_NHC2	1.99	2.27	180	ECIHOO	1.94	2.27	179
AuCl_NHC3	1.99	2.27	180				
AuCl_NHC4	1.99	2.27	180	ECIHUU	1.96	2.26	175
AuCl_NHC5	2.01	2.27	180				
AuCl_NHC6	1.99	2.27	180				
AuCl_NHC7	1.99	2.27	180	ECIJAC	1.98	2.29	177
AuCl_NHC1b	1.97	2.26	180				
AuCl_NHC2b	1.99	2.26	180				
AuCl_NHC3b	1.98	2.26	180				
AuCl_NHC4b	1.99	2.27	180				
AuCl_NHC5b	2.01	2.27	179				
AuCl_NHC6b	1.98	2.27	179				
AuCl_NHC7b	1.99	2.27	180				

Stellenbosch University https://scholar.sun.ac.za

The neutral AuCl_NHCx complexes (Table 5-2) display very little variation in their optimised parameters, and there is good agreement between the optimised geometries and crystal structures. As with the Au_2NHCx complexes, the longest Au-NHC distance is observed for the complexes featuring the t-Bu N-substituent. Shorter Au-C bond distances are observed than in the cationic Au_2NHCx complexes

Good agreement between the optimised geometry and crystal structure was also found for Auranofin (Table 5-3). The Au-P and Au-S bond lengths in the optimised structures of the other Au-Phos/Au-Thio complexes are also very similar. The preference of Au for linear coordination is also displayed in these complexes.

Table 5-3: Geometric parameters of Au-Phos/Thio complexes. Auranofin and the Thio complex are neutral, while the other complexes carry a +1 charge.

Complex	Optimised geometry			CSD REF	Crystal structure		
	Au-P (Å)	Au-S (Å)	P-Au-S (°)		Au-P (Å)	Au-S (Å)	P-Au-S (°)
Auranofin	2.27	2.32	169	AGLPAU	2.26	2.29	174
	Au-S	**Au-C**	**S-Au-C**				
Thio1-Au-NHC5	2.30	2.04	180				
	Au-P	**Au-C**	**P-Au-C**				
Phos4-Au-NHC5	2.30	2.07	179				
Phos1-Au-NHC3b	2.31	2.06	180				
Phos2-Au-NHC3b	2.31	2.06	179				
Phos3-Au-NHC3b	2.32	2.05	179				
Phos4-Au-NHC3b	2.31	2.05	179				

The geometries of the ligand exchange products of the above complexes with $SeCH_3^-$, $SeCF_3^-$ were also optimised. The complexes are linear as well, and Au-Se bond distances are largely conserved (Au-Se distance is ~2.4 Å in $SeCH_3^-$ species and 2.41 Å in $SeCF_3^-$ species). Log files of the calculations have been included in the ESI.

5.2 Atoms in Molecules and electrostatic potential

Atoms in molecules analysis was performed for the above complexes. We were mainly concerned with the ESP properties, but the molecular graphs of some of the complexes proved interesting.

Table 5-4: H···H and Au···H distances and BCP e^- densities.

	H···H (Å)	ρ (e bohr^{-3})	$\nabla^2\rho$ (e bohr^{-5})
Au_2NHC4	2.4	0.002	0.007
Au_2NHC5	2.1	0.009	0.026
Au_2NHC6	2.4	0.006	0.019
	2.5	0.004	0.015
	2.5	0.004	0.014
	2.4	0.005	0.017
	2.4	0.006	0.019
Au_2NHC7	2.6	0.003	0.009
	2.5	0.004	0.010
	2.6	0.003	0.009
	Au···H (Å)		
Au_2NHC5	2.5	0.018	0.051
	2.8	0.011	0.031
Au_2NHC6	3.2	0.006	0.017

Stellenbosch University https://scholar.sun.ac.za

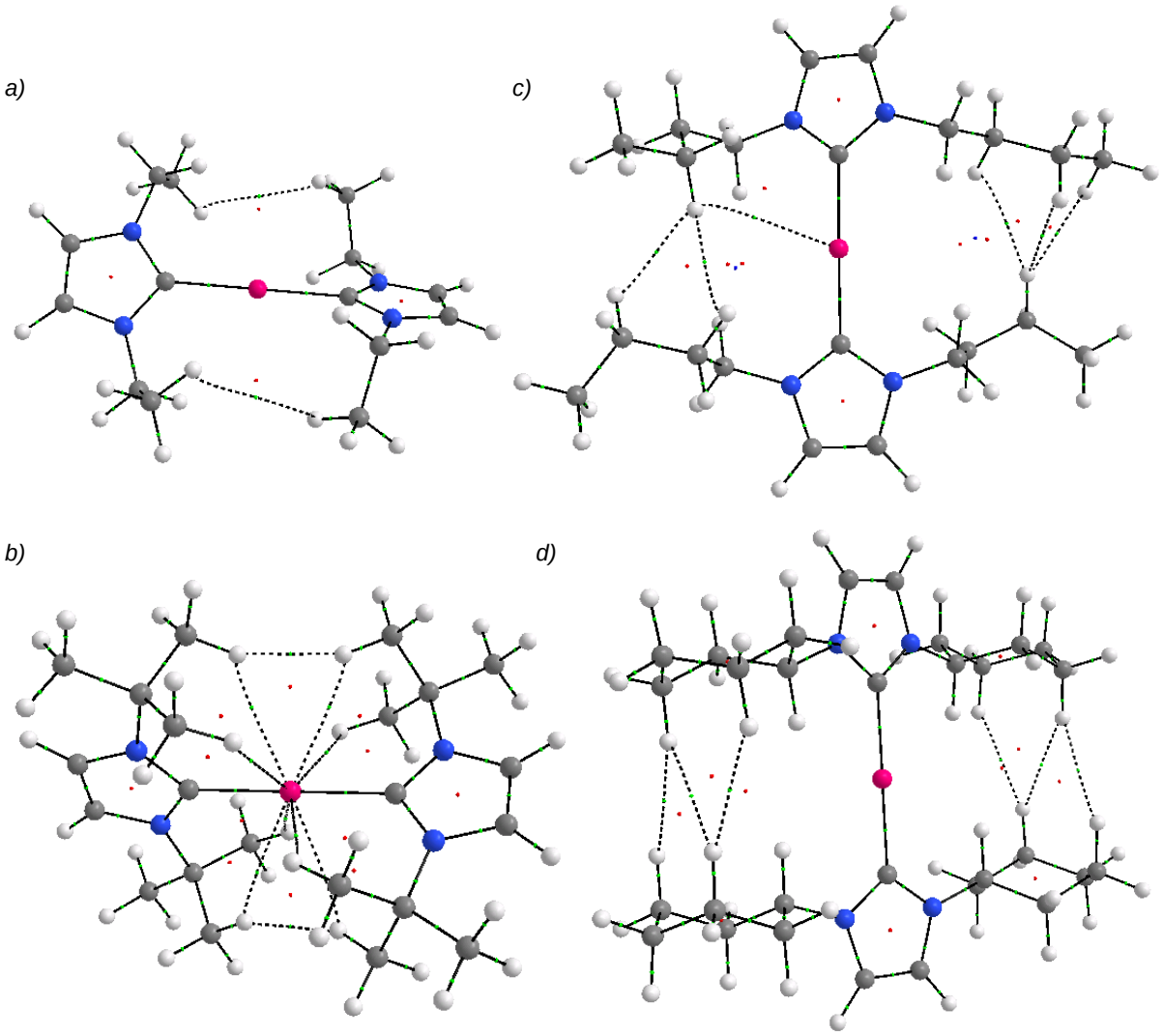

Figure 5-4: Molecular graphs of a) Au_2NHC3, b) Au_2NHC5, c) Au_2NHC6, d) Au_2NHC7.

Bond paths and bond critical points of low electron density (ρ) are observed between H···H and Au···H pairs in the molecular graphs of a number of the Au-NHC complexes (Figure 5-4a to d, and also in their benzimidazolylidene versions). The longest H···H contact displaying such a critical point is found in Au_2NHC3 (Figure 5-4 a). In this complex the H atoms are separated by a distance of ~3 Å, which exceeds the sum of their vdW radii (2.4 Å), casting doubt on the existence of a stabilising interaction. The shortest H···H distance, 2.1 Å, is encountered in Au_2NHC5 (Figure 5-4 b). This is well within the sum of the vdW radii. The rest of the H···H contacts approximately match the sum of the vdW radii. The electron density at these BCPs is low (Table 5-4), and in the range commonly found for dispersion interactions, which seem unlikely for small and hard H atoms.

For the congested H atoms the conventional wisdom is that there should be steric repulsion between them instead of a stabilising interaction.[3] The apparent H···H bonds found in planar biphenyl has been a topic of discussion in the literature, and it has been questioned whether

Stellenbosch University https://scholar.sun.ac.za

Table 5-3: ESP values and volume of Au-NHC complexes.

Complex	Max	Min	Avg	Volume
	(kcal mol^{-1})			(bohr^3)
Au_2NHC1	118	62	83	1332
Au_2NHC2	86	58	74	1938
Au_2NHC3	86	56	69	2570
Au_2NHC4	83	53	64	3163
Au_2NHC5	79	52	62	3640
Au_2NHC6	83	43	61	3791
Au_2NHC7	80	45	58	4554
Au_2NHC1b	115	46	69	2114
Au_2NHC2b	77	43	65	2715
Au_2NHC3b	79	42	63	3344
Au_2NHC4b	75	41	60	3904
Au_2NHC5b	73	39	59	4375
Au_2NHC6b	76	40	57	4571
Au_2NHC7b	75	38	55	5264

a BCP is necessarily associated with a stabilising interaction. The H···H BCPs and bond paths discussed above are most likely not indicative of a stabilising interaction, and are not likely to hinder ligand dissociation.

Three types of Au···H bond paths can be identified in the molecular graphs of Au_2NHC5 and Au_2NHC6 (Figure 5-4 b and c). The Au···H distance in Au_2NHC6 is longer than the sum of vdW radii, and the electron density at the BCP is low (compare reference 4). In Au_2NHC5 there are eight Au···H BCPs of low electron density, with interatomic separations of 2.5 Å and 2.8 Å (sum of vdW radii 2.8 Å). The electron density at these critical points is significantly higher than what is found for Au_2NHC6, the electron density of 0.018 *e* bohr^{-3} being about twice what is normally found for vdW interactions.[5] This is high enough to suggest that a stabilising interaction may be occurring. The stabilising nature of the interaction should be confirmed by checking for the presence of attractive Ehrenfest force,[3] however, the use of an ECP for Au prevents the calculation of this quantity. It is interesting to note that the shortest H···H contact is found for this complex, perhaps as a side effect of establishing the short Au···H contacts. Further characterisation of these interactions falls outside the scope of this work. If these interactions are in fact stabilising, they are likely to contribute little to the overall molecular stabilisation (with the exception of the Au_2NHC5 Au···H interactions) given their low BCP electron densities.

Table 5-4: ESP parameters and volume of AuCl_NHC complexes.

Complex	Max	Min	Avg	Volume
	(kcal mol^{-1})			(bohr^3)
AuCl_NHC1	61	-42	3	1038
AuCl_NHC2	40	-43	3	1340
AuCl_NHC3	39	-43	2	1652
AuCl_NHC4	39	-44	3	1954
AuCl_NHC5	35	-43	2	2200
AuCl_NHC6	31	-42	3	2266
AuCl_NHC7	37	-44	3	2641
AuCl_NHC1b	60	-41	4	1429
AuCl_NHC2b	33	-41	3	1729
AuCl_NHC3b	33	-41	3	2040
AuCl_NHC4b	31	-42	3	2325
AuCl_NHC5b	30	-42	2	2558
AuCl_NHC6b	31	-42	3	2656
AuCl_NHC7b	31	-42	2	3002

The ESP properties of the Au complexes were considered next (extensive numerical data may be found in the ESI). An isodensity surface at an electron density of 0.001 *e* bohr^{-3} was used to define the volume. The ESP distribution can reveal

Stellenbosch University https://scholar.sun.ac.za

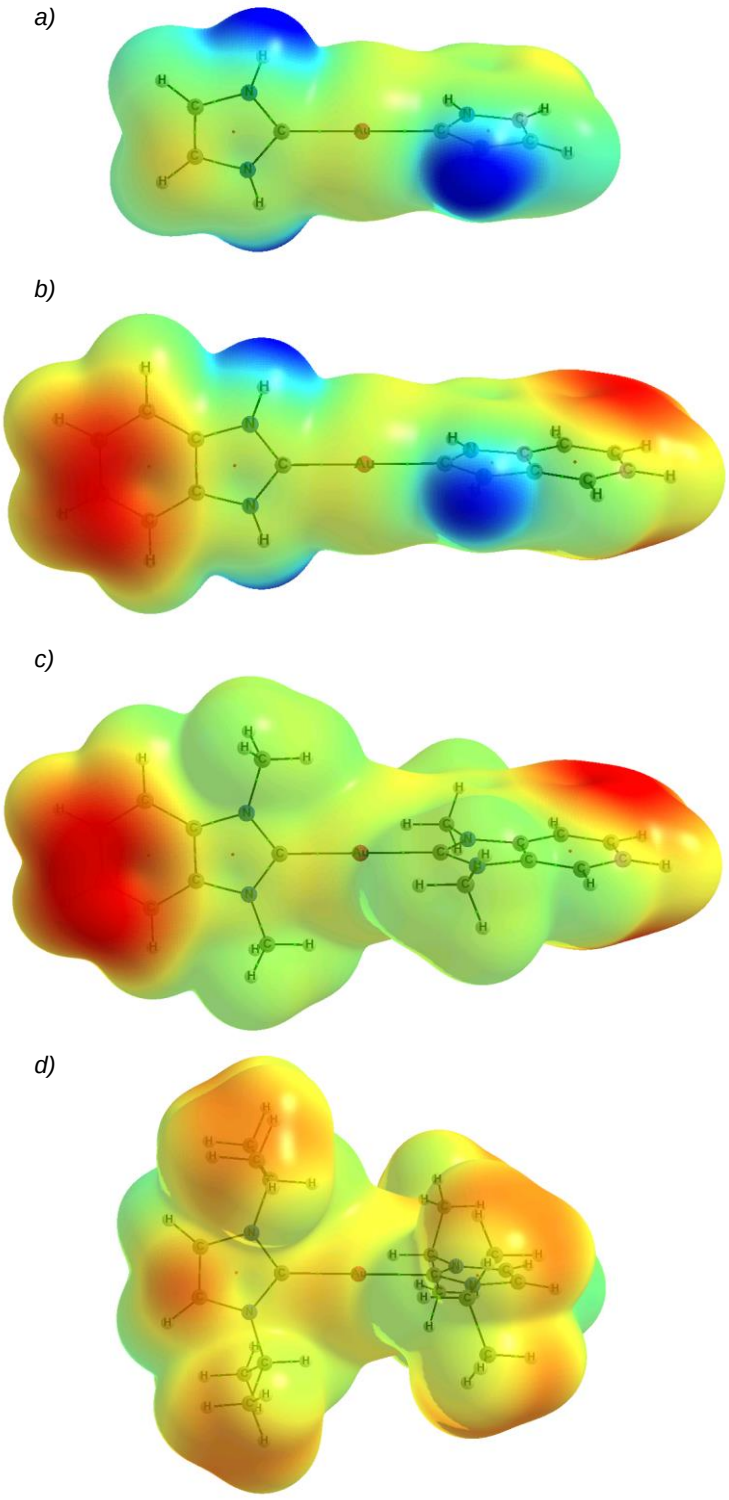

Figure 5-5: ESP maps of a) Au_2NHC1, b) Au_2NHC1b, c) Au_2NHC2b, and d) Au_2NHC4.
Red = 46 kcal mol^{-1}, Blue = 115 kcal mol^{-1}.

how a molecule is likely to engage in weak interactions, and is also related to its solubility properties.

The Au-NHC complexes are very similar in terms of their charge distribution (Table 5-5). Besides the NHC1(b) outliers, there is little variation in the maximum, minimum, and average potentials on the molecular surface. A general decrease in these values is however observed with increasing volume. For the Au_NHCxb complexes, the maximum ESP tends to decrease more slowly with volume than the minimum, resulting in more variation across the molecular surface. The regions of charge accumulation and depletion can easily be discerned in ESP maps of the complexes.

The ESP maps of Au_2NHC1, Au_2NHC1b, and Au_2NHC2b appear in Figure 5-5a to c. The colour scale has been chosen according to the maximum and minimum charge areas of Au_2NHC1b, which has the largest ESP spread among the three complexes. The most positive areas (indicated in blue) on the isosurfaces of both Au_2NHC1 and Au_2NHC1b occur close to the N-substituent, which corresponds to H atoms for these complexes. The areas of relative charge accumulation on these species (both isosurfaces are entirely positive) are quite different, however. The least

Stellenbosch University https://scholar.sun.ac.za

positive area on the Au_2NHC1 is found in proximity to the aromatic carbons of the NHC rings. In Au_2NHC1b much more electron density is concentrated above and below the benzenoid ring, as evidenced by the red colour on the isosurface. When the N-substituent H atoms are replaced with alkyl fragments (e.g. Au_2NHC2b and Au_2NHC4, Figure 5-6 c and d), a much more homogeneous charge distribution is observed. The ESP around Au in these complexes is close to the molecular surface average. The above observations are consistent with the results of a prior theoretical study, and the reputation of these complexes as nonpolar.[6]

Table 5-5: ESP parameters and volume of Au-Phos and Au-Thio complexes.

Complex	Max	Min	Avg	Volume
	(kcal mol^{-1})			(bohr^3)
Phos1-Au-NHC3b	89	45	69	2538
Phos2-Au-NHC3b	83	44	66	2988
Phos3-Au-NHC3b	79	43	64	3408
Phos4-Au-NHC3b	78	41	58	4877
Phos4-Au-NHC5	80	40	58	4152
Auranofin	25	-40	1	4175
Thio1-Au-NHC5	33	-41	-1	5578

The AuCl-NHC complexes show much greater variation in ESP over the entire molecular surface (Table 5-6), but the charge distribution across the NHC ligand is again very homogenous. Interestingly, the Au isosurface average ESP is slightly negative for these complexes, demonstrating the electronegativity of Au. The Cl atom exhibits the most negative ESP, while the NHC ligands appear mostly positive.

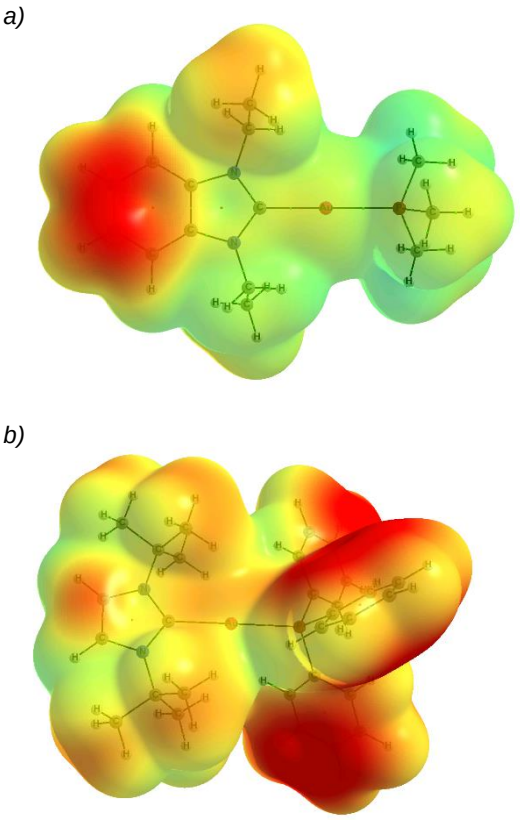

Figure 5-6: ESP maps of a) Phos1-Au-NHC3b and b) Phos4-Au-NHC5. Same colour scale mapping as Figure 5-5.

Five cationic and two neutral complexes containing Phos and Thio ligands were also investigated (Table 5-7). The cationic Au-Phos complexes are similar to the Au-NHC complexes in terms of their homogenous ESP distribution (although maximum – minimum is slightly higher for the Phos complexes) and the trends with molecular volume. In the complexes where the Phos ligand has alkyl substituents (Phos1 to Phos3) the most positive ESP regions occur around them, while the least positive ESP is found near the aromatic C atoms of the NHC ring (Figure 5-6a). In contrast, in the Phos4 (Phos4 = P(Phenyl)$_3$) complexes, the areas of least positive ESP are found near the phosphine

Stellenbosch University https://scholar.sun.ac.za

phenyl rings, while the highest charge depletion occurs near the aromatic H atoms on the NHC ring (Figure 5-6b).

The neutral complexes, Auranofin and Thio1-Au-NHC5, are similar to the neutral AuCl_NHC complexes in terms of ESP parameters. The lowest ESP is found on the isosurface apportioned to the Thio1 ligand, especially near the electronegative S and O atoms.

5.3 Conclusions

The good agreement between the geometric parameters of the complexes established by geometry optimisation and those found in crystal structures validates our choice of model chemistry. The biggest difference between the optimised structures and crystal structures is found in the N-C···(Au)···C-N dihedral angles. By scanning this parameter we were able to demonstrate that the barrier to rotation is low, so that although the parameters differ between optimised geometry and crystal structure, the energy is not significantly affected.

The ESP distributions of the Au-NHC complexes were found to be homogenous, and in this sense similar to the Au-Phos complexes. This indicates that there should be little preference in terms of a specific site for coordination in a vdW complex if electrostatic attraction is the dominating interaction between the two monomers. Additionally, the molecular size of the cationic Au complexes was found to be related to their ESP properties. As the charge is spread over a larger volume, the ESP on the molecular surface becomes more homogenous.

Stellenbosch University https://scholar.sun.ac.za

References

(1) Allen, F. H. *Acta Crystallogr. Sect. B Struct. Sci.* **2002**, *58*, 380–388.

(2) Pacheco, E. A.; Tiekienk, E. R. T.; Whitehouse, M. W. *Gold Chemistry: Applications and Future Directions in the Life Sciences*; Mohr, F., Ed.; Wiley-VCH: Weinheim, Germany, **2009**, 284

(3) Dillen, J. *Int. J. Quantum Chem.* **2013**, *113*, 2143–2153.

(4) Groenewald, F.; Dillen, J.; Raubenheimer, H. G.; Esterhuysen, C. *Angew. Chem. Int. Ed.* **2015**, *7602*, 1694–1698.

(5) Nakanishi, W.; Hayashi, S.; Narahara, K. *J. Phys. Chem. A* **2008**, *112*, 13593–13599.

(6) Rubbiani, R.; Salassa, L.; De Almeida, A.; Casini, A.; Ott, I. *ChemMedChem* **2014**, *9*, 1205–1210.

Stellenbosch University https://scholar.sun.ac.za

6 Solubility

The efficacy of a drug is dependent on its solubility in both water, the major constituent of the liquid in the body's circulatory system and cell interiors, and the lipid bilayers of cell membranes, which must be crossed by the drug if it is to have an effect within the cell. As such, the solubility of a drug in polar and non-polar media is of great interest in drug design, and a means of predicting solubility (and relating it to properties of a drug molecule) can be very useful in the drug design process.

6.1 Free energy of hydration

The free energies of hydration for the Au complexes, ligands, and products of ligand exchange reactions were calculated using the COSMO-RS continuum solvation model,[1] using the Au and Se parameters described in Chapter 3. The results are shown in Tables 6-1 to 6-4.

The cationic, bis-ligated Au complexes (Table 6-1) are greatly stabilised by the continuum solvent model (up to 52 kcal mol^{-1} in the case of Au_2NHC1), as expected for charged species. Among the Au_NHCxb complexes the most stabilising ΔG_{solv} is found for Au_2NHC1b, with the same N-substituent as Au_2NHC1. The greater charge polarisation in

Table 6-1: Free energies of hydration for cationic Au complexes, a) bis-ligated and b) mono-ligated.

a)

Complex	Charge (*e*)	ΔG_{solv} (kcal mol^{-1})
Au_2NHC1	1	-52.41
Au_2NHC2	1	-35.24
Au_2NHC3	1	-33.44
Au_2NHC4	1	-30.43
Au_2NHC5	1	-29.21
Au_2NHC6	1	-30.69
Au_2NHC7	1	-27.08
Au_2NHC1b	1	-49.55
Au_2NHC2b	1	-32.70
Au_2NHC3b	1	-31.00
Au_2NHC4b	1	-28.95
Au_2NHC5b	1	-28.09
Au_2NHC6b	1	-27.93
Au_2NHC7b	1	-25.89
Phos1-Au-NHC3b	1	-34.17
Phos2-Au-NHC3b	1	-32.06
Phos3-Au-NHC3b	1	-30.71
Phos4-Au-NHC5	1	-28.56
Phos4-Au-NHC3b	1	-29.26

b)

Complex	Charge (*e*)	ΔG_{solv} (kcal mol^{-1})
Au_NHC1	1	-60.62
Au_NHC2	1	-47.84
Au_NHC3	1	-45.27
Au_NHC4	1	-42.96
Au_NHC5	1	-41.27
Au_NHC6	1	-42.72
Au_NHC7	1	-39.55
Au_NHC1b	1	-57.22
Au_NHC2b	1	-45.13
Au_NHC3b	1	-42.82
Au_NHC4b	1	-41.03
Au_NHC5b	1	-39.52
Au_NHC6b	1	-40.23
Au_NHC7b	1	-37.95
Au_Phos1	1	-50.82
Au_Phos2	1	-45.99
Au_Phos3	1	-42.51
Au_Phos4	1	-37.34

Stellenbosch University https://scholar.sun.ac.za

Au_2NHC1 and Au_2NHC1b, as seen in their ESP maps in Figure 5-6, results in greater stabilisation upon solvation. A few kcal mol^{-1} difference is observed between the Au_2NHCx and Au_2NHCxb species, In general a decrease in the magnitude of ΔG_{solv} is seen as the size of the species increases, consistent with the decreased charge polarisation found in the larger complexes. The Au-Phos complexes have very similar ΔG_{solv} values to Au-NHC complexes of approximately the same volume (molecular volumes in Tables 5-5 and 5-7).

The mono-ligated, cationic Au-NHC complexes undergo even more stabilisation by the continuum solvent than the bis-ligated species, as the charge is now being concentrated within a smaller molecular volume. The NHC1 and NHC1b ligand complexes are once again the most stabilised, and the effect of size is again evident.

Table 6-2: Free energies of hydration of neutral Au complexes, a) bis-ligated and b) mono-ligated.

	Complex	Charge (*e*)	ΔG_{solv} (kcal mol^{-1})
a)	AuCl_NHC1	0	-18.61
	AuCl_NHC2	0	-11.02
	AuCl_NHC3	0	-10.11
	AuCl_NHC4	0	-9.74
	AuCl_NHC5	0	-8.68
	AuCl_NHC6	0	-9.18
	AuCl_NHC7	0	-8.55
	AuCl_NHC1b	0	-17.25
	AuCl_NHC2b	0	-9.41
	AuCl_NHC3b	0	-8.61
	AuCl_NHC4b	0	-8.16
	AuCl_NHC5b	0	-7.93
	AuCl_NHC6b	0	-7.49
	AuCl_NHC7b	0	-6.81
	Auranofin	0	-15.50
	Thio1-Au-NHC5	0	-16.62
b)	Au_Thio1	0	-14.63
	AuCl	0	-5.43
	$AuSeCH_3$	0	-2.60
	$AuSeCF_3$	0	-2.45

Table 6-3: Free energies of hydration of ligands, a) neutral and b) anionic.

	Complex	Charge (*e*)	ΔG_{solv} (kcal mol^{-1})
a)	NHC1	0	-8.10
	NHC2	0	-3.37
	NHC3	0	-2.99
	NHC4	0	-2.76
	NHC5	0	-1.25
	NHC6	0	-2.25
	NHC7	0	-2.09
	NHC1b	0	-7.82
	NHC2b	0	-2.73
	NHC3b	0	-2.35
	NHC4b	0	-2.02
	NHC5b	0	-0.39
	NHC6b	0	-1.76
	NHC7b	0	-1.00
	Phos1	0	0.42
	Phos2	0	0.88
	Phos3	0	1.05
	Phos4	0	-0.59
b)	Cl	-1	-70.28
	Thio1	-1	-60.20
	$SeCH_3$	-1	-57.80
	$SeCF_3$	-1	-51.99

The neutral complexes of Table 6-2 exhibit more moderate ΔG_{solv} values, with the NHC1 and NHC1b species again appearing as outliers. The ΔG_{solv} of the bis-ligated species Auranofin

Stellenbosch University https://scholar.sun.ac.za

and Thio1-Au-NHC5, as well as the mono-ligated Au_Thio1 undergo more solvent stabilisation than the other neutral complexes. Comparing the ESP maps of Au_Thio1, with relatively higher stabilisation, and AuCl, with quite modest stabilisation, it is not entirely clear why Au_Thio1 should be so stabilised by hydration (Figure 6-1). AuCl has a larger depletion of charge at the Au atom in line with the coordination bond than Au_Thio1 as evidenced by the blue regions on the isosurfaces. Charge accumulation on Cl is limited by the electronegativity of Au in the AuCl complex, while the O atoms in the thioglucose effectively polarise charge towards themselves, indicated by the orange colour of the isosurface in their vicinity. These O atoms may act as H-bond acceptors, leading to higher solvent stabilisation. Relatively high solvent stabilisation is also seen for the two other complexes containing the Thio1 ligand, Auranofin and Thio1-Au-NHC5, implicating the thioglucose ligand.

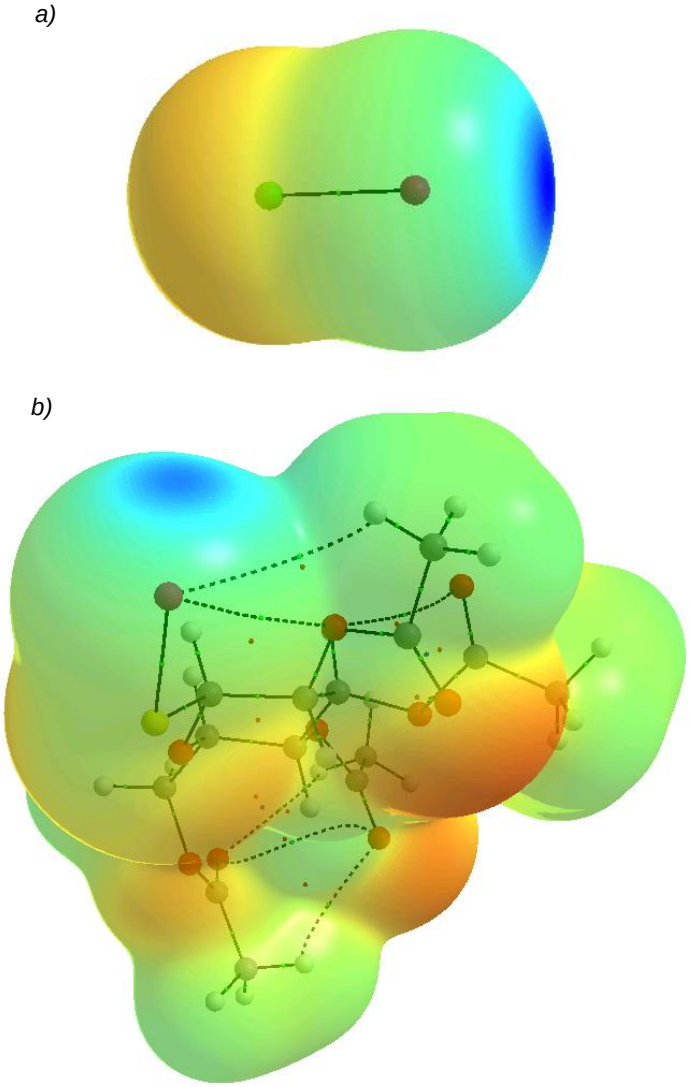

Figure 6-1: ESP maps of a) AuCl and b) Au_Thio1. Red = -32 kcal mol^{-1}, Blue = 76 kcal mol^{-1}.

The neutral ligands (Table 6-3a) are only weakly stabilised by the continuum solvent, with the exception of NHC1 and NHC1b. The ESP map of NHC1 (Figure 6-2) reveals relatively high charge accumulation on the carbene and charge depletion on the N-substituent H atoms, which accounts for the relatively high solvent stabilisation. Interestingly, three of the four phosphine ligands show small *positive* ΔG_{solv}. Phos4, which bears three phenyl groups, is the only phosphine ligand to have a nominally negative ΔG_{solv}, which is unusual given its reputation as a lipophilic moiety. This is, however, consistent with the greater charge polarisation observed in the ESP map of Phos4-Au-NHC5 (Figure 5-7).

Stellenbosch University https://scholar.sun.ac.za

The anionic ligands (Table 6-3b) are the most stabilised of the species considered. Contributing to this stabilisation is their small size, with the Cl^- displaying the highest stabilisation at 70 kcal mol^{-1}. Although they are of comparable size, the ΔG_{solv} values of the Se fragments differ by almost 6 kcal mol^{-1}, consistent with the higher charge polarisation found in $SeCH_3^-$.

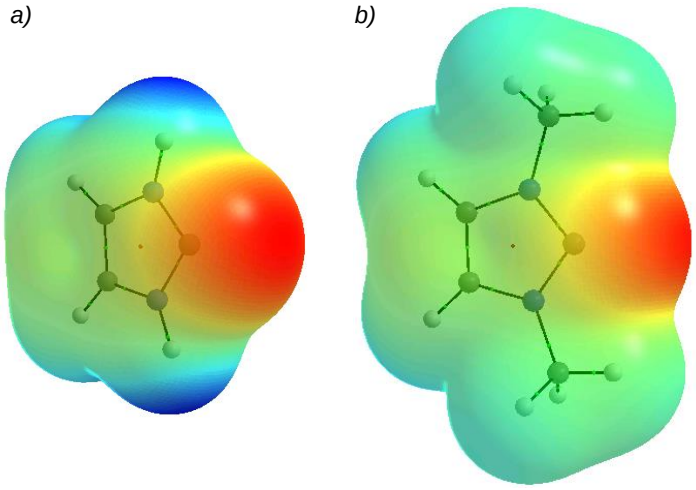

Figure 6-2: ESP maps of a) NHC1 and b) NHC1b. Red = -49 kcal mol^{-1}, Blue = 41 kcal mol^{-1}.

The ΔG_{solv} values of the coordination complexes containing the Se fragments as ligands (Table 6-4) are comparable to those of the other neutral complexes and the same trends are observed. The $SeCH_3^-$ coordination complexes are slightly more stabilised than the $SeCF_3^-$ species, mirroring what was seen for the lone ligands.

Table 6-2: Free energies of hydration of Au complexes with a) $SeCH_3^-$ and b) $SeCF_3^-$ ligands.

a)

Complex	Charge (*e*)	ΔG_{solv} (kcal mol^{-1})
$AuSeCH_3$_NHC1	0	-16.24
$AuSeCH_3$_NHC2	0	-9.19
$AuSeCH_3$_NHC3	0	-8.22
$AuSeCH_3$_NHC4	0	-8.05
$AuSeCH_3$_NHC5	0	-6.98
$AuSeCH_3$_NHC6	0	-7.46
$AuSeCH_3$_NHC7	0	-7.03
$AuSeCH_3$_NHC1b	0	-14.54
$AuSeCH_3$_NHC2b	0	-7.47
$AuSeCH_3$_NHC3b	0	-6.66
$AuSeCH_3$_NHC4b	0	-6.35
$AuSeCH_3$_NHC5b	0	-6.07
$AuSeCH_3$_NHC6b	0	-5.67
$AuSeCH_3$_NHC7b	0	-5.17
$AuSeCH_3$_Phos1	0	-6.91
$AuSeCH_3$_Phos2	0	-5.99
$AuSeCH_3$_Phos3	0	-5.64
$AuSeCH_3$_Phos4	0	-5.31

b)

Complex	Charge (*e*)	ΔG_{solv} (kcal mol^{-1})
$AuSeCF_3$_NHC1	0	-16.19
$AuSeCF_3$_NHC2	0	-8.19
$AuSeCF_3$_NHC3	0	-7.05
$AuSeCF_3$_NHC4	0	-6.55
$AuSeCF_3$_NHC5	0	-5.86
$AuSeCF_3$_NHC6	0	-5.91
$AuSeCF_3$_NHC7	0	-5.22
$AuSeCF_3$_NHC1b	0	-14.63
$AuSeCF_3$_NHC2b	0	-6.61
$AuSeCF_3$_NHC3b	0	-5.64
$AuSeCF_3$_NHC4b	0	-5.32
$AuSeCF_3$_NHC5b	0	-5.02
$AuSeCF_3$_NHC6b	0	-4.72
$AuSeCF_3$_NHC7b	0	-3.78
$AuSeCF_3$_Phos1	0	-6.59
$AuSeCF_3$_Phos2	0	-5.31
$AuSeCF_3$_Phos3	0	-4.87
$AuSeCF_3$_Phos4	0	-4.37

Stellenbosch University https://scholar.sun.ac.za

6.2 Lipophilicity

A measure of the lipophilicity of a range of Au complexes was obtained by calculating the octanol-water partition coefficient (*Log P*) using COSMO-RS. The results are shown in Tables 6-5 and 6-6, along with the average ESP and molecular volume calculated by the AIM approach. Experimental *Log P* values for five of the cationic Au-NHC complexes (as discussed in Chapter 1) are also included for comparison.[2]

It is immediately evident that the calculated *Log P* values are grossly overestimated (Table 6-5), *i.e.* the continuum solvent model overestimates the affinity of the complexes for octanol relative to water. This is likely primarily due to the absence of the counterions, Cl^- and Br^-, in the calculation. In the physical experiment these anions are likely to have a low affinity for the octanol layer and a high affinity for the water layer (Table 6-3 – Cl^- stabilised by 70 kcal mol^{-1}). Besides the neglect of this stabilisation, the potential difference established at the octanol-water interface by the differential partitioning of the Au complexes and counterions in the two solvent layers is also not accounted for in the calculation. This potential difference will limit the partitioning of the Au complexes into the octanol layer. The estimated solvent model parameters used for Au may have an effect, but this is not easily predictable. Assuming that any error originating from the estimated parameters will affect the individual Au complex *Log P* values to the same extent, the trends in the data can still provide meaningful insight.

Table 6-3: Average ESP, volume, and Log P of cationic Au complexes.

Complex	ESP average (kcal mol^{-1})	Volume ($bohr^3$)	logP (calc)	logP (exp)
Au_2NHC1	83	1332	3.4	
Au_2NHC2	74	1938	4.8	-1.09
Au_2NHC3	69	2570	6.3	-0.83
Au_2NHC4	64	3163	9.0	
Au_2NHC5	62	3640	8.9	0.3
Au_2NHC6	61	3791	9.6	1.09
Au_2NHC7	58	4554	11.7	1.73
Au_2NHC1b	69	2114	6.0	
Au_2NHC2b	65	2715	7.0	
Au_2NHC3b	63	3344	8.4	
Au_2NHC4b	60	3904	10.3	
Au_2NHC5b	59	4375	10.6	
Au_2NHC6b	57	4571	11.6	
Au_2NHC7b	55	5264	13.3	
Phos1-Au-NHC3b	69	2538	6.6	
Phos2-Au-NHC3b	66	2988	7.8	
Phos3-Au-NHC3b	64	3408	8.6	
Phos4-Au-NHC5	58	4152	10.2	
Phos4-Au-NHC3b	58	4877	10.2	

Stellenbosch University https://scholar.sun.ac.za

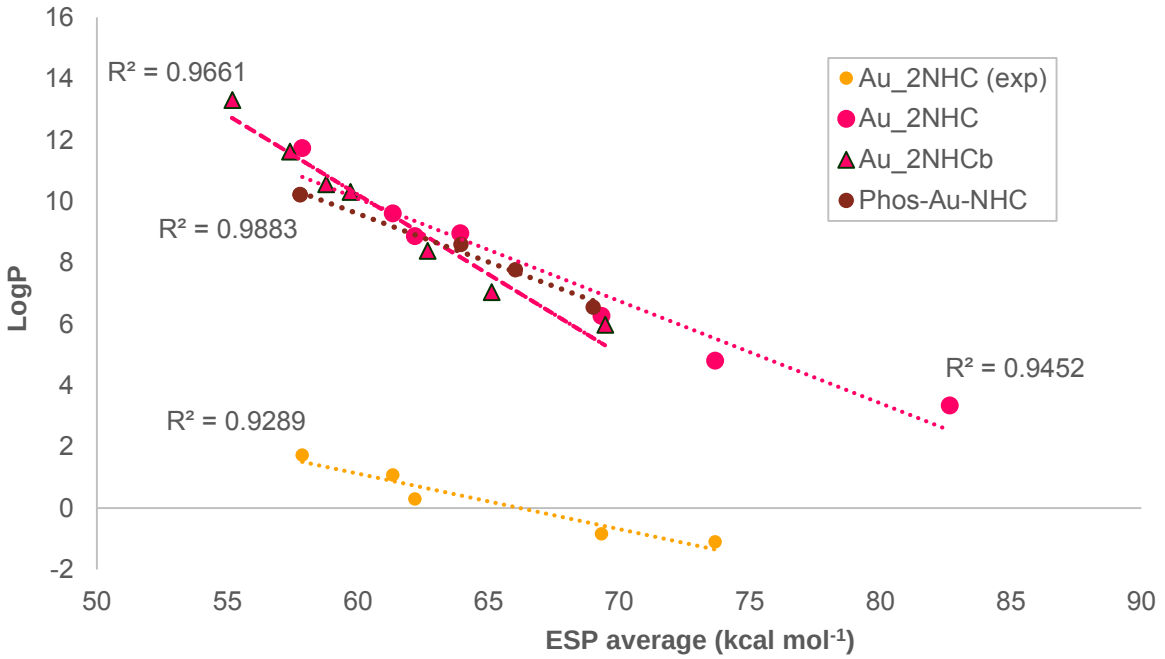

Figure 6-3: Log P relation to ESP average, cationic Au complexes.

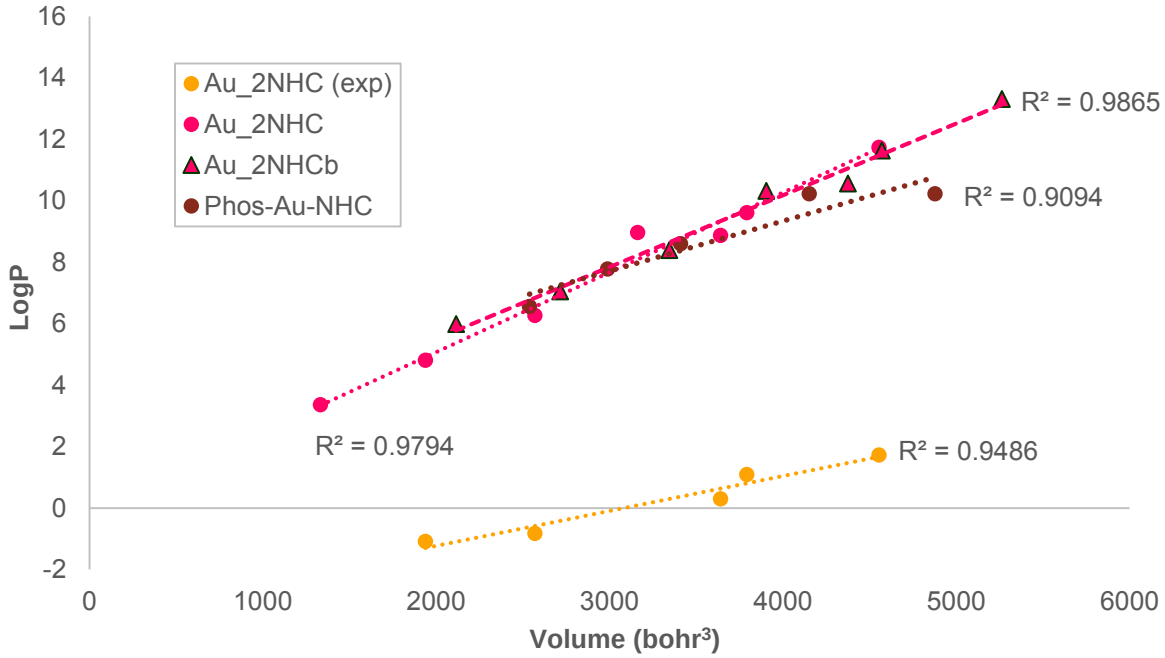

Figure 6-4: Log P relation to Volume, cationic Au complexes.

Stellenbosch University https://scholar.sun.ac.za

For the cationic complexes (Table 6-5), *Log P* is observed to increase as the average ESP decreases and the molecular volume increases. Plotting *Log P* as a function of the average ESP (Figure 6-3) and the volume (Figure 6-4) reveals linear trends with coefficients of determination close to unity. This is the case for both the calculated and experimental *Log P* values. Despite the large nominal differences in calculated and experimental *Log P* values, prediction of the relative lipophilicity of such delocalised lipophilic cations may be possible by using this approach. Also of note is the clustering together of NHC and phosphine *Log P* values on the graphs, suggesting that NHC ligands are indeed a good substitute for phosphine ligands when trying to achieve a certain lipophilicity. The neutral complexes also display *Log P* values correlated with molecular volume (Table 6-6, Figure 6-5). Thio1-Au-NHC5 and Auranofin do not fit the trend however, indicating that only sufficiently similar species can be compared in this fashion.

Table 6-4: volume and Log P of neutral Au complexes.

Complex	Volume (bohr^3)	logP (calc)
AuCl_NHC1	1038	0.9
AuCl_NHC2	1340	1.8
AuCl_NHC3	1652	2.8
AuCl_NHC4	1954	3.7
AuCl_NHC5	2200	4.2
AuCl_NHC6	2266	4.9
AuCl_NHC7	2641	6.0
AuCl_NHC1b	1429	2.3
AuCl_NHC2b	1729	3.0
AuCl_NHC3b	2040	4.0
AuCl_NHC4b	2325	4.9
AuCl_NHC5b	2558	5.2
AuCl_NHC6b	2656	6.0
AuCl_NHC7b	3002	6.8
Auranofin	4175	4.8
Thio1-Au-NHC5	5578	5.4

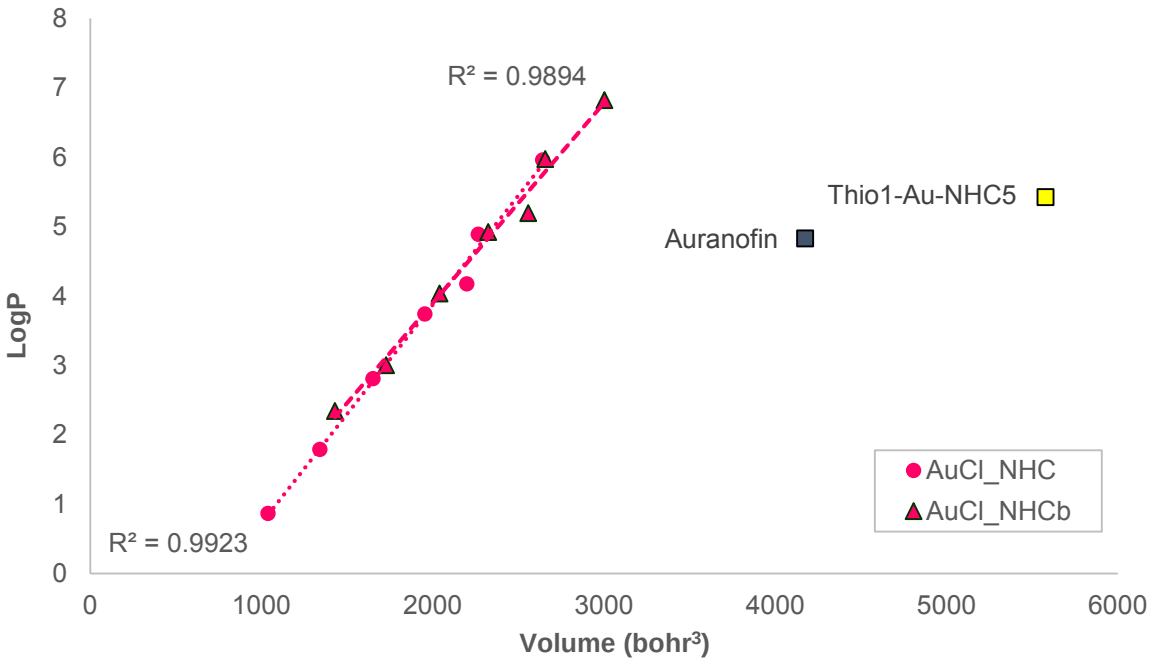

Figure 6-3: Log P relation to Volume, neutral Au complexes.

Stellenbosch University https://scholar.sun.ac.za

6.3 Conclusions

NHC ligands have attracted interest as replacements for phosphine ligands in drug design, specifically due to the lipophilic character of their complexes with Au. Our results show that they are indeed quite similar in terms of their solubility properties, both in terms of their hydration free energies and lipophilicity.

Although we could not correlate our free energies of hydration to experimental values, relative values could be rationalised and the expected high stabilisation for small charged species is observed.

We were able to show strong correlation between the average ESP on the molecular surface of the Au-NHC and Au-Phos complexes with their lipophilicity, and also a relation to the volume. This is probably related to the more homogenous charge distributions exhibited by the larger complexes, but also the volume-surface area connection, as the COSMO-RS model accounts for vdW-type interactions between solute and solvent. We have shown that although our calculated Log P values differ significantly from experimental values, that both show a linear relation to the molecular volume which may be useful in predicting the lipophilicity of related compounds.

Our theoretical results confirm that varying the N-substituent of an NHC ligand in an Au complex is an effective approach to fine-tuning the lipophilicity of such a complex.

References

(1) SCM, Theoretical Chemistry, Vrije Universiteit: Amsterdam, The Netherlands **2014**.

(2) Baker, M. V; Barnard, P. J.; Berners-Price, S. J.; Brayshaw, S. K.; Hickey, J. L.; Skelton, B. W.; White, A. H. *Dalton Trans.* **2006**, *6*, 3708–3715.

Stellenbosch University https://scholar.sun.ac.za

7 Au···Se vdW complexes

Au(I) is known to prefer an associative mechanism in its ligand exchange reactions with thiols.[1] This implies the formation of a three-coordinate transition state before one of the original ligands dissociates and a new coordination bond is formed. The reactant vdW complex may hint at the structure of the transition state occurring later along the reaction path, and reveal aspects hindering or helping its formation. We therefore investigated the vdW complexes of the cationic Au-NHC coordination complexes with the Se fragments, $SeCH_3^-$ and $SeCF_3^-$, with an interest in how the identity of the NHC ligand would influence vdW complex formation. The geometries of various combinations were optimised and their geometric parameters were scrutinised. We then performed Atoms in Molecules (AIM) analysis on the resulting structures, looking specifically at the properties of the bond critical points (BCPs) connecting the Au complexes and Se fragments. This was followed by calculation of the association energy in both the gas and solvated phase, and energy decomposition analysis (EDA) of the gas phase interaction energy.

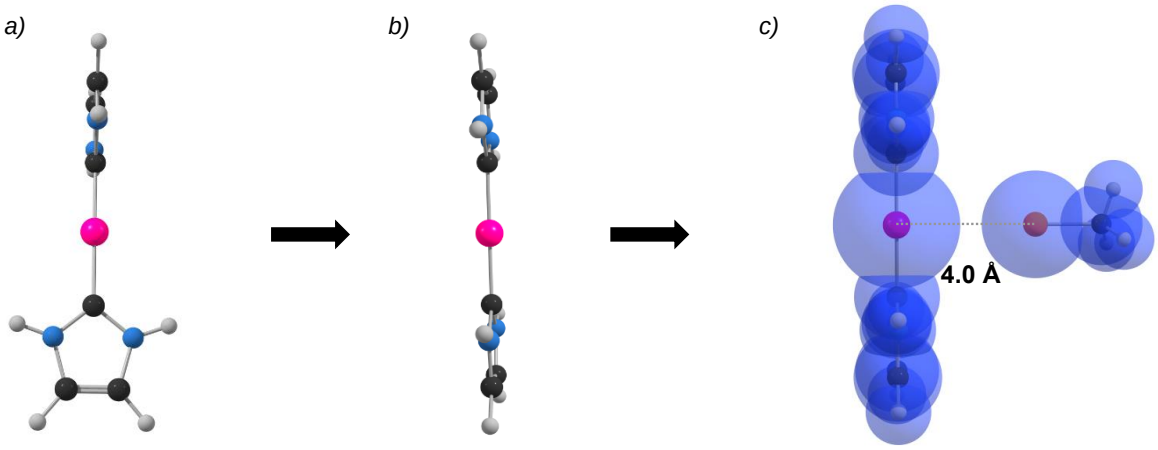

Figure 7-1: a) Optimised geometry of Au_2NHC1, b) co-planar optimised geometry, c) starting geometry for optimisation of $SeCH_3^-$ adduct with Au_2NHC1. Spheres illustrate vdW radii of atoms.

7.1 Geometry optimisation

Before optimising the geometries of various combinations of the Au-NHC complexes with Se fragments, we first optimised the Au complexes in a co-planar arrangement of NHC ligands. The co-planar arrangement simplified the construction of symmetrical starting geometries for optimisation (Figure 7-1). The barrier to rotation of the ligands was estimated to be low (Chapter 5), so energetically there is little difference between the minimum energy structures of the Au complexes and their co-planar conformers. The monomers were placed a distance of 4 Å apart so that no overlap of their vdW radii occurred. As before, geometry optimisation was performed at the PBE0-D3/TZVP level of theory.

Stellenbosch University https://scholar.sun.ac.za

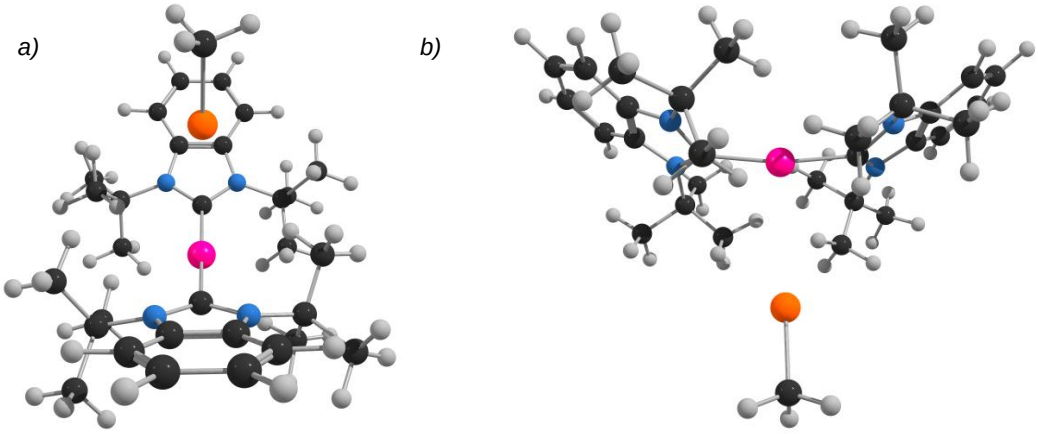

Figure 7-2: Au_2NHC5b with $SeCH_3^-$ placed a) inside and b) outside the "bowl" of the complex.

Constraining the N-C···(Au)···C-N dihedral angle during geometry optimisation of the Au complexes in most cases led to symmetrical Au complexes, such that starting geometries for the vdW complexes where the Se fragment was placed above or below the plane of the NHC were equivalent. In the case of Au_2NHC5b, however, a bowl-shaped structure resulted from optimisation. We elected to create two starting geometries each for the Au_2NHC5b/$SeCH_3^-$ and Au_2NHC5b/$SeCF_3^-$ combinations, placing the Se fragment inside or outside the “bowl” (Figure 7-2). The same minimum energy structure of the $SeCH_3^-$ vdW complexes was obtained after geometry optimisation, while different minimum energy structures were obtained for the $SeCF_3^-$ vdW complexes.

The energetic cost of deforming the Au complex is a key impediment to the formation of the vdW complex, and even more so the transition state. We therefore performed single point energy calculations on the distorted conformers of the Au complexes found in the vdW complexes, and calculated the difference in energy between the undistorted and distorted conformers (ΔE_{deform}). These energies are reported in Table 7-1, along with selected geometric parameters of the optimised vdW complexes.

The optimised structures of $SeCH_3^-$ and $SeCF_3^-$ with Au_2NHC1 are shown in Figure 7-3. Close contacts occur between the Se atom and the H atoms at the N-substituent positions (sum of Se and H vdW radii = 3.1 Å), as well as Au (sum of vdW radii of Se and Au = 3.6 Å) . From the ESP maps of the Se fragments (Chapter 4) and the Au complexes (Chapter 5) it could be anticipated that the monomers would arrange themselves in this sort of fashion, since the H atoms are the sites of highest positive ESP in the Au complexes, and in the Se fragments the most negative ESP is found close to the Se atom. The C-Se···H angle in both vdW complexes is approximately 90°. This is consistent with what was seen in the ESP maps – the region of highest negative ESP occurs in a ring around Se, orthogonal to the Se-C bond

Stellenbosch University https://scholar.sun.ac.za

axis. The Au···Se contacts in the two structures occur at approximately the same distance, but a distinct difference is observed in the Se···H distances. The shorter Se···H distance found in the $SeCH_3^-$ vdW structure relative to the $SeCF_3^-$ (~2.2 Å versus 2.4 Å) is consistent with the greater charge accumulation near Se observed in the ESP map of this species leading to stronger Coulombic forces between the monomers. The vdW complexes with Au_2NHC1b are practically identical to the vdW complexes of Au_2NHC1 in terms of the manner of Se fragment coordination.

Table 7-1: Geometric parameters of vdW complexes and deformation energies of Au complexes.

Se fragment (-1)	Au complex (+1)	Au···Se	Au-C	C-Se···Au	C-Au-C	ΔE_{deform}
		(Å)		(°)		(kcal mol^{-1})
$SeCH_3$	Au_2NHC1	3.46	2.02	82	168	7.9
$SeCH_3$	Au_2NHC2	2.74	2.03	103	167	5.7
$SeCH_3$	Au_2NHC3	2.75	2.03	103	168	4.2
$SeCH_3$	Au_2NHC4	2.77	2.03	106	169	4.1
$SeCH_3$	Au_2NHC5	2.77	2.10	102	167	9.8
$SeCH_3$	Au_2NHC6	2.75	2.04	105	167	4.3
$SeCH_3$	Au_2NHC7	2.77	2.04	106	169	4.2
$SeCH_3$	Au_2NHC1b	3.46	2.02	85	169	7.8
$SeCH_3$	Au_2NHC2b	2.68	2.03	102	163	7.4
$SeCH_3$	Au_2NHC3b	2.68	2.03	103	165	6.1
$SeCH_3$	Au_2NHC4b	2.70	2.03	107	170	6.1
$SeCH_3$	Au_2NHC5b	2.66	2.11	100	162	12.7
$SeCH_3$	Au_2NHC6b	2.70	2.03	101	162	6.3
$SeCH_3$	Au_2NHC7b	2.70	2.06	105	168	11.8
$SeCF_3$	Au_2NHC1	3.53	2.02	86	170	4.9
$SeCF_3$	Au_2NHC2	3.09	2.03	91	176	2.3
$SeCF_3$	Au_2NHC3	3.07	2.03	92	174	1.5
$SeCF_3$	Au_2NHC4	3.00	2.03	110	177	1.7
$SeCF_3$	Au_2NHC5	3.92	2.05	121	179	1.1
$SeCF_3$	Au_2NHC6	3.13	2.04	95	175	1.5
$SeCF_3$	Au_2NHC7	3.13	2.03	89	176	2.0
$SeCF_3$	Au_2NHC1b	3.52	2.02	86	170	4.8
$SeCF_3$	Au_2NHC2b	2.92	2.03	94	171	3.5
$SeCF_3$	Au_2NHC3b	2.94	2.03	93	171	2.4
$SeCF_3$	Au_2NHC4b	2.95	2.03	91	172	1.9
$SeCF_3$	Au_2NHC5b_i	2.87	2.09	98	170	7.3
$SeCF_3$	Au_2NHC5b_o	3.04	2.11	99	162	10.7
$SeCF_3$	Au_2NHC6b	2.91	2.03	94	168	3.0
$SeCF_3$	Au_2NHC7b	2.96	2.06	97	175	8.1

Stellenbosch University https://scholar.sun.ac.za

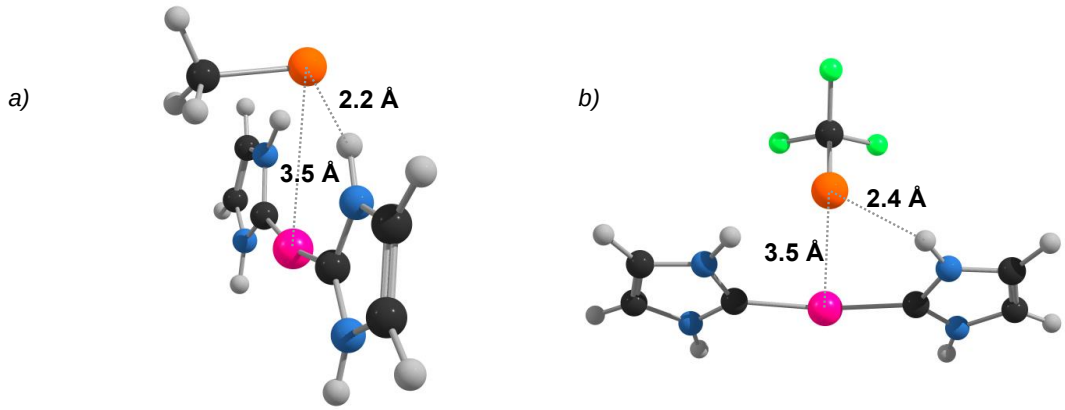

Figure 7-3: vdW complexes of Au_2NHC1 with a) $SeCH_3^-$ and b) $SeCF_3^-$ with illustrated close contacts.

Where the dominant interaction leading to the formation of a vdW complex in the above combinations appears to be between Se and H atoms at the N-substituent positions, the geometries of the vdW complexes with the rest of the Au(I) species suggest a strong stabilising interaction between Au and Se: the sum of the vdW radii of Au and Se is ~3.6 Å, and only in one optimised vdW complex (Au_2NHC5 with $SeCF_3^-$) is a longer Au···Se distance found. In fact, in most cases the Au···Se distance is closer to the length of the Au-Se coordination bond found in previously optimised structures (~2.4 Å) than to the vdW distance. Since the region surrounding Au in the coordination complexes is not the region of highest positive ESP, this could indicate that any stabilising interaction between the Au and Se is not merely electrostatic in nature.

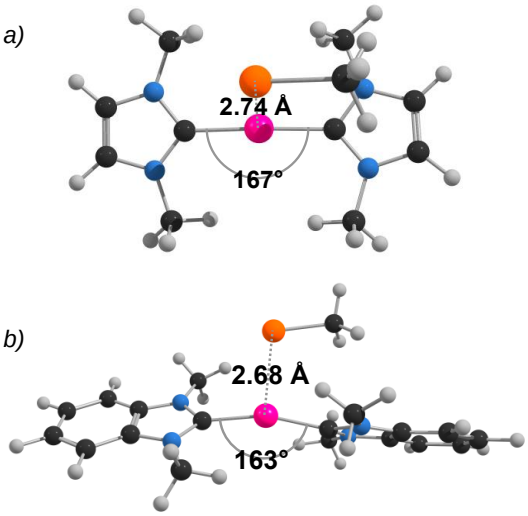

Figure 7-4: vdW complex of $SeCH_3^-$ with a) Au_2NHC2 and b) Au_2NHC2b.

Although the vdW complexes containing the Au_2NHCx and Au_2NHCxb species (imidazolylidene and benzimidazolylidene ligands) are for the most part almost identical in terms of the manner of coordination, the Au···Se distance in the Au_2NHCxb vdW complexes is slightly shorter (Figure 7-4), while slight increases in the Se···H distances are observed (Figure 7-5). Greater deformation of the C-Au-C angle is also observed for the Au_2NHCxb complexes, coupled with a higher ΔE_{deform}. This makes sense if the manner of $SeCH_3^-$ coordination is determined by the interplay of the Se···H and Au···Se interactions – in the Au_2NHCxb complexes, the positive charge is spread out over a larger area, leading to weaker electrostatic interactions between Se and the ligands, and elongation of these short contacts. At the same time $SeCH_3^-$ is less constrained in approaching the Au atom, as the ligands are now bending further away from the Se fragment.

Stellenbosch University https://scholar.sun.ac.za

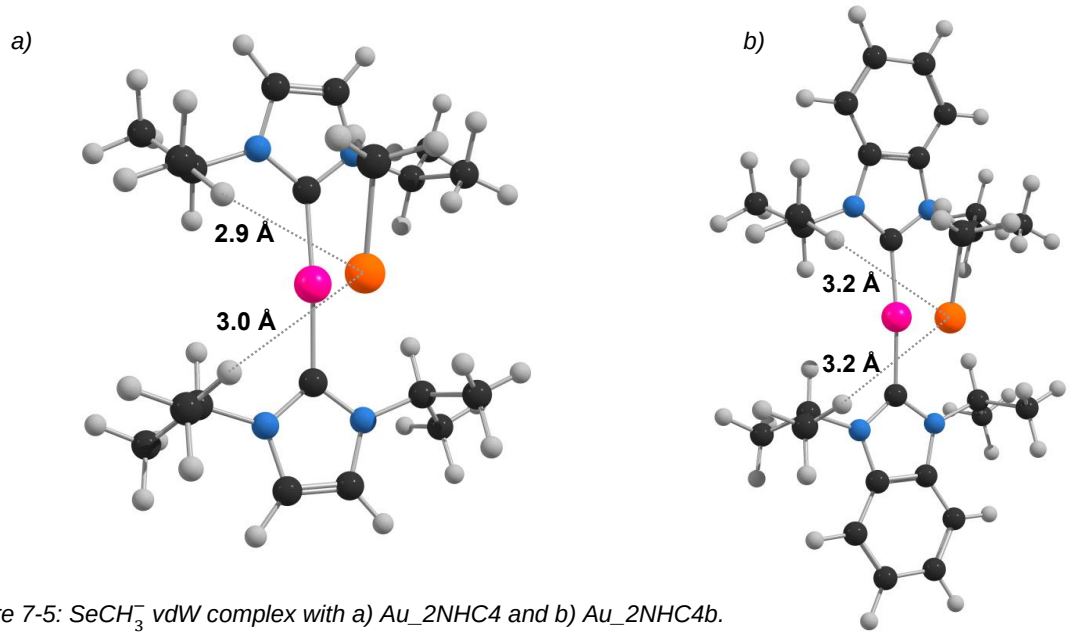

Figure 7-5: $SeCH_3^-$ vdW complex with a) Au_2NHC4 and b) Au_2NHC4b.

The Au···Se distances found in the vdW complexes containing $SeCH_3^-$ are somewhat shorter than those found for the $SeCF_3^-$-containing vdW complexes. A greater deformation of the Au complexes is also observed for the $SeCH_3^-$ species, in the C-Au-C angle as well as the deformation energy. Another conspicuous difference is found in the C-Se···Au angles. For the $SeCF_3^-$ vdW complexes, these angles are in most cases appreciably smaller. Short contacts are also observed between the F atoms and H atoms (sum of vdW radii = 2.7 Å) on the N-substituents, in some cases (e.g. vdW complex of Au_2NHC7b with $SeCF_3^-$, Figure 7-6), suggesting stabilising F···H interactions. Attractive electrostatic interactions between the F atoms and positively-charged Au complexes seem likely given the accumulation of electron density on F discussed in Chapter 4. The longer Au···Se distances found in the $SeCF_3^-$ vdW complexes are also consistent with the reduced charge density on Se in the $SeCF_3^-$ fragment resulting in a decreased attraction of Se to the Au complex.

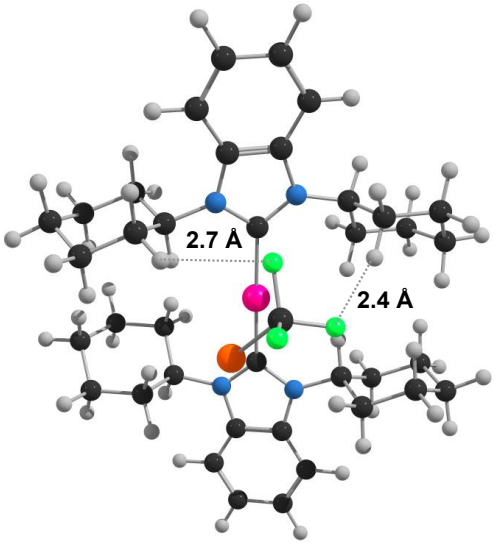

Figure 7-6: Au_2NHC7b/$SeCF_3^-$ vdW complex.

The Au···Se distance appears to be largely unaffected by the identity of the N-substituent on the NHC ligands, at least in the $SeCH_3^-$ vdW complexes, where little deviation is observed. The greater variation observed in the $SeCF_3^-$ species may be attributable to competing F···H interactions. NHC5

Stellenbosch University https://scholar.sun.ac.za

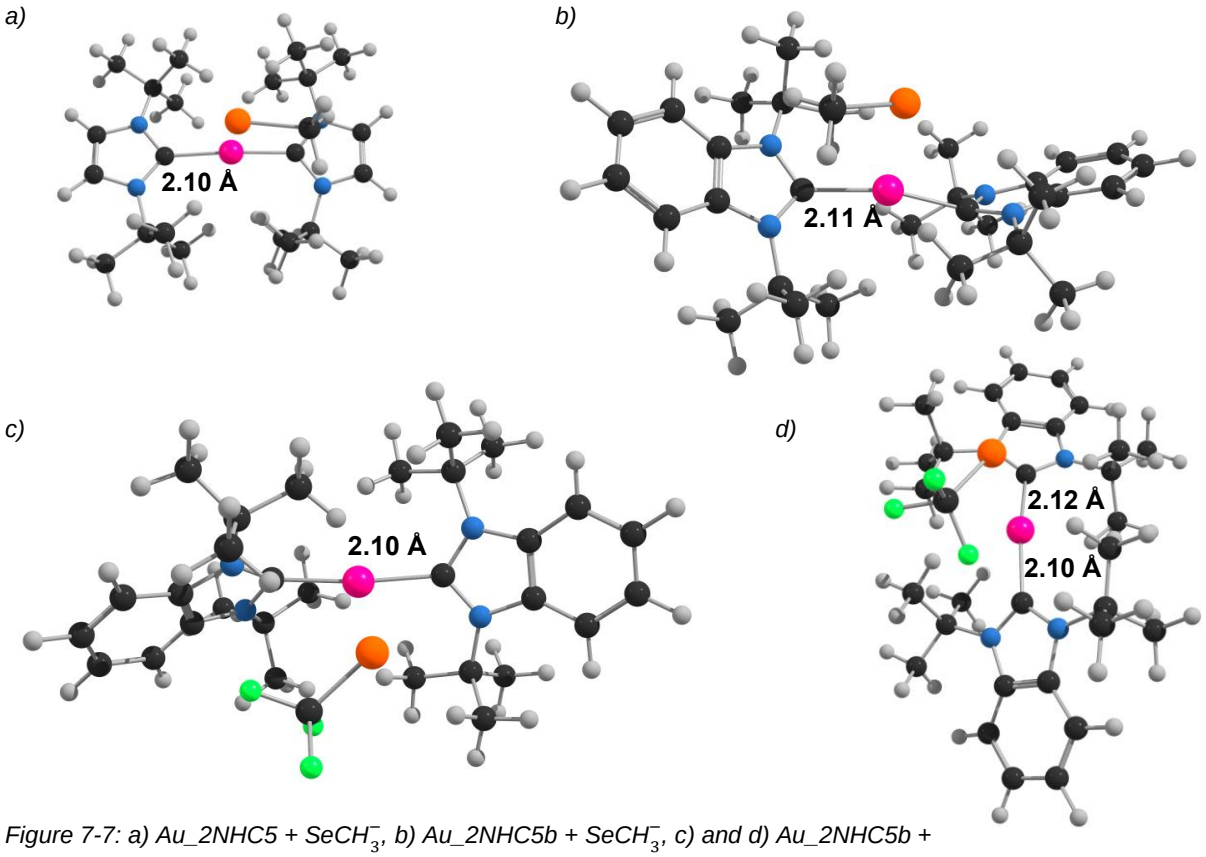

Figure 7-7: a) Au_2NHC5 + $SeCH_3^-$, b) Au_2NHC5b + $SeCH_3^-$, c) and d) Au_2NHC5b + $SeCF_3^-$ (two conformations) with longer than average Au-C bond distances.

and NHC5b appear to be exceptions – the vdW complexes containing these ligands all show especially high deformation energies and/or structural differences from the other vdW complexes. Unlike the other Au complexes, in these structures elongation of the Au-C bond occurs with vdW complex formation (Figure 7-7). In the case of the vdW complex formed between Au_2NHC5 and $SeCF_3^-$ (Figure 7-8), the Au···Se distance, 3.9 Å, is beyond the sum of the vdW radii, 3.6 Å. The planes of the NHC rings are approximately orthogonal to each other, presumably in an orientation which minimises steric clashes. The Au-C bonds are not elongated, and many short Se···H and F···H contacts are observed. The deformation energy is low, as little deformation of the Au_2NHC5 structure has occurred.

The suspected interactions between F and H are troublesome for our analysis, as this sort of interaction would not occur between an Au complex and the TrxR active site. However, in most vdW complexes exhibiting short F···H contacts, the dominant interaction (based on the mode of coordination alone) still appears to be between Au and Se.

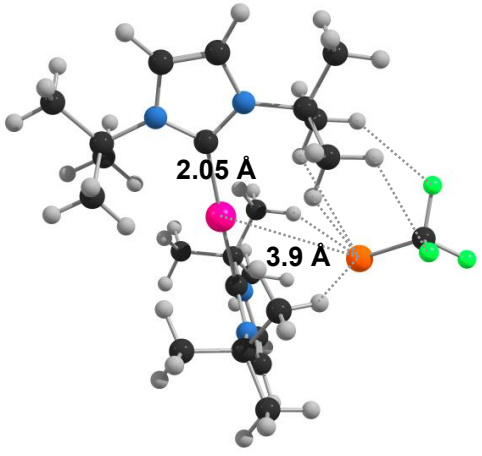

Figure 7-8: Au_2NHC5/$SeCF_3^-$ vdW complex.

Stellenbosch University https://scholar.sun.ac.za

7.2 Atoms in Molecules

In order to confirm the above hypothesis by assessing the relative importance of the different intermolecular interactions in stabilising the vdW complexes, AIM analysis was performed. While effective core potentials (ECPs) can be used in the accurate calculation of interaction energies and geometry optimisation, energy densities (and a number of other properties) for ECP atoms are incorrect. We therefore performed single point calculations in ADF (using the optimised geometries from G09 calculations) with an all electron basis set and the ZORA method, generating wave function files for use in the AIM program, eDensity. The molecular graphs were examined to identify the different weak interactions present, and the BCP properties were examined in order to classify the bonds according to the scheme set forth by Nakanishi (Table 7-2).[2] In this scheme, weak intermolecular interactions are classified according to the following BCP properties: the electron density, ρ, the Laplacian of the electron density, $\nabla^2\rho$, and the total energy density, H. The results are shown in Tables 7-3 to 7-6. Some intramolecular BCPs and bond paths (as well as RCPs and CCPs) have been omitted from the figures for clarity.

Table 7-2: BCP properties of weak interactions. CT-MC = Charge Transfer in Molecular Complex, CT-TBP = Charge Transfer in Trigonal Bipyramidal adducts.

Interaction	ρ (*e* bohr^{-3})	$\nabla^2\rho$ (*e* bohr^{-5})	H (a.u.)
vdW	0.00 < ρ < 0.01	0.00 < $\nabla^2\rho$ < 0.04	0.000 < H < 0.002
H-bond	0.01 < ρ < 0.04	0.04 < $\nabla^2\rho$ < 0.12	-0.004 < H < 0.002
CT-MC	0.01 < ρ < 0.03	0.02 < $\nabla^2\rho$ < 0.06	-0.001 < H < 0.002
CT-TBP	0.03 < ρ < 0.12	-0.01 < $\nabla^2\rho$ < 0.10	-0.060 < H < -0.003

The molecular graphs reveal many apparent stabilising interactions taking place between the Au complexes and Se fragments. The vdW complexes of Au_2NHC1 and Au_2NHC1b with the Se fragments all resemble each other in terms of BCPs as well as geometry. In these complexes two Se···H interactions as well as an Au···Se interaction are identified by the presence of BCPs and bond paths (Figure 7-9). Little difference is observed between the vdW complexes containing the NHCx and NHCxb ligands, as expected from their similar geometries. The shorter bond distances and higher BCP ρ values (for both Se···H and Au···Se) observed in the vdW complexes containing $SeCH_3^-$ relative to $SeCF_3^-$ indicate that electrostatics contribute to these interactions, that is, the greater charge polarisation towards Se in $SeCH_3^-$.leads to stronger interactions. The Se···H BCP properties suggest that these interactions are similar to other H-bonds, while the Au···Se resembles a vdW interaction, *i.e.* a weaker, dispersion-based interaction.

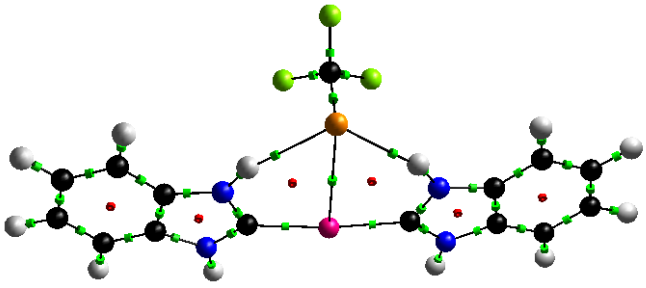

Figure 7-9: Molecular graph of Au_2NHC1b/$SeCF_3^-$.

Stellenbosch University https://scholar.sun.ac.za

Table 7-3: Some properties of the BCPs of Au_2NHCx/$SeCH_3^-$ vdW complexes (atomic units).

Se fragment (-1)	Au complex (+1)	Au···Se				Se···H/C				H/F/C···H/C/N			
		Distance (Å)	ρ	$\nabla^2\rho$	H	Distance (Å)	ρ	$\nabla^2\rho$	H	Distance (Å)	ρ	$\nabla^2\rho$	H
$SeCH_3$	Au_2NHC1	3.46	0.02	0.03	0.000	2.25	0.03	0.04	-0.004				
						2.25	0.03	0.04	-0.004				
$SeCH_3$	Au_2NHC2	2.74	0.05	0.10	-0.010	3.02	0.01	0.02	0.001	2.38	0.01	0.02	0.001
						2.90	0.01	0.02	0.001				
$SeCH_3$	Au_2NHC3	2.75	0.05	0.10	-0.010	3.00	0.01	0.02	0.001	2.51	0.00	0.02	0.001
						2.97	0.01	0.02	0.001				
$SeCH_3$	Au_2NHC4	2.77	0.05	0.10	-0.009	2.96	0.01	0.02	0.001	2.72	0.01	0.03	0.001
						2.94	0.01	0.02	0.001				
						2.96	0.01	0.02	0.001				
						2.94	0.01	0.02	0.001				
$SeCH_3$	Au_2NHC5	2.77	0.05	0.09	-0.009	2.71	0.01	0.03	0.001	2.39	0.01	0.02	0.001
						2.69	0.01	0.03	0.001	2.79	0.01	0.02	0.001
$SeCH_3$	Au_2NHC6	2.75	0.05	0.10	-0.009	2.90	0.01	0.02	0.001	2.42	0.01	0.02	0.001
						3.25	0.01	0.01	0.001	2.67	0.01	0.03	0.001
$SeCH_3$	Au_2NHC7	2.77	0.05	0.10	-0.009	3.18	0.01	0.02	0.001	2.74	0.01	0.03	0.001
						3.18	0.01	0.01	0.001	2.82	0.01	0.02	0.001
						3.05	0.01	0.02	0.001	2.72	0.01	0.03	0.001
						2.97	0.01	0.02	0.001				

Stellenbosch University https://scholar.sun.ac.za

Table 7-4: Some properties of the BCPs of Au_2NHCxb/$SeCH_3^-$ vdW complexes (atomic units).

Se fragment (-1)	Au complex (+1)	Au···Se				Se···H/C				H/F/C···H/C/N			
		Distance (Å)	ρ	$\nabla^2\rho$	H	Distance (Å)	ρ	$\nabla^2\rho$	H	Distance (Å)	ρ	$\nabla^2\rho$	H
$SeCH_3$	Au_2NHC1b	3.46	0.02	0.03	0.000	2.25	0.03	0.04	-0.004				
						2.25	0.03	0.04	-0.004				
$SeCH_3$	Au_2NHC2b	2.68	0.06	0.11	-0.013					2.81	0.01	0.02	0.001
$SeCH_3$	Au_2NHC3b	2.68	0.06	0.11	-0.013					2.47	0.01	0.02	0.001
										2.48	0.00	0.02	0.001
										2.91	0.01	0.02	0.001
$SeCH_3$	Au_2NHC4b	2.70	0.06	0.10	-0.011	3.17	0.01	0.02	0.001	2.71	0.01	0.03	0.001
						3.15	0.01	0.01	0.001				
						3.15	0.01	0.01	0.001				
						3.17	0.01	0.02	0.001				
$SeCH_3$	Au_2NHC5b	2.66	0.06	0.11	-0.014	2.79	0.01	0.03	0.001	2.76	0.00	0.01	0.001
						2.78	0.01	0.03	0.001	2.75	0.01	0.03	0.001
$SeCH_3$	Au_2NHC6b	2.70	0.06	0.10	-0.012	2.90	0.01	0.02	0.001	2.81	0.01	0.02	0.001
						2.86	0.01	0.03	0.001				
$SeCH_3$	Au_2NHC7b	2.70	0.06	0.11	-0.012	3.03	0.01	0.02	0.001	3.06	0.00	0.02	0.001
						3.07	0.01	0.02	0.001	2.74	0.01	0.03	0.001

Stellenbosch University https://scholar.sun.ac.za

Table 7-5: Some properties of the BCPs of Au_2NHCx/$SeCF_3^-$ vdW complexes (atomic units).

Se fragment (-1)	Au complex (+1)	Au···Se				Se···H/C				H/F/C···H/C/N			
		Distance (Å)	ρ	$\nabla^2\rho$	H	Distance (Å)	ρ	$\nabla^2\rho$	H	Distance (Å)	ρ	$\nabla^2\rho$	H
$SeCF_3$	Au_2NHC1	3.53	0.01	0.03	0.000	2.38	0.02	0.04	-0.001				
						2.38	0.02	0.04	-0.001				
$SeCF_3$	Au_2NHC2	3.09	0.03	0.06	-0.003	2.87	0.01	0.03	0.001	2.61	0.01	0.02	0.001
						2.75	0.01	0.03	0.001	3.08	0.01	0.03	0.002
$SeCF_3$	Au_2NHC3	3.07	0.03	0.06	-0.003	2.89	0.01	0.03	0.001	3.07	0.01	0.03	0.002
						2.75	0.01	0.03	0.001	2.45	0.01	0.03	0.002
										2.58	0.01	0.02	0.001
$SeCF_3$	Au_2NHC4	3.00	0.03	0.07	-0.003	3.00	0.01	0.02	0.001	3.07	0.01	0.03	0.002
						3.22	0.01	0.01	0.001	2.77	0.00	0.02	0.001
						3.14	0.01	0.02	0.001	2.68	0.01	0.02	0.001
						3.09	0.01	0.02	0.001				
$SeCF_3$	Au_2NHC5	3.92	-	-	-	3.15	0.01	0.02	0.001	2.66	0.01	0.02	0.001
						2.80	0.01	0.03	0.001	2.57	0.01	0.03	0.002
						2.94	0.01	0.02	0.001	2.56	0.01	0.03	0.002
						3.13	0.01	0.02	0.001				
						3.33	0.01	0.03	0.001				
$SeCF_3$	Au_2NHC6	3.13	0.03	0.06	-0.002	3.23	0.01	0.01	0.001	3.10	0.01	0.03	0.002
						2.74	0.01	0.03	0.001	2.76	0.01	0.02	0.001
						3.02	0.01	0.02	0.001	2.71	0.01	0.03	0.001
										2.56	0.01	0.02	0.001
										2.63	0.01	0.02	0.001
										2.79	0.00	0.02	0.001
$SeCF_3$	Au_2NHC7	3.13	0.03	0.06	-0.002	2.77	0.01	0.03	0.001	2.59	0.01	0.02	0.001
						3.00	0.01	0.02	0.001	2.62	0.01	0.02	0.001
						3.24	0.01	0.01	0.001	2.55	0.01	0.02	0.001
										3.09	0.01	0.03	0.002

Stellenbosch University https://scholar.sun.ac.za

Table 7-6: Some properties of the BCPs of Au_2NHCxb/$SeCF_3^-$ vdW complexes (atomic units).

Se fragment (-1)	Au complex (+1)	Au···Se				Se···H/C				H/F/C···H/C/N			
		Distance (Å)	ρ	$\nabla^2\rho$	H	Distance (Å)	ρ	$\nabla^2\rho$	H	Distance (Å)	ρ	$\nabla^2\rho$	H
$SeCF_3$	Au_2NHC1b	3.52	0.01	0.03	0.000	2.37	0.03	0.04	-0.001				
						2.37	0.03	0.04	-0.001				
$SeCF_3$	Au_2NHC2b	2.92	0.04	0.08	-0.005	2.87	0.01	0.03	0.001	2.64	0.01	0.03	0.002
						3.17	0.01	0.02	0.001	3.06	0.01	0.03	0.002
$SeCF_3$	Au_2NHC3b	2.94	0.04	0.08	-0.005	2.93	0.01	0.02	0.001	2.43	0.01	0.03	0.002
						2.80	0.01	0.03	0.001	3.09	0.01	0.03	0.002
$SeCF_3$	Au_2NHC4b	2.95	0.04	0.08	-0.005	3.05	0.01	0.02	0.001	2.54	0.01	0.03	0.002
						3.15	0.01	0.02	0.001	2.48	0.01	0.03	0.002
										2.71	0.00	0.02	0.001
										3.11	0.01	0.02	0.001
$SeCF_3$	Au_2NHC5b_i	2.87	0.04	0.08	-0.006	2.76	0.01	0.03	0.001	2.43	0.01	0.03	0.002
						2.82	0.01	0.03	0.001	2.61	0.01	0.02	0.001
										2.73	0.01	0.02	0.001
										3.08	0.01	0.03	0.002
$SeCF_3$	Au_2NHC5b_o	3.04	0.03	0.07	-0.003	2.72	0.01	0.03	0.001	2.59	0.01	0.03	0.002
						2.70	0.01	0.03	0.001	2.49	0.01	0.03	0.002
$SeCF_3$	Au_2NHC6b	2.91	0.04	0.08	-0.005	2.82	0.01	0.03	0.001	2.60	0.01	0.03	0.001
						2.93	0.01	0.02	0.001	2.61	0.00	0.02	0.001
										3.07	0.01	0.03	0.002
$SeCF_3$	Au_2NHC7b	2.96	0.04	0.08	-0.005	2.99	0.01	0.02	0.001	2.73	0.00	0.02	0.001
						3.12	0.01	0.02	0.001	2.42	0.01	0.03	0.002
						3.00	0.01	0.02	0.001	2.96	0.00	0.01	0.001
										3.07	0.01	0.03	0.001

Stellenbosch University https://scholar.sun.ac.za

A greater variety of intermolecular interactions are observed in the vdW complexes containing the NHC2 and NHC2b ligands (Figure 7-10). In addition to Au···Se and Se···H BCPs, BCPs are found for H···H, H···N, F···H and F···C contacts. The properties of these BCPs indicate that the interactions resemble weak vdW interactions. The Au···Se BCP displays a much higher ρ than in the NHC1(b) complexes and has properties similar to those of charge transfer complexes.[2] Based on this characterisation and the short Au···Se distances observed, this appears to be a *strong* intermolecular interaction. A higher Au···Se BCP ρ is observed in the NHCxb complexes, combined with a shorter Au···Se distance, a higher deformation energy of the Au complex, and generally longer distances between the other atoms connected by bond paths. The same is observed for (most of) the other vdW complexes. This suggests that for the vdW complexes containing NHCxb ligands, the Au···Se interaction is more important than for those containing NHCx ligands. The ancillary interactions between the Se fragments and larger Au complexes, with their more spread out charge distribution, should be weaker (if these interactions are primarily electrostatic), which favours the formation of a stronger Au···Se interaction.

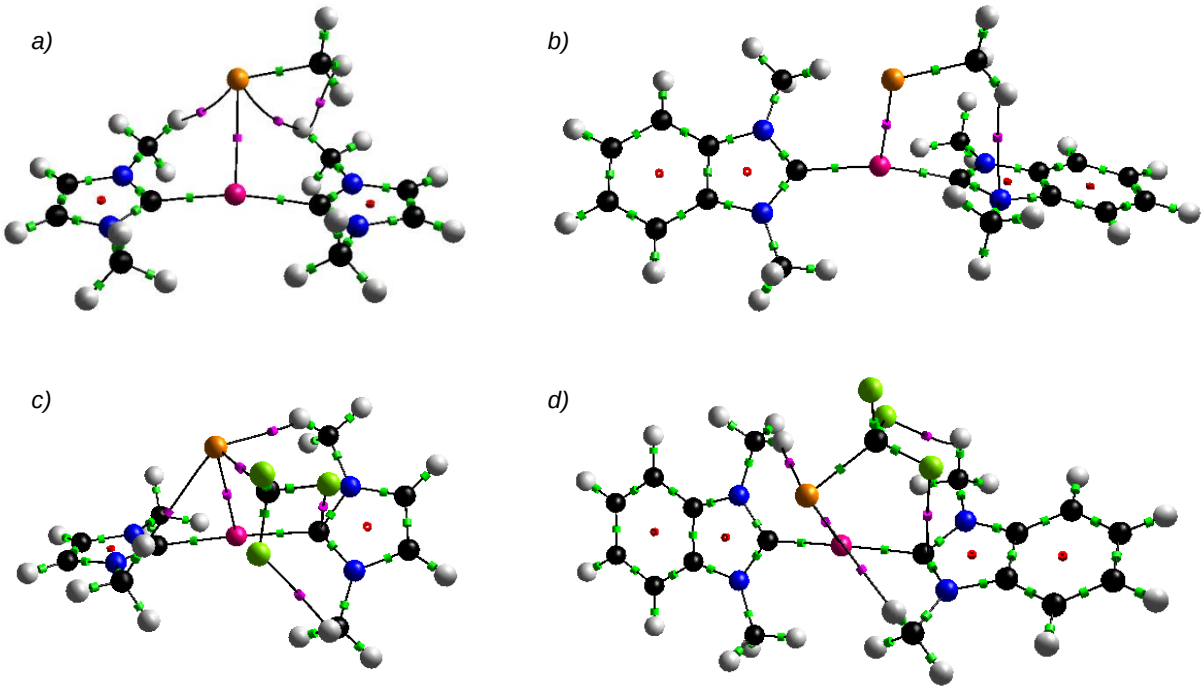

Figure 7-10: Molecular graphs of vdW complexes of a) Au_2NHC2/SeCH$_3^-$, b) Au_2NHC2b/SeCH$_3^-$, c) Au_2NHC2/SeCF$_3^-$, and d) Au_2NHC2b/SeCF$_3^-$. BCPs of interest indicated in pink.

In the other complexes apparent interactions also occur between H and C, F and N, and Se and C, all resembling weak vdW interactions, each probably contributing far less to the stabilisation of the vdW complex than the strong Au···Se charge transfer interaction. More of these interactions occur in the vdW complexes with SeCF$_3^-$ than with SeCH$_3^-$ – the F atoms are more negatively charged than the H atoms and simultaneously less charge is polarised

Stellenbosch University https://scholar.sun.ac.za

toward the Se in $SeCF_3^-$ (Chapter 4), leading to weaker intermolecular interactions. The most extreme case is in the vdW complex of Au_2NHC5/$SeCF_3^-$ (Figure 7-11), where no Au···Se interaction is evident. Instead, the Se coordinates to four H atoms and a C atom, while three F···H BCPs are observed. ΔE_{deform} for this complex, at 1 kcal mol^{-1}, is lower than any of the other deformation energies, suggesting that the deformation of the Au complexes is related to the establishment of the Au···Se interaction. In the Au_2NHC5/$SeCH_3^-$ and Au_2NHC5b/$SeCF_3^-$ vdW complexes, the Au···Se interaction again appears as an apparently strongly stabilising charge transfer interaction, based on the short Au···Se distances and BCP properties.

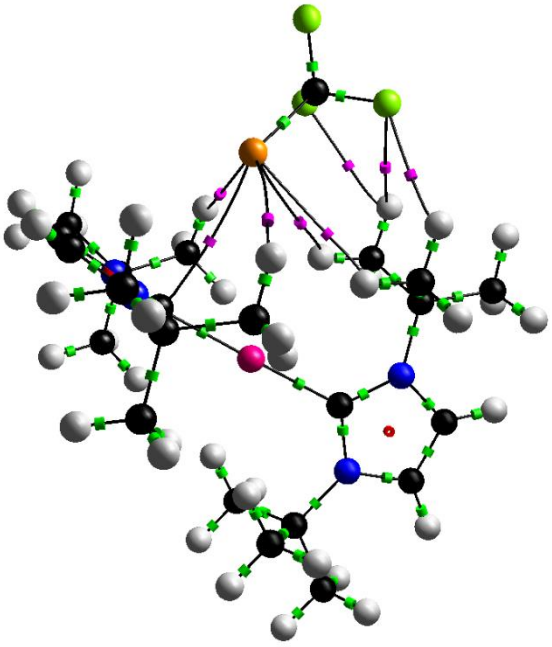

Figure 7-11: Molecular graph of Au_2NHC5/$SeCF_3^-$ vdW complex. BCPs of interest indicated in pink.

7.3 Free energies of association

The free energies of association of the vdW complexes in the gas and solvated phase in the rigid rotor-harmonic oscillator approximation ($\Delta G_{gas,RRHO}$ and ΔG_{aq}) were calculated by the method described in Chapter 3. In this way we hoped to gain a measure of the strength of the interaction between the monomers, the spontaneity of their association, and the effect of the Au complex ligands. The results are shown in Table 7-7, along with the Au···Se distance, the electronic association energy, ΔE_{gas}, calculated as the energy difference between the vdW complex and unperturbed monomers, and ΔE_{deform}. The basis set superposition error (BSSE) was also calculated using the Counterpoise method,[3] but was found to be of negligible magnitude compared to the gas phase interaction energies, hence no corrections were applied to any energy values. The raw data used in the above calculations is included in the ESI.

The results in Table 7-7 suggest that formation of a vdW complex is favoured in the gas phase, with both ΔE_{gas} and $\Delta G_{gas,RRHO}$ being strongly stabilising. However, this appears not to be the case in solution, where only the vdW complexes of Au_2NHC1 and Au_2NHC1b with $SeCH_3^-$ exhibit negative values for ΔG_{aq}, which is probably due to strongly stabilising electrostatic interactions between Se and the H atoms at the N-substituent positions. This lack of stabilisation in solution is most likely an artefact of the method chosen to calculate the free energies – in solution, the electrostatic interactions between the monomers are dampened as a result of dielectric screening, which leads to longer equilibrium distances for weak

Stellenbosch University https://scholar.sun.ac.za

intermolecular interactions. We can therefore assume that less deformation of the monomers due to steric repulsion will take place in an interaction occurring in solution and that ΔE_{deform} will be lower. When applying the method described in Chapter 3 to the calculation of the free energy of association of various cationic amines with a cucurbituril host molecule, Sure *et al.*[4] included counterions in their host-guest structures to balance charges, performed geometry optimisation in continuum solvent, performed gas phase single point calculations on the

Table 7-7: Association energies of vdW complexes.

Se fragment (-1)	Au complex (+1)	Au···Se	ΔE_{deform}	ΔE_{gas}	$\Delta G_{gas,RRHO}$	ΔG_{aq}
		(Å)	(kcal mol^{-1})			
$SeCH_3$	Au_2NHC1	3.46	7.9	-107.5	-95.9	-2.1
$SeCH_3$	Au_2NHC2	2.74	5.7	-89.8	-75.7	4.7
$SeCH_3$	Au_2NHC3	2.75	4.2	-91.7	-77.1	3.8
$SeCH_3$	Au_2NHC4	2.77	4.1	-90.6	-75.4	3.6
$SeCH_3$	Au_2NHC5	2.77	9.8	-81.8	-65.1	12.7
$SeCH_3$	Au_2NHC6	2.75	4.3	-89.8	-75.0	4.1
$SeCH_3$	Au_2NHC7	2.77	4.2	-88.3	-72.2	5.0
$SeCH_3$	Au_2NHC1b	3.46	7.8	-107.4	-95.4	-3.1
$SeCH_3$	Au_2NHC2b	2.68	7.4	-93.1	-79.3	2.0
$SeCH_3$	Au_2NHC3b	2.68	6.1	-95.5	-80.0	1.1
$SeCH_3$	Au_2NHC4b	2.70	6.1	-93.9	-78.8	1.2
$SeCH_3$	Au_2NHC5b	2.66	12.7	-88.9	-75.2	5.4
$SeCH_3$	Au_2NHC6b	2.70	6.3	-91.3	-77.7	1.3
$SeCH_3$	Au_2NHC7b	2.70	11.8	-85.5	-70.3	7.4
$SeCF_3$	Au_2NHC1	3.53	4.9	-94.8	-80.7	6.4
$SeCF_3$	Au_2NHC2	3.09	2.3	-80.4	-64.6	10.5
$SeCF_3$	Au_2NHC3	3.07	1.5	-80.4	-64.6	9.5
$SeCF_3$	Au_2NHC4	3.00	1.7	-78.0	-61.4	9.9
$SeCF_3$	Au_2NHC5	3.92	1.1	-70.4	-54.4	11.7
$SeCF_3$	Au_2NHC6	3.13	1.5	-78.4	-62.1	9.7
$SeCF_3$	Au_2NHC7	3.13	2.0	-77.7	-60.7	9.1
$SeCF_3$	Au_2NHC1b	3.52	4.8	-94.5	-79.9	6.1
$SeCF_3$	Au_2NHC2b	2.92	3.5	-80.9	-65.8	9.1
$SeCF_3$	Au_2NHC3b	2.94	2.4	-81.9	-65.4	8.7
$SeCF_3$	Au_2NHC4b	2.95	1.9	-81.3	-65.3	7.9
$SeCF_3$	Au_2NHC5b_i	2.87	7.3	-75.3	-59.8	13.2
$SeCF_3$	Au_2NHC5b_o	3.04	10.7	-69.8	-50.8	18.0
$SeCF_3$	Au_2NHC6b	2.91	3.0	-79.7	-64.2	8.0
$SeCF_3$	Au_2NHC7b	2.96	8.1	-72.7	-55.8	14.6

Stellenbosch University https://scholar.sun.ac.za

continuum solvent-optimised structures to determine ΔE_{gas}, and used gas phase frequencies calculated for the *cationic* host-guest structures for the calculation of entropy. This laborious process is computationally expensive, and without much precedent in the literature - we therefore followed the method used to good effect on neutral adducts by the same group.[5] Assuming greater distances between the monomers in the solvent phase adduct, ΔE_{deform} should be lower, while $\Delta G_{gas,RRHO}$ should be less stabilising. The effect on ΔG_{aq} is therefore unclear and limited inferences should be made from the data. In the cases where ΔG_{aq} is higher than ΔE_{deform}, that is, more destabilising, a reasonable assumption can be made that the association of the monomers is *not* beneficial in aqueous medium.

The sterically congested vdW complexes containing the NHC5 and NHC5b ligands have some of the highest ΔG_{aq} values among the complexes studied, and even when ΔE_{deform} is considered these interactions still appear unfavourable in solution. This is consistent with the findings of Hickey *et al.*[6] who estimated rate constants for the exchange of NHC ligands with Cys and Sec, and found that the Au complexes with NHC ligands contributing to steric congestion at the metal centre underwent exchange at a much slower rate than complexes with less bulky ligands.

In the vdW complexes containing NHCxb ligands, where electrostatic interactions between Se and the Au complex ligands are presumed to be less important, generally shorter Au···Se distances are observed along with less positive ΔG_{aq} values despite the energy required to deform the Au complexes. The benzimidazolylidene ligands therefore appear to be superior to the imidazolylidene ligands in terms of facilitating the formation of a vdW complex with one of the Se fragments.

There is no apparent trend in the data with increasing size of the N-substituents of the NHC ligands – steric bulk near the metal centre, as exhibited by the complexes with NHC5(b) and NHC7(b), appears to be more decisive in whether vdW complex-formation is favourable.

7.4 Energy decomposition analysis

Energy decomposition analysis (EDA) of the Au complex-Se fragment interaction was also performed to elucidate the contribution of the various energy terms to the association energy (Table 7-7), following the method detailed in Chapter 3. The relative stabilisation of the NHC1/NHC1b-containing vdW complexes is apparently caused by a lack of Pauli repulsion, as opposed to especially strong electrostatic interactions. Relatively high Pauli repulsion is found in the Au_2NHC5/$SeCH_3^-$, and Au_2NHC5b/$SeCH_3^-$ vdW complexes, as well as Au_2NHC5b_i/$SeCF_3^-$ conformer with the relatively shorter Au···Se distance (Figure 7-7 d). Conversely, especially low Pauli repulsion is found for Au_2NHC5/$SeCF_3^-$, where a short

Stellenbosch University https://scholar.sun.ac.za

Au···Se contact is not established, and in the Au_2NHC5b_o/$SeCF_3^-$ conformer (Figure 7-7 c) which exhibits a longer Au···Se distance. This illustrates that Pauli repulsion is an impediment to the formation of these vdW complexes.

Table 7-8: vdW complex EDA with ΔE_{gas} and Au complex deformation energy. Total energy = Coulomb (electrostatic) interaction + Pauli (exchange) repulsion + Orbital energy + Dispersion

Se fragment (-1)	Au complex (+1)	Au···Se (Å)	ΔE (kcal mol^{-1})						
			BDE	ΔE_{deform}	Total	Coulomb	Pauli	Orbital	Dispers
$SeCH_3$	Au_2NHC1	3.46	107.5	7.9	-115.3	-126.1	55.4	-40.0	-4.7
$SeCH_3$	Au_2NHC2	2.74	89.8	5.7	-94.9	-154.2	111.1	-46.5	-5.3
$SeCH_3$	Au_2NHC3	2.75	91.7	4.2	-95.2	-152.4	110.4	-46.8	-6.4
$SeCH_3$	Au_2NHC4	2.77	90.6	4.1	-94.1	-147.0	107.9	-47.5	-7.5
$SeCH_3$	Au_2NHC5	2.77	81.8	9.8	-90.5	-146.7	114.1	-50.1	-7.8
$SeCH_3$	Au_2NHC6	2.75	89.8	4.3	-93.1	-145.4	106.1	-46.8	-7.1
$SeCH_3$	Au_2NHC7	2.77	88.3	4.2	-91.6	-141.6	105.2	-47.0	-8.1
$SeCH_3$	Au_2NHC1b	3.46	107.4	7.8	-115.0	-124.2	56.3	-42.3	-4.8
$SeCH_3$	Au_2NHC2b	2.68	93.1	7.4	-99.8	-166.7	127.0	-54.7	-5.5
$SeCH_3$	Au_2NHC3b	2.68	95.5	6.1	-100.4	-166.2	128.5	-56.0	-6.7
$SeCH_3$	Au_2NHC4b	2.70	93.9	6.1	-98.7	-157.5	120.8	-54.2	-7.8
$SeCH_3$	Au_2NHC5b	2.66	88.9	12.7	-100.5	-175.8	144.7	-60.9	-8.6
$SeCH_3$	Au_2NHC6b	2.70	91.3	6.3	-96.5	-158.2	122.5	-54.6	-6.2
$SeCH_3$	Au_2NHC7b	2.70	85.5	11.8	-96.5	-156.3	123.8	-55.5	-8.5
$SeCF_3$	Au_2NHC1	3.53	94.8	4.9	-100.7	-105.9	38.0	-27.9	-4.9
$SeCF_3$	Au_2NHC2	3.09	80.4	2.3	-83.0	-102.1	51.4	-25.9	-6.3
$SeCF_3$	Au_2NHC3	3.07	80.4	1.5	-81.9	-101.2	53.7	-27.5	-6.9
$SeCF_3$	Au_2NHC4	3.00	78.0	1.7	-79.8	-99.7	56.5	-28.8	-7.8
$SeCF_3$	Au_2NHC5	3.92	70.4	1.1	-70.9	-69.4	23.0	-16.7	-7.9
$SeCF_3$	Au_2NHC6	3.13	78.4	1.5	-80.1	-92.9	47.8	-27.0	-8.0
$SeCF_3$	Au_2NHC7	3.13	77.7	2.0	-79.0	-90.5	47.6	-27.1	-9.0
$SeCF_3$	Au_2NHC1b	3.52	94.5	4.8	-100.6	-104.2	38.8	-29.9	-5.2
$SeCF_3$	Au_2NHC2b	2.92	80.9	3.5	-84.7	-113.8	68.2	-32.6	-6.5
$SeCF_3$	Au_2NHC3b	2.94	81.9	2.4	-84.9	-112.3	68.3	-34.0	-7.0
$SeCF_3$	Au_2NHC4b	2.95	81.3	1.9	-83.2	-109.4	67.2	-32.7	-8.3
$SeCF_3$	Au_2NHC5b_i	2.87	75.3	7.3	-83.4	-120.0	84.9	-39.1	-9.2
$SeCF_3$	Au_2NHC5b_o	3.04	69.8	10.7	-80.6	-99.6	59.4	-32.4	-8.0
$SeCF_3$	Au_2NHC6b	2.91	79.7	3.0	-83.3	-111.4	70.6	-35.3	-7.3
$SeCF_3$	Au_2NHC7b	2.96	72.7	8.1	-81.2	-104.1	66.3	-34.2	-9.2

Stellenbosch University https://scholar.sun.ac.za

The dispersion component of the interaction is of the order of a few kcal mol^{-1}, which should be significant in solution where electrostatic effects are not as important. In general, dispersion forces increase with surface area, and greater dispersion stabilisation with increasing size of the Au complex is indeed observed, although a linear trend is not evident.

A substantial contribution from the Au···Se interaction to the orbital term is evident, as this term is relatively small in the Au_2NHC5/$SeCF_3^-$ vdW complex which displays no Au···Se interaction, and is smaller by ~7kcal mol^{-1} in the Au_2NHC5b_i/$SeCF_3^-$ conformer with the slightly longer Au···Se distance (longer by 0.17 Å). The orbital term is also larger for the $SeCH_3^-$ species in which greater charge polarisation towards Se is observed (Chapter 4). The identity of the NHC ligands in the Au complex make little difference to this term, therefore tweaking the ligand in order to increase this stabilisation appears to an unsound strategy.

7.5 Conclusions

A study of the vdW complexes of the Se fragments with the Au complexes has revealed a multitude of ancillary interactions that make interpretation of the data more difficult. Nevertheless, the data strongly suggests that the Au···Se interaction dominates in determining the manner of coordination found in most of the vdW complexes. This is the case for both $SeCH_3^-$ and $SeCF_3^-$-containing vdW complexes, although the Au···Se interaction appears to be weaker with the less nucleophilic $SeCF_3^-$.

In the vdW complexes containing NHCxb ligands, shorter Au···Se distances are observed, which could be correlated to higher electron density at the BCPs between these atoms, and more deformation of the Au-NHC complexes from their isolated minimum energy state. This was ascribed to weaker ancillary electrostatic interactions hampering the formation of a stronger Au···Se interaction.

The interaction of the Se fragments with the Au complexes is found in general to *not* be favourable in solution – this was attributed to the underestimation of our method of the distances separating monomers leading to more energetically costly deformation of the Au complexes when forming an adduct with a Se fragment. In solution, the distances separating the monomers is assumed to be higher, with a concomitantly lower deformation energy. These longer distances will lead to a reduced attraction between the monomers, however, so the effect on the free energy of association in water is ambiguous.

The identity of the NHC ligand in terms of its N-substituent is found not to have a large effect on the Au···Se distance, the properties of BCPs of this interaction, or the energies of association, except in the case of NHC1/NHC1b and NHC5/NHC5b ligands. In the former, H-bonding between Se and H and the avoidance of Pauli repulsion dominate in determining

Stellenbosch University https://scholar.sun.ac.za

the complex geometry. In the latter, steric interactions prevent a strong Au···Se interaction from occurring in the case of Au_2NHC5/$SeCF_3^-$, while in Au_2NHC5/$SeCH_3^-$ and both Au_2NHC5b/$SeCF_3^-$ conformers the energy required to deform the Au complex is so substantial that the interaction is only favourable in the gas phase. However, the strongest Au···Se interaction, based on the distance separating the atoms and the extent of the deformation of the Au complex taking place, may be found in the vdW complex of Au_2NHC5b/$SeCH_3^-$.

References

(1) Isab, A.; Sadler, P. *J. Chem. Soc. Dalt. Trans.* **1982**, 135–141.

(2) Nakanishi, W.; Hayashi, S.; Narahara, K. *J. Phys. Chem. A* **2008**, *112* (51), 13593–13599.

(3) Boys, S.; Bernardi, F. *Mol. Phys.* **1970**, *19*, 553–566.

(4) Sure, R.; Antony, J.; Grimme, S. *J. Phys. Chem. B* **2014**, *118* (12), 3431–3440.

(5) Grimme, S. *Chem. - Eur. J.* **2012**, *18* (32), 9955–9964.

(6) Hickey, J. L.; Ruhayel, R. a.; Barnard, P. J.; Baker, M. V.; Berners-Price, S. J.; Filipovska, A. *J. Am. Chem. Soc.* **2008**, *130* (I), 12570–12571.

Stellenbosch University https://scholar.sun.ac.za

8 Ligand exchange reactions

Numerous studies have provided evidence that the anti-cancer properties of Au(I) complexes with non-chelating ligands derive from their ability to metallate the Se-containing active site of the TrxR enzyme, inhibiting the enzyme and leading to oxidative stress and apoptosis. In a first step towards understanding the role of ligand exchange in this process, the energetics of ligand exchange reactions of relevant Au(I) complexes with the small model compounds $SeCH_3^-$ and $SeCF_3^-$ were investigated. Bond dissociation energies (BDEs) were calculated for a range of Au-NHC and Au-Phosphine complexes, as well as dissociation of the Se fragments from mixed ligand complexes and the effect of the ligands were evaluated. The dissociation of the Se fragments from mixed ligand complexes was also studied to determine the effect of the remaining ligand on the Au-Se coordination bond strength, as well as the effect of the Se fragment on the Au-ligand bond strength. The free energies of the ligand exchange reactions was also estimated, to gain insight into the spontaneity of these reactions. Finally, energy decomposition analysis (EDA) was performed for the different bond dissociations to assess the contributions of the different energy terms in the stability of these bonds.

8.1 Bond dissociation energies

Bond dissociation electronic energies (ΔE_{gas}) as well as free energies in the gas ($\Delta G_{gas,RRHO}$) and solvated phase (ΔG_{aq}) were calculated (as described in Chapter 3) for a range of cationic and neutral complexes. The data used in the calculation of the free energies are included in the ESI.

ΔE_{gas} for the dissociation of an NHC ligand from its cationic Au-NHC complex (Table 8-1) in general increases with increasing ligand size (molecular volume defined by a 0.001 *e* bohr^{-3} isodensity surface), though a strong trend is not evident in the data. The NHC5 (Figure 5-2 b) and NHC5b dissociations appear as obvious outliers, being a few kcal mol^{-1} less strongly bound to their coordination complexes, most likely due to unfavourable steric interactions between the bulky tertiary-butyl N-substituents and the metal centre. This is supported by the slightly longer Au-C bond lengths found in the cationic Au-NHC and neutral AuCl complexes (Table 8-2) with the NHC5/NHC5b ligands, and a larger contribution from Pauli repulsion observed in the vdW complexes containing these ligands (Section 7-4). The trend in the size is largely absent from the free energies, both in the gas phase and solution, attributable to the increase in entropy and decrease in solvent stabilisation with increasing size. The dissociation energies of NHCx and NHCxb species (imidazolylidene and benzimidazolylidene) ligands also do not differ appreciably, in accordance with the similar Au-C bond lengths found in NHCx and NHCxb species.

Stellenbosch University https://scholar.sun.ac.za

Table 8-1: Bond dissociation energies and free energies (gas and solvated phase) - cationic Au complexes.

Reactant	Products		ΔE_{gas}	$\Delta G_{gas,RRHO}$	ΔG_{aq}
			(kcal mol^{-1})		
Au_2NHC1$^+$	Au_NHC1$^+$	NHC1^0	91.8	74.8	58.4
Au_2NHC2$^+$	Au_NHC2$^+$	NHC2^0	92.5	75.0	59.0
Au_2NHC3$^+$	Au_NHC3$^+$	NHC3^0	94.1	74.7	59.8
Au_2NHC4$^+$	Au_NHC4$^+$	NHC4^0	93.5	75.4	60.1
Au_2NHC5$^+$	Au_NHC5$^+$	NHC5^0	90.2	69.7	56.4
Au_2NHC6$^+$	Au_NHC6$^+$	NHC6^0	95.2	74.4	60.1
Au_2NHC7$^+$	Au_NHC7$^+$	NHC7^0	97.0	78.0	63.5
Au_2NHC1b$^+$	Au_NHC1b$^+$	NHC1b^0	90.1	72.6	57.1
Au_2NHC2b$^+$	Au_NHC2b$^+$	NHC2b^0	90.6	72.1	56.9
Au_2NHC3b$^+$	Au_NHC3b$^+$	NHC3b^0	91.9	74.4	60.2
Au_2NHC4b$^+$	Au_NHC4b$^+$	NHC4b^0	91.5	72.8	58.7
Au_2NHC5b$^+$	Au_NHC5b$^+$	NHC5b^0	81.4	61.0	49.2
Au_2NHC6b$^+$	Au_NHC6b$^+$	NHC6b^0	95.1	74.4	60.3
Au_2NHC7b$^+$	Au_NHC7b$^+$	NHC7b^0	96.0	75.1	62.0
Phos1-Au-NHC3b$^+$	Au_Phos1$^+$	NHC3b^0	88.0	71.0	52.0
Phos2-Au-NHC3b$^+$	Au_Phos2$^+$	NHC3b^0	85.7	68.1	51.8
Phos3-Au-NHC3b$^+$	Au_Phos3$^+$	NHC3b^0	83.8	66.0	51.9
Phos4-Au-NHC3b$^+$	Au_Phos4$^+$	NHC3b^0	83.9	80.0	69.6
Phos4-Au-NHC5$^+$	Au_Phos4$^+$	NHC5^0	85.9	79.2	69.2
Phos1-Au-NHC3b$^+$	Au_NHC3b$^+$	Phos1^0	74.1	58.8	50.6
Phos2-Au-NHC3b$^+$	Au_NHC3b$^+$	Phos2^0	78.2	61.1	51.2
Phos3-Au-NHC3b$^+$	Au_NHC3b$^+$	Phos3^0	81.9	64.5	53.4
Phos4-Au-NHC3b$^+$	Au_NHC3b$^+$	Phos4^0	76.6	59.9	45.7
Phos4-Au-NHC5$^+$	Au-NHC5$^+$	Phos4^0	77.7	59.0	45.7

a) *b)* *c)* *d)*

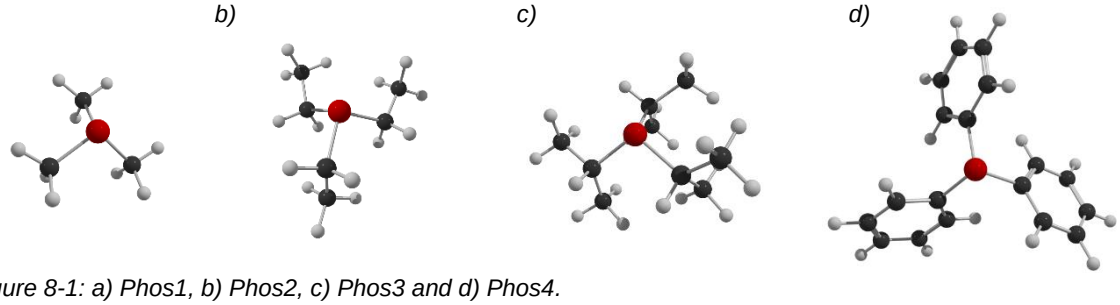

Figure 8-1: a) Phos1, b) Phos2, c) Phos3 and d) Phos4.

Stellenbosch University https://scholar.sun.ac.za

Similarly to other studies,[1,2] the phosphine ligands (Figure 8-1) are observed to have lower BDEs than the NHC ligands, in terms of the electronic and free dissociation energies. As with the NHC ligands, counteracting effects of increasing entropy and decreasing solvent stabilisation are observed as the size of the complexes increase. The low ΔG_{aq} is therefore attributed to a lower than expected (given the size of the ligand) electronic interaction energy between the phosphine ligand and the mono-ligated complex.

The Phos4 ligand (triphenylphosphine) has a substantially lower ΔG_{aq} than the alkyl phosphine ligands. The electron withdrawing phenyl substituents decrease the sigma donating ability of the Phos4 ligand, resulting in a weaker Au-P coordination bond. Interestingly, this appears to affect the dissociation of an NHC from an Au-Phos4 complex – the NHC ligands are more strongly bound (in terms of ΔG_{aq}) to the Au-Phos4 complex by almost 20 kcal mol^{-1} relative to the other Au-Phos complexes. In a mixed ligand complex containing an NHC and phosphine ligand, especially a phosphine ligand bearing electron-withdrawing substituents, the phosphine ligand can be expected to dissociate before the NHC ligand.

The NHC ligands in the complexes bearing alkyl phosphine ligands (Phos1 – 3) have lower BDEs than their counterparts in the homo-ligated NHC complexes. Further discussion of this point is deferred to section 8-3, which concerns the energy decomposition analysis of the ligand dissociations.

The neutral AuCl-NHC complex dissociation energies are shown in Table 8-2. For dissociation of Cl^- ligands the difference between the gas and solvent phase energies is striking, owing to the high solvent stabilisation of the Cl^- ion (~70 kcal mol^{-1}). Separating a negatively charged Cl^- from a positively charged Au-NHC fragment is very unfavourable in the gas phase, but in solution the Cl^- ligands demonstrate higher lability than any of the other ligands studied, in agreement with a previous study which found a lower BDE for Cl^- relative to NHC and phosphine ligands.[1] The identity of the NHC ligand (including the absence or presence of the benzimidazolylidene moiety) appears to make little difference to ΔG_{aq} for Cl^- dissociation, but ΔE_{gas} is found to decrease with increasing size of the NHC ligand. The atomic basin charges (Table 8-3), as determined by the AIM approach, show little variation in the different complexes. This suggests that the differing ΔE_{gas} values stem from the interaction of the Cl charge distribution with that of the NHC ligands and not the metal centre.

Stellenbosch University https://scholar.sun.ac.za

Table 8-2: Bond dissociation energies and free energies (gas and solvated phase) - neutral Au complexes.

Reactant	Products		ΔE_{gas}	$\Delta G_{gas,RRHO}$	ΔG_{aq}
			(kcal mol^{-1})		
AuCl_NHC1^0	Au_NHC1$^+$	Cl$^-$	160.7	151.2	38.9
AuCl_NHC2^0	Au_NHC2$^+$	Cl$^-$	157.5	148.0	40.9
AuCl_NHC3^0	Au_NHC3$^+$	Cl$^-$	156.3	146.5	41.1
AuCl_NHC4^0	Au_NHC4$^+$	Cl$^-$	154.4	145.4	41.9
AuCl_NHC5^0	Au_NHC5$^+$	Cl$^-$	154.0	144.1	41.2
AuCl_NHC6^0	Au_NHC6$^+$	Cl$^-$	154.9	145.1	41.3
AuCl_NHC7^0	Au_NHC7$^+$	Cl$^-$	152.4	142.9	41.6
AuCl_NHC1b^0	Au_NHC1b$^+$	Cl$^-$	160.2	150.4	40.2
AuCl_NHC2b^0	Au_NHC2b$^+$	Cl$^-$	157.7	148.0	42.0
AuCl_NHC3b^0	Au_NHC3b$^+$	Cl$^-$	156.6	147.3	42.9
AuCl_NHC4b^0	Au_NHC4b$^+$	Cl$^-$	155.3	145.6	42.4
AuCl_NHC5b^0	Au_NHC5b$^+$	Cl$^-$	153.2	143.5	41.6
AuCl_NHC6b^0	Au_NHC6b$^+$	Cl$^-$	155.4	145.6	42.6
AuCl_NHC7b^0	Au_NHC7b$^+$	Cl$^-$	154.0	143.9	42.5
Auranofin^0	Au_Phos2$^+$	Thio1$^-$	155.3	137.0	46.3
Thio1-Au-NHC5^0	Au-NHC5$^+$	Thio1$^-$	157.3	137.7	52.8
AuCl_NHC1^0	AuCl^0	NHC1^0	79.3	63.5	68.5
AuCl_NHC2^0	AuCl^0	NHC2^0	81.9	67.0	69.2
AuCl_NHC3^0	AuCl^0	NHC3^0	83.9	67.4	69.0
AuCl_NHC4^0	AuCl^0	NHC4^0	83.9	68.6	70.2
AuCl_NHC5^0	AuCl^0	NHC5^0	81.0	64.1	66.1
AuCl_NHC6^0	AuCl^0	NHC6^0	85.0	68.1	69.6
AuCl_NHC7^0	AuCl^0	NHC7^0	85.0	68.9	69.9
AuCl_NHC1b^0	AuCl^0	NHC1b^0	78.9	63.8	67.8
AuCl_NHC2b^0	AuCl^0	NHC2b^0	81.2	65.5	66.8
AuCl_NHC3b^0	AuCl^0	NHC3b^0	82.8	67.3	68.1
AuCl_NHC4b^0	AuCl^0	NHC4b^0	82.8	66.8	67.6
AuCl_NHC5b^0	AuCl^0	NHC5b^0	71.7	55.3	57.5
AuCl_NHC6b^0	AuCl^0	NHC6b^0	84.1	67.9	68.2
AuCl_NHC7b^0	AuCl^0	NHC7b^0	83.6	66.9	67.3
Auranofin^0	Au_Thio1^0	Phos2^0	68.3	50.5	52.2
Thio1-Au-NHC5^0	Au_Thio1^0	NHC5^0	78.6	58.2	59.0

Stellenbosch University https://scholar.sun.ac.za

The anionic Thio1⁻ ligand is not as labile as Cl⁻, especially in its complex with Au_NHC5. The Thio1⁻ solvent stabilisation is less than that of Cl⁻ by approximately 10 kcal mol^{-1}, and this is only somewhat negated by the favourable entropy change for this dissociation. The difference in Thio1 lability from the Au-NHC and Au-phosphine complexes appears to originate from the solvation free energy – the Au_Phos2 fragment is more stabilised than Au_NHC5 by ~5 kcal mol^{-1}. The higher solvent stabilisation of Au_Phos2 can be related to its smaller volume, which implies a higher concentration of charge.

The gas phase dissociation of an NHC ligand from one of these neutral complexes incurs a smaller energetic penalty than dissociation from the corresponding cationic complex, but the reverse is observed in solution. Since there is more electron density on Au in these complexes it seems intuitive that a σ-donating ligand, such as an NHC, would be less strongly bound than to a cationic species. However, solvation effects make the difference – whereas these are favourable for the dissociation of an NHC from one of the cationic complexes, the opposite is the case for the neutral complexes. AuCl might be expected to have a more polarised charge distribution (leading to stronger solvent stabilisation) than the neutral bis-ligated complexes, but the atomic charges suggest otherwise. The Cl ESP in AuCl is less negative than in the Cl-containing complexes, with an atomic basin charge of -0.37 *e* compared to approximately -0.57 *e* in the complexes. More electron density from the NHC ligand can be polarised toward Cl than from only the relatively electronegative Au. Slightly shorter Au-C bond lengths than in the cationic complexes are also observed for the AuCl_NHC species, consistent with stronger bonding.

Table 8-3: Au and Cl atomic basin charges, neutral complexes.

Complex	q (e)	
	Au	Cl
AuCl_NHC1	0.22	-0.56
AuCl_NHC2	0.22	-0.57
AuCl_NHC3	0.22	-0.57
AuCl_NHC4	0.21	-0.57
AuCl_NHC5	0.22	-0.57
AuCl_NHC6	0.22	-0.57
AuCl_NHC7	0.21	-0.57
AuCl_NHC1b	0.23	-0.56
AuCl_NHC2b	0.23	-0.56
AuCl_NHC3b	0.23	-0.57
AuCl_NHC4b	0.22	-0.57
AuCl_NHC5b	0.24	-0.57
AuCl_NHC6b	0.23	-0.57
AuCl_NHC7b	0.23	-0.57

As in the cationic complexes, the NHCx and NHCxb ligands do not differ significantly in terms of their dissociation energies and the effect of varying the N-substituent can only be observed in ΔE_{gas}. The expected order of lability in the solvent phase, Cl⁻ > Phos > NHC, is again observed. Similarly to the cationic complexes, the sterically demanding NHC5 and NHC5b ligands are observed to have lower BDEs than the other ligands, though they appear more strongly bound in the neutral complexes than even the least labile NHC in the cationic complexes.

Stellenbosch University https://scholar.sun.ac.za

Table 8-4: Bond dissociation energies and free energies (gas and solvated phase) - Au-$SeCH_3^-$ complexes.

Reactant	Products		ΔE_{gas}	$\Delta G_{gas,RRHO}$	ΔG_{aq}
			(kcal mol^{-1})		
$AuSeCH_3$_NHC1^0	Au_NHC1$^+$	$SeCH_3^-$	169.3	155.5	53.3
$AuSeCH_3$_NHC2^0	Au_NHC2$^+$	$SeCH_3^-$	166.0	151.6	55.2
$AuSeCH_3$_NHC3^0	Au_NHC3$^+$	$SeCH_3^-$	164.8	150.2	55.3
$AuSeCH_3$_NHC4^0	Au_NHC4$^+$	$SeCH_3^-$	162.8	149.0	56.3
$AuSeCH_3$_NHC5^0	Au_NHC5$^+$	$SeCH_3^-$	163.5	148.5	56.4
$AuSeCH_3$_NHC6^0	Au_NHC6$^+$	$SeCH_3^-$	163.6	148.7	55.7
$AuSeCH_3$_NHC7^0	Au_NHC7$^+$	$SeCH_3^-$	160.9	146.5	56.1
$AuSeCH_3$_NHC1b^0	Au_NHC1b$^+$	$SeCH_3^-$	169.0	154.3	53.8
$AuSeCH_3$_NHC2b^0	Au_NHC2b$^+$	$SeCH_3^-$	166.5	151.9	56.5
$AuSeCH_3$_NHC3b^0	Au_NHC3b$^+$	$SeCH_3^-$	165.4	151.2	57.2
$AuSeCH_3$_NHC4b^0	Au_NHC4b$^+$	$SeCH_3^-$	164.1	149.3	56.9
$AuSeCH_3$_NHC5b^0	Au_NHC5b$^+$	$SeCH_3^-$	163.4	148.3	57.1
$AuSeCH_3$_NHC6b^0	Au_NHC6b$^+$	$SeCH_3^-$	164.4	149.4	57.0
$AuSeCH_3$_NHC7b^0	Au_NHC7b$^+$	$SeCH_3^-$	163.1	148.3	57.7
$AuSeCH_3$_Phos1^0	Au_Phos1$^+$	$SeCH_3^-$	167.4	152.0	50.2
$AuSeCH_3$_Phos2^0	Au_Phos2$^+$	$SeCH_3^-$	163.7	149.0	51.2
$AuSeCH_3$_Phos3^0	Au_Phos3$^+$	$SeCH_3^-$	160.4	145.6	50.9
$AuSeCH_3$_Phos4^0	Au_Phos4$^+$	$SeCH_3^-$	160.4	158.8	69.0
$AuSeCH_3$_NHC1^0	$AuSeCH_3^0$	NHC1^0	62.1	46.0	51.6
$AuSeCH_3$_NHC2^0	$AuSeCH_3^0$	NHC2^0	64.6	48.8	52.1
$AuSeCH_3$_NHC3^0	$AuSeCH_3^0$	NHC3^0	66.6	49.3	52.0
$AuSeCH_3$_NHC4^0	$AuSeCH_3^0$	NHC4^0	66.5	50.5	53.2
$AuSeCH_3$_NHC5^0	$AuSeCH_3^0$	NHC5^0	64.6	46.8	50.0
$AuSeCH_3$_NHC6^0	$AuSeCH_3^0$	NHC6^0	67.9	50.0	52.6
$AuSeCH_3$_NHC7^0	$AuSeCH_3^0$	NHC7^0	67.7	50.7	53.0
$AuSeCH_3$_NHC1b^0	$AuSeCH_3^0$	NHC1b^0	62.0	45.9	50.1
$AuSeCH_3$_NHC2b^0	$AuSeCH_3^0$	NHC2b^0	64.1	47.7	49.8
$AuSeCH_3$_NHC3b^0	$AuSeCH_3^0$	NHC3b^0	65.8	49.4	51.1
$AuSeCH_3$_NHC4b^0	$AuSeCH_3^0$	NHC4b^0	65.8	48.9	50.6
$AuSeCH_3$_NHC5b^0	$AuSeCH_3^0$	NHC5b^0	56.1	38.5	41.6
$AuSeCH_3$_NHC6b^0	$AuSeCH_3^0$	NHC6b^0	67.3	50.0	51.3
$AuSeCH_3$_NHC7b^0	$AuSeCH_3^0$	NHC7b^0	67.0	49.6	51.2
$AuSeCH_3$_Phos1^0	$AuSeCH_3^0$	Phos1^0	53.9	38.0	42.8
$AuSeCH_3$_Phos2^0	$AuSeCH_3^0$	Phos2^0	56.6	40.2	44.5
$AuSeCH_3$_Phos3^0	$AuSeCH_3^0$	Phos3^0	58.9	42.2	46.3
$AuSeCH_3$_Phos4^0	$AuSeCH_3^0$	Phos4^0	53.4	36.9	39.1

Stellenbosch University https://scholar.sun.ac.za

Table 8-5: Bond dissociation energies and free energies (gas and solvated phase) - neutral Au-$SeCF_3^-$ complexes.

Reactant	Products		ΔE_{gas}	$\Delta G_{gas,RRHO}$	ΔG_{aq}
			(kcal mol^{-1})		
$AuSeCF_3$_NHC1^0	Au_NHC1$^+$	$SeCF_3^-$	151.1	136.6	40.2
$AuSeCF_3$_NHC2^0	Au_NHC2$^+$	$SeCF_3^-$	148.3	133.2	41.6
$AuSeCF_3$_NHC3^0	Au_NHC3$^+$	$SeCF_3^-$	147.4	131.7	41.5
$AuSeCF_3$_NHC4^0	Au_NHC4$^+$	$SeCF_3^-$	145.5	130.2	41.8
$AuSeCF_3$_NHC5^0	Au_NHC5$^+$	$SeCF_3^-$	146.2	130.4	43.0
$AuSeCF_3$_NHC6^0	Au_NHC6$^+$	$SeCF_3^-$	145.2	128.8	40.0
$AuSeCF_3$_NHC7^0	Au_NHC7$^+$	$SeCF_3^-$	144.3	128.3	42.0
$AuSeCF_3$_NHC1b^0	Au_NHC1b$^+$	$SeCF_3^-$	150.5	135.1	40.5
$AuSeCF_3$_NHC2b^0	Au_NHC2b$^+$	$SeCF_3^-$	148.4	133.1	42.6
$AuSeCF_3$_NHC3b^0	Au_NHC3b$^+$	$SeCF_3^-$	147.6	132.4	43.2
$AuSeCF_3$_NHC4b^0	Au_NHC4b$^+$	$SeCF_3^-$	146.4	130.8	43.1
$AuSeCF_3$_NHC5b^0	Au_NHC5b$^+$	$SeCF_3^-$	145.8	129.8	43.3
$AuSeCF_3$_NHC6b^0	Au_NHC6b$^+$	$SeCF_3^-$	147.0	130.6	43.1
$AuSeCF_3$_NHC7b^0	Au_NHC7b$^+$	$SeCF_3^-$	146.1	129.9	43.7
$AuSeCF_3$_Phos1^0	Au_Phos1$^+$	$SeCF_3^-$	148.4	133.5	37.3
$AuSeCF_3$_Phos2^0	Au_Phos2$^+$	$SeCF_3^-$	145.3	129.8	37.1
$AuSeCF_3$_Phos3^0	Au_Phos3$^+$	$SeCF_3^-$	142.1	126.6	37.0
$AuSeCF_3$_Phos4^0	Au_Phos4$^+$	$SeCF_3^-$	141.6	139.2	54.2
$AuSeCF_3$_NHC1^0	$AuSeCF_3^0$	NHC1^0	68.7	52.2	57.8
$AuSeCF_3$_NHC2^0	$AuSeCF_3^0$	NHC2^0	71.7	55.4	57.8
$AuSeCF_3$_NHC3^0	$AuSeCF_3^0$	NHC3^0	74.0	55.9	57.5
$AuSeCF_3$_NHC4^0	$AuSeCF_3^0$	NHC4^0	74.0	56.7	58.0
$AuSeCF_3$_NHC5^0	$AuSeCF_3^0$	NHC5^0	72.1	53.7	55.8
$AuSeCF_3$_NHC6^0	$AuSeCF_3^0$	NHC6^0	74.2	55.0	56.2
$AuSeCF_3$_NHC7^0	$AuSeCF_3^0$	NHC7^0	75.9	57.6	58.2
$AuSeCF_3$_NHC1b^0	$AuSeCF_3^0$	NHC1b^0	68.2	51.7	56.1
$AuSeCF_3$_NHC2b^0	$AuSeCF_3^0$	NHC2b^0	70.8	53.9	55.3
$AuSeCF_3$_NHC3b^0	$AuSeCF_3^0$	NHC3b^0	72.8	55.6	56.4
$AuSeCF_3$_NHC4b^0	$AuSeCF_3^0$	NHC4b^0	72.8	55.3	56.1
$AuSeCF_3$_NHC5b^0	$AuSeCF_3^0$	NHC5b^0	63.3	44.9	47.0
$AuSeCF_3$_NHC6b^0	$AuSeCF_3^0$	NHC6b^0	74.6	56.1	56.6
$AuSeCF_3$_NHC7b^0	$AuSeCF_3^0$	NHC7b^0	74.7	56.2	56.5
$AuSeCF_3$_Phos1^0	$AuSeCF_3^0$	Phos1^0	59.6	44.5	49.1
$AuSeCF_3$_Phos2^0	$AuSeCF_3^0$	Phos2^0	62.9	46.0	49.7
$AuSeCF_3$_Phos3^0	$AuSeCF_3^0$	Phos3^0	65.4	48.2	51.7
$AuSeCF_3$_Phos4^0	$AuSeCF_3^0$	Phos4^0	59.4	42.3	43.6

Stellenbosch University https://scholar.sun.ac.za

A large difference in the gas and solvent phase dissociation of $SeCH_3^-$ or $SeCF_3^-$ from the Au-NHC species (Tables 8-4 and 8-5) is observed, but to a lesser extent than Cl^-. Solvent phase dissociation energies of $SeCH_3^-$ are almost as high as for NHC dissociation from a cationic complex, but $SeCF_3^-$ is considerably less strongly bound, as expected from the relative Se atomic basin charges (-0.72 and -0.46 *e* respectively). The greater concentration of electron density on Se in $SeCH_3^-$ relative to $SeCF_3^-$ may be responsible, but $SeCF_3^-$ in the gas phase is also expected to be more stable due to less charge polarisation over the molecule. The higher charge polarisation in $SeCH_3^-$ relative to $SeCF_3^-$ does result in stronger solvent stabilisation (almost 6 kcal mol^{-1}), but this is not enough to result in more facile dissociation of $SeCH_3^-$ in solution.

Continuing the trend, the identity of the NHC ligand does not appear to make much of a difference in how easily the Se ligands dissociate from a complex. Dissociation from an NHC1- or NHC1b-containing complex in solution is somewhat more facile, owing to the greater solvent stabilisation of the cationic Au_NHC1 and Au_NHC1b fragments. Likewise, the various NHC ligands have very similar ΔG_{aq} values, while ΔE_{gas} increases slightly with increasing size of the NHC. As before, the NHC5 and NHC5b ligands are the most labile, regardless of phase.

The NHC ligands are bound more weakly to the $AuSeCH_3^0$ species than they are in the cationic complexes and far more weakly than in the AuCl complexes. The energy associated with NHC dissociation from the $AuSeCF_3^0$ species falls between that of the AuCl and $AuSeCH_3^0$ species. Solvent phase dissociation of a Phos ligand from one of the AuSe complexes is more facile than NHC dissociation, especially for Phos4. For the dissociation of the $SeCH_3^-$ fragment from Au-Phos4 the opposite is true – at 69 kcal mol^{-1} this is the most stable Au-Se coordination bond identified. It appears that a stronger Au-Se coordination bond will form when the opposing ligand is a *weaker* σ-donor.

8.2 Reaction energies

The change in the Gibbs free energy of a reaction reveals whether the reaction will occur spontaneously or not. Spontaneity of ligand exchange with the TrxR active site Se is a desirable property for these Au(I) prodrugs, and so the Gibbs free energy change for ligand exchange reactions with the TrxR proxies, $SeCH_3^-$ (Table 8-6) and $SeCF_3^-$ (Table 8-7), was investigated. Although exchange of an NHC ligand with either Se fragment is predicted to occur spontaneously in the gas phase, this is not the case in solution, the only exceptions being the reactions involving the NHC5 ligand, which has been remarked on before.

Stellenbosch University https://scholar.sun.ac.za

Table 8-6: Ligand exchange reactions with $SeCH_3^-$.

Reactants		Products		ΔE_{gas}	$\Delta G_{gas,RRHO}$	ΔG_{aq}
				(kcal mol^{-1})		
Au_2NHC1$^+$	$SeCH_3^-$	$AuSeCH_3$_NHC1^0	NHC1^0	-77.5	-80.7	5.2
Au_2NHC2$^+$	$SeCH_3^-$	$AuSeCH_3$_NHC2^0	NHC2^0	-73.6	-76.7	3.8
Au_2NHC3$^+$	$SeCH_3^-$	$AuSeCH_3$_NHC3^0	NHC3^0	-70.8	-75.5	4.5
Au_2NHC4$^+$	$SeCH_3^-$	$AuSeCH_3$_NHC4^0	NHC4^0	-69.4	-73.6	3.8
Au_2NHC5$^+$	$SeCH_3^-$	$AuSeCH_3$_NHC5^0	NHC5^0	-73.2	-78.8	0.0
Au_2NHC6$^+$	$SeCH_3^-$	$AuSeCH_3$_NHC6^0	NHC6^0	-68.5	-74.4	4.4
Au_2NHC7$^+$	$SeCH_3^-$	$AuSeCH_3$_NHC7^0	NHC7^0	-63.8	-68.4	7.3
Au_2NHC1b$^+$	$SeCH_3^-$	$AuSeCH_3$_NHC1b^0	NHC1b^0	-78.9	-81.7	3.3
Au_2NHC2b$^+$	$SeCH_3^-$	$AuSeCH_3$_NHC2b^0	NHC2b^0	-75.9	-79.8	0.5
Au_2NHC3b$^+$	$SeCH_3^-$	$AuSeCH_3$_NHC3b^0	NHC3b^0	-73.5	-76.8	3.0
Au_2NHC4b$^+$	$SeCH_3^-$	$AuSeCH_3$_NHC4b^0	NHC4b^0	-72.5	-76.5	1.8
Au_2NHC5b$^+$	$SeCH_3^-$	$AuSeCH_3$_NHC5b^0	NHC5b^0	-82.0	-87.3	-7.9
Au_2NHC6b$^+$	$SeCH_3^-$	$AuSeCH_3$_NHC6b^0	NHC6b^0	-69.3	-75.0	3.3
Au_2NHC7b$^+$	$SeCH_3^-$	$AuSeCH_3$_NHC7b^0	NHC7b^0	-67.1	-73.2	4.3
Phos1-Au-NHC3b$^+$	$SeCH_3^-$	$AuSeCH_3$_Phos1^0	NHC3b^0	-79.4	-81.0	1.7
Phos2-Au-NHC3b$^+$	$SeCH_3^-$	$AuSeCH_3$_Phos2^0	NHC3b^0	-78.0	-80.9	0.6
Phos3-Au-NHC3b$^+$	$SeCH_3^-$	$AuSeCH_3$_Phos3^0	NHC3b^0	-76.6	-79.6	1.0
Phos4-Au-NHC3b$^+$	$SeCH_3^-$	$AuSeCH_3$_Phos4^0	NHC3b^0	-76.5	-78.8	0.6
Phos4-Au-NHC5$^+$	$SeCH_3^-$	$AuSeCH_3$_Phos4^0	NHC5^0	-74.5	-79.6	0.2
Phos1-Au-NHC3b$^+$	$SeCH_3^-$	$AuSeCH_3$_NHC3b^0	Phos1^0	-91.3	-92.4	-6.6
Phos2-Au-NHC3b$^+$	$SeCH_3^-$	$AuSeCH_3$_NHC3b^0	Phos2^0	-87.1	-90.1	-6.0
Phos3-Au-NHC3b$^+$	$SeCH_3^-$	$AuSeCH_3$_NHC3b^0	Phos3^0	-83.4	-86.7	-3.8
Phos4-Au-NHC3b$^+$	$SeCH_3^-$	$AuSeCH_3$_NHC3b^0	Phos4^0	-88.8	-91.3	-11.5
Phos4-Au-NHC5$^+$	$SeCH_3^-$	$AuSeCH_3$_NHC5^0	Phos4^0	-85.7	-89.5	-10.8
AuCl_NHC1^0	$SeCH_3^-$	$AuSeCH_3$_NHC1^0	Cl^-	-8.6	-4.3	-14.4
AuCl_NHC2^0	$SeCH_3^-$	$AuSeCH_3$_NHC2^0	Cl^-	-8.5	-3.6	-14.3
AuCl_NHC3^0	$SeCH_3^-$	$AuSeCH_3$_NHC3^0	Cl^-	-8.5	-3.7	-14.3
AuCl_NHC4^0	$SeCH_3^-$	$AuSeCH_3$_NHC4^0	Cl^-	-8.5	-3.6	-14.4
AuCl_NHC5^0	$SeCH_3^-$	$AuSeCH_3$_NHC5^0	Cl^-	-9.4	-4.4	-15.2
AuCl_NHC6^0	$SeCH_3^-$	$AuSeCH_3$_NHC6^0	Cl^-	-8.8	-3.6	-14.4
AuCl_NHC7^0	$SeCH_3^-$	$AuSeCH_3$_NHC7^0	Cl^-	-8.5	-3.6	-14.5
AuCl_NHC1b^0	$SeCH_3^-$	$AuSeCH_3$_NHC1b^0	Cl^-	-8.8	-3.9	-13.6
AuCl_NHC2b^0	$SeCH_3^-$	$AuSeCH_3$_NHC2b^0	Cl^-	-8.8	-3.9	-14.4
AuCl_NHC3b^0	$SeCH_3^-$	$AuSeCH_3$_NHC3b^0	Cl^-	-8.8	-3.8	-14.3
AuCl_NHC4b^0	$SeCH_3^-$	$AuSeCH_3$_NHC4b^0	Cl^-	-8.8	-3.8	-14.4
AuCl_NHC5b^0	$SeCH_3^-$	$AuSeCH_3$_NHC5b^0	Cl^-	-10.2	-4.8	-15.5
AuCl_NHC6b^0	$SeCH_3^-$	$AuSeCH_3$_NHC6b^0	Cl^-	-9.0	-3.8	-14.4
AuCl_NHC7b^0	$SeCH_3^-$	$AuSeCH_3$_NHC7b^0	Cl^-	-9.1	-4.4	-15.2

Stellenbosch University https://scholar.sun.ac.za

Table 8-7: Ligand exchange reactions with $SeCF_3^-$.

Reactants		Products		ΔE_{gas}	$\Delta G_{gas,RRHO}$	ΔG_{aq}
				(kcal mol^{-1})		
Au_2NHC1$^+$	$SeCF_3^-$	AuSeCF$_3$_NHC1^0	NHC1^0	-59.3	-61.9	18.2
Au_2NHC2$^+$	$SeCF_3^-$	AuSeCF$_3$_NHC2^0	NHC2^0	-55.9	-58.3	17.4
Au_2NHC3$^+$	$SeCF_3^-$	AuSeCF$_3$_NHC3^0	NHC3^0	-53.4	-57.1	18.3
Au_2NHC4$^+$	$SeCF_3^-$	AuSeCF$_3$_NHC4^0	NHC4^0	-52.1	-54.8	18.3
Au_2NHC5$^+$	$SeCF_3^-$	AuSeCF$_3$_NHC5^0	NHC5^0	-56.0	-60.7	13.4
Au_2NHC6$^+$	$SeCF_3^-$	AuSeCF$_3$_NHC6^0	NHC6^0	-50.0	-54.4	20.1
Au_2NHC7$^+$	$SeCF_3^-$	AuSeCF$_3$_NHC7^0	NHC7^0	-47.2	-50.3	21.4
Au_2NHC1b$^+$	$SeCF_3^-$	AuSeCF$_3$_NHC1b^0	NHC1b^0	-60.4	-62.5	16.6
Au_2NHC2b$^+$	$SeCF_3^-$	AuSeCF$_3$_NHC2b^0	NHC2b^0	-57.9	-61.0	14.3
Au_2NHC3b$^+$	$SeCF_3^-$	AuSeCF$_3$_NHC3b^0	NHC3b^0	-55.7	-58.0	17.0
Au_2NHC4b$^+$	$SeCF_3^-$	AuSeCF$_3$_NHC4b^0	NHC4b^0	-54.8	-58.0	15.6
Au_2NHC5b$^+$	$SeCF_3^-$	AuSeCF$_3$_NHC5b^0	NHC5b^0	-64.4	-68.7	5.9
Au_2NHC6b$^+$	$SeCF_3^-$	AuSeCF$_3$_NHC6b^0	NHC6b^0	-51.9	-56.2	17.2
Au_2NHC7b$^+$	$SeCF_3^-$	AuSeCF$_3$_NHC7b^0	NHC7b^0	-50.0	-54.8	18.3
Phos1-Au-NHC3b$^+$	$SeCF_3^-$	AuSeCF$_3$_Phos1^0	NHC3b^0	-60.4	-62.5	14.7
Phos2-Au-NHC3b$^+$	$SeCF_3^-$	AuSeCF$_3$_Phos2^0	NHC3b^0	-59.5	-61.7	14.7
Phos3-Au-NHC3b$^+$	$SeCF_3^-$	AuSeCF$_3$_Phos3^0	NHC3b^0	-58.3	-60.6	14.9
Phos4-Au-NHC3b$^+$	$SeCF_3^-$	AuSeCF$_3$_Phos4^0	NHC3b^0	-57.7	-59.2	15.3
Phos4-Au-NHC5$^+$	$SeCF_3^-$	AuSeCF$_3$_Phos4^0	NHC5^0	-55.7	-60.0	14.9
Phos1-Au-NHC3b$^+$	$SeCF_3^-$	AuSeCF$_3$_NHC3b^0	Phos1^0	-73.5	-73.6	7.4
Phos2-Au-NHC3b$^+$	$SeCF_3^-$	AuSeCF$_3$_NHC3b^0	Phos2^0	-69.4	-71.3	8.0
Phos3-Au-NHC3b$^+$	$SeCF_3^-$	AuSeCF$_3$_NHC3b^0	Phos3^0	-65.7	-67.9	10.2
Phos4-Au-NHC3b$^+$	$SeCF_3^-$	AuSeCF$_3$_NHC3b^0	Phos4^0	-71.0	-72.5	2.5
Phos4-Au-NHC5$^+$	$SeCF_3^-$	AuSeCF$_3$_NHC5^0	Phos4^0	-68.4	-71.4	2.7
AuCl_NHC1^0	$SeCF_3^-$	AuSeCF$_3$_NHC1^0	Cl^-	9.6	14.5	-1.3
AuCl_NHC2^0	$SeCF_3^-$	AuSeCF$_3$_NHC2^0	Cl^-	9.2	14.8	-0.7
AuCl_NHC3^0	$SeCF_3^-$	AuSeCF$_3$_NHC3^0	Cl^-	8.8	14.7	-0.5
AuCl_NHC4^0	$SeCF_3^-$	AuSeCF$_3$_NHC4^0	Cl^-	8.8	15.2	0.1
AuCl_NHC5^0	$SeCF_3^-$	AuSeCF$_3$_NHC5^0	Cl^-	7.8	13.7	-1.8
AuCl_NHC6^0	$SeCF_3^-$	AuSeCF$_3$_NHC6^0	Cl^-	9.7	16.3	1.3
AuCl_NHC7^0	$SeCF_3^-$	AuSeCF$_3$_NHC7^0	Cl^-	8.1	14.6	-0.4
AuCl_NHC1b^0	$SeCF_3^-$	AuSeCF$_3$_NHC1b^0	Cl^-	9.7	15.3	-0.4
AuCl_NHC2b^0	$SeCF_3^-$	AuSeCF$_3$_NHC2b^0	Cl^-	9.3	14.9	-0.6
AuCl_NHC3b^0	$SeCF_3^-$	AuSeCF$_3$_NHC3b^0	Cl^-	9.0	15.0	-0.4
AuCl_NHC4b^0	$SeCF_3^-$	AuSeCF$_3$_NHC4b^0	Cl^-	8.9	14.8	-0.6
AuCl_NHC5b^0	$SeCF_3^-$	AuSeCF$_3$_NHC5b^0	Cl^-	7.4	13.7	-1.7
AuCl_NHC6b^0	$SeCF_3^-$	AuSeCF$_3$_NHC6b^0	Cl^-	8.4	15.0	-0.5
AuCl_NHC7b^0	$SeCF_3^-$	AuSeCF$_3$_NHC7b^0	Cl^-	7.9	14.0	-1.3

Stellenbosch University https://scholar.sun.ac.za

Exchange with $SeCF_3^-$, which is presumed to bear a greater resemblance to Se in the TrxR active site, is more unlikely than with $SeCH_3^-$. Based on the number of studies that have found Au-NHC fragments bonded not just to the Se-containing active site, but to other regions of TrxR as well, this is an unexpected result. The solvent model is the most likely source of error here - ions are known to be problematic, and continuum solvation models suffer from the fundamental drawback that they cannot account for specific interaction between solute and solvent molecules (*e.g.* H-bonding and charge-transfer-to-solvent).[3]

Based on the ESP maps of the NHC ligands, which show high charge concentration at the carbene position, it seems likely that specific interactions between solvent molecules and the ligand would occur. The reaction free energies for NHC exchange are scattered and do not show any dependence on the size of the NHC ligand. The greater lability of the phosphine ligands is evident here as it was in the bond dissociation energies. Exchange with $SeCH_3^-$ is predicted to occur spontaneously, but not exchange with $SeCF_3^-$. Exchange of Cl^- with $SeCH_3^-$ occurs spontaneously in the gas and solvated phase, but solvent stabilisation of Cl^- is necessary for exchange with $SeCF_3^-$.

8.3 Energy decomposition analysis

EDA was performed to gain insight into the nature of the Au-ligand bonds. Good agreement was found between the bonding energies as calculated by ADF and the electronic dissociation energies calculated with G09, although it should be noted that the EDA fragment geometries have not been allowed to relax, *i.e.* this calculation is based on the geometry the fragments assume in the coordination complex. The total energy term is therefore more akin to an interaction energy than a BDE. Au_2NHC5 once again was the exception, showing a significant difference in G09 and ADF energies, but the G09 interaction energy of the unrelaxed Au_NHC5 and NHC5 fragments showed good agreement with the ADF bonding energy.

The small increase in bonding energy with increasing molecular volume of the cationic Au-NHC complexes is reflected in the individual terms it is composed of (Table 8-8). The surprisingly high Coulomb and Pauli energies of the Au-NHC7 bond appear to be erroneous, as similarly high values are not observed for Au-NHC7b, while the other imidazolylidene-benzimidazolylidene pairs differ very little from each other in terms of the individual energy terms contained in the total bonding energy. It is unclear whether this result is due to the underlying chemistry or a problem during the calculations. There is some indication that stabilising interactions may be occurring between the cyclohexane rings in Au_2NHC7 (Chapter 5), but this is likely to be a dispersion interaction not exceeding a few kcal mol^{-1}.

Stellenbosch University https://scholar.sun.ac.za

Table 8-8: EDA of cationic Au-NHC and Au-phosphine complexes. Total energy = Coulomb (electrostatic) interaction + Pauli (exchange) repulsion + Orbital energy + Dispersion.

Reactant	Products		ΔE (kcal mol^{-1})				
			Total	Coulomb	Pauli	Orbital	Dispers
Au_2NHC1$^+$	Au_NHC1$^+$	NHC1^0	-92.3	-198.7	171.6	-63.2	-2.0
Au_2NHC2$^+$	Au_NHC2$^+$	NHC2^0	-93.9	-200.8	175.4	-65.1	-3.4
Au_2NHC3$^+$	Au_NHC3$^+$	NHC3^0	-95.9	-202.8	178.8	-66.0	-6.0
Au_2NHC4$^+$	Au_NHC4$^+$	NHC4^0	-95.0	-202.7	178.8	-66.4	-4.6
Au_2NHC5$^+$	Au_NHC5$^+$	NHC5^0	-96.2	-200.1	184.3	-70.7	-9.6
Au_2NHC6$^+$	Au_NHC6$^+$	NHC6^0	-98.7	-203.5	181.5	-67.4	-9.3
Au_2NHC7$^+$	Au_NHC7$^+$	NHC7^0	-97.7	-232.4	217.1	-72.2	-10.2
Au_2NHC1b$^+$	Au_NHC1b$^+$	NHC1b^0	-90.8	-195.3	171.5	-64.9	-2.2
Au_2NHC2b$^+$	Au_NHC2b$^+$	NHC2b^0	-92.1	-197.0	174.9	-66.6	-3.6
Au_2NHC3b$^+$	Au_NHC3b$^+$	NHC3b^0	-93.9	-199.3	178.2	-67.2	-5.6
Au_2NHC4b$^+$	Au_NHC4b$^+$	NHC4b^0	-93.2	-199.9	180.1	-68.1	-5.3
Au_2NHC5b$^+$	Au_NHC5b$^+$	NHC5b^0	-90.0	-191.1	183.1	-72.2	-9.9
Au_2NHC6b$^+$	Au_NHC6b$^+$	NHC6b^0	-97.1	-200.4	181.7	-68.9	-9.5
Au_2NHC7b$^+$	Au_NHC7b$^+$	NHC7b^0	-98.2	-202.0	185.9	-70.7	-11.5
Phos1-Au-NHC3b$^+$	Au_Phos1$^+$	NHC3b^0	-90.5	-192.3	174.5	-68.3	-4.4
Phos2-Au-NHC3b$^+$	Au_Phos2$^+$	NHC3b^0	-88.1	-191.9	176.7	-67.8	-5.1
Phos3-Au-NHC3b$^+$	Au_Phos3$^+$	NHC3b^0	-86.4	-192.7	179.6	-67.6	-5.7
Phos4-Au-NHC3b$^+$	Au_Phos4$^+$	NHC3b^0	-87.2	-194.8	181.9	-68.7	-5.6
Phos4-Au-NHC5$^+$	Au_Phos4$^+$	NHC5^0	-91.3	-199.8	189.7	-72.4	-8.8
Phos1-Au-NHC3b$^+$	Au_NHC3b$^+$	Phos1^0	-78.1	-169.9	158.3	-63.3	-3.2
Phos2-Au-NHC3b$^+$	Au_NHC3b$^+$	Phos2^0	-82.3	-171.3	159.5	-65.3	-5.1
Phos3-Au-NHC3b$^+$	Au_NHC3b$^+$	Phos3^0	-86.1	-173.5	160.9	-66.9	-6.6
Phos4-Au-NHC3b$^+$	Au_NHC3b$^+$	Phos4^0	-79.7	-150.0	145.5	-68.9	-6.3
Phos4-Au-NHC5$^+$	Au-NHC5$^+$	Phos4^0	-81.1	-154.0	150.7	-69.5	-8.3

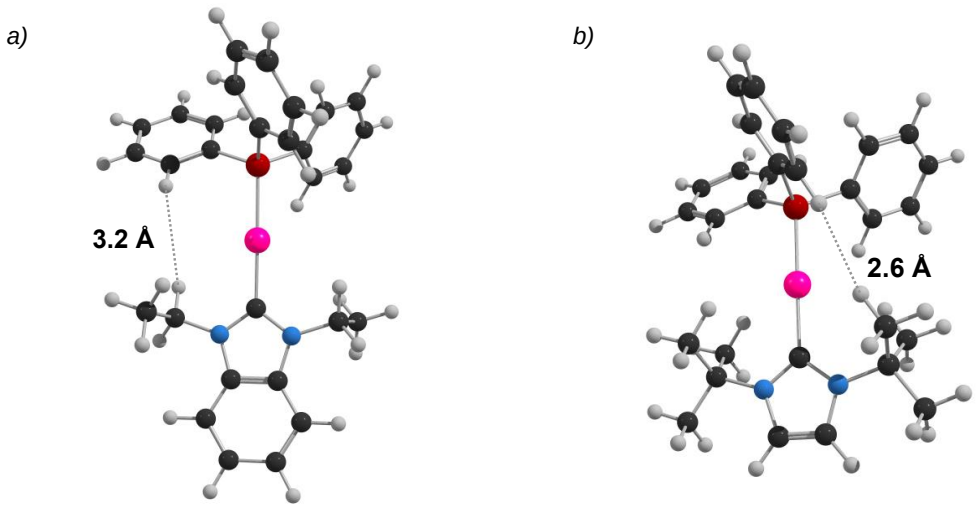

Figure 8-2: a) Phos4-Au-NHC3b and b) Phos4-Au-NHC5 with shortest H···H distance indicated.

Stellenbosch University https://scholar.sun.ac.za

Table 8-9: EDA of AuCl-NHC and other neutral complexes. Total energy = Coulomb (electrostatic) interaction + Pauli (exchange) repulsion + Orbital energy + Dispersion.

Reactant	Products		ΔE (kcal mol^{-1})				
			Total	Coulomb	Pauli	Orbital	Dispers
AuCl_NHC1^0	Au_NHC1$^+$	Cl$^-$	-155.5	-203.1	112.4	-64.6	-0.3
AuCl_NHC2^0	Au_NHC2$^+$	Cl$^-$	-152.5	-200.0	112.4	-64.5	-0.4
AuCl_NHC3^0	Au_NHC3$^+$	Cl$^-$	-151.2	-198.3	112.1	-64.5	-0.5
AuCl_NHC4^0	Au_NHC4$^+$	Cl$^-$	-149.4	-196.3	112.0	-64.5	-0.5
AuCl_NHC5^0	Au_NHC5$^+$	Cl$^-$	-149.0	-194.7	112.0	-65.4	-0.9
AuCl_NHC6^0	Au_NHC6$^+$	Cl$^-$	-149.8	-196.3	111.9	-64.8	-0.7
AuCl_NHC7^0	Au_NHC7$^+$	Cl$^-$	-147.5	-193.9	111.6	-64.6	-0.6
AuCl_NHC1b^0	Au_NHC1b$^+$	Cl$^-$	-155.0	-201.7	113.3	-66.4	-0.3
AuCl_NHC2b^0	Au_NHC2b$^+$	Cl$^-$	-152.8	-199.4	113.4	-66.4	-0.5
AuCl_NHC3b^0	Au_NHC3b$^+$	Cl$^-$	-151.6	-197.9	113.2	-66.3	-0.5
AuCl_NHC4b^0	Au_NHC4b$^+$	Cl$^-$	-150.4	-196.5	113.1	-66.4	-0.6
AuCl_NHC5b^0	Au_NHC5b$^+$	Cl$^-$	-148.3	-193.6	112.3	-66.0	-1.0
AuCl_NHC6b^0	Au_NHC6b$^+$	Cl$^-$	-150.5	-196.1	112.9	-66.6	-0.7
AuCl_NHC7b^0	Au_NHC7b$^+$	Cl$^-$	-149.1	-194.1	112.6	-66.8	-0.9
Auranofin^0	Au_Phos2$^+$	Thio1$^-$	-157.7	-225.1	150.4	-75.4	-7.6
Thio1-Au-NHC5^0	Au-NHC5$^+$	Thio1$^-$	-158.6	-221.6	148.2	-75.2	-10.0
AuCl_NHC1^0	AuCl^0	NHC1^0	-78.3	-217.1	204.9	-64.2	-1.9
AuCl_NHC2^0	AuCl^0	NHC2^0	-81.4	-218.9	205.3	-64.9	-3.0
AuCl_NHC3^0	AuCl^0	NHC3^0	-83.9	-221.1	206.8	-65.5	-4.1
AuCl_NHC4^0	AuCl^0	NHC4^0	-83.5	-220.9	207.0	-65.8	-3.7
AuCl_NHC5^0	AuCl^0	NHC5^0	-83.2	-221.4	211.4	-67.8	-5.5
AuCl_NHC6^0	AuCl^0	NHC6^0	-84.8	-220.5	206.5	-66.0	-4.9
AuCl_NHC7^0	AuCl^0	NHC7^0	-84.5	-221.5	207.2	-66.1	-4.2
AuCl_NHC1b^0	AuCl^0	NHC1b^0	-77.8	-217.4	207.4	-65.7	-2.1
AuCl_NHC2b^0	AuCl^0	NHC2b^0	-80.6	-219.0	207.7	-66.3	-3.1
AuCl_NHC3b^0	AuCl^0	NHC3b^0	-82.5	-220.9	209.1	-66.7	-4.0
AuCl_NHC4b^0	AuCl^0	NHC4b^0	-82.4	-221.2	209.8	-67.1	-3.9
AuCl_NHC5b^0	AuCl^0	NHC5b^0	-77.5	-219.3	216.0	-68.9	-5.2
AuCl_NHC6b^0	AuCl^0	NHC6b^0	-84.1	-221.2	209.1	-67.1	-4.9
AuCl_NHC7b^0	AuCl^0	NHC7b^0	-83.9	-221.4	210.8	-67.9	-5.4
Auranofin^0	Au_Thio1^0	Phos2^0	-67.3	-191.1	194.0	-62.4	-7.7
Thio1-Au-NHC5^0	Au_Thio1^0	NHC5^0	-78.2	-209.9	209.7	-66.5	-11.6

The input and output of the calculation were examined for errors, but neither the structural specification or numerical quality seem to be involved. Due to time constraints, further investigation of the above result falls outside the scope of this study.

Stellenbosch University https://scholar.sun.ac.za

The Pauli repulsion energy term for the Au-NHC5 and Au-NHC5b bond is slightly higher than would be expected based on molecular volume, despite being longer than the other Au-NHC bonds, supporting the notion that the relatively low bond dissociation energy is indeed related to the relief of steric strain. The similarity of the orbital energy terms for the Au-NHC complexes confirms that the N-substituent has little effect on the electronic properties of the carbene. As with the BDEs, the EDA reveals that the Au-phosphine bond is weaker than the Au-NHC bond, and that in the mixed ligand complexes the NHC ligands are marginally more weakly bound. In the Phos-Au-NHC3b complexes, this is a consequence of a lower Coulomb stabilisation term (relative to that observed for NHC3b in the bis-ligated cationic Au-NHC complexes), while a relatively large Pauli repulsion term (related to apparent congestion at the metal centre, Figure 8-2) causes weaker bonding of the NHC ligand in Phos4-Au-NHC5.

The weakness of the Au-Phos4 bond relative to the other Au-Phos bond can now be seen to originate from the Coulomb term, which is ~20 kcal mol^{-1} less stabilising for the Au-Phos4 complexes. This could be a result of less facile charge polarisation from the Phos4 ligand towards the Au-NHC fragment owing to the presence of more electron withdrawing phenyl substituents (relative to the alkyl substituents of the other phosphine ligands).

The strength of the Au-Cl bond in the gas phase appears not to stem from particularly stabilising Coulomb or orbital terms, but from relatively low Pauli repulsion between Cl^- and the Au-NHC fragment (Table 8-8). Unlike the NHC ligands, dispersion does not meaningfully contribute to the Au-Cl bond strength. As with the BDEs, the strength of the Au-Cl bond is observed to weaken slightly as the size of the NHC ligand increases. This is almost entirely due to changes in the Coulomb attraction term. Since the atomic basin charges of Cl in the AuCl_NHC complexes are not observed to change significantly with an increase in the size of the NHC ligand, this trend in Au-Cl bond energy decreasing with an increase in size of the opposing NHC ligand may be the result of the positive charge on the Au_NHC fragment being distributed over a larger volume, effectively increasing the average distance between the Cl and Au-NHC charge distributions.

The orbital energy term of the Au-NHC bonds in these neutral complexes is on par with that found for the cationic complexes, but the Coulomb and Pauli terms differ significantly. This relatively high Coulomb stabilisation results from the large charge polarisation taking place when the two neutral fragments are brought together – the ESP on the NHC ligands in the AuCl_NHC complexes are the areas of highest potential, indicating that Cl effectively draws the electron density toward itself. The shorter Au-C bond lengths of the neutral complexes is a result of this greater electrostatic attraction, and the cause of the increase in Pauli repulsion.

Stellenbosch University https://scholar.sun.ac.za

Table 8-10: EDA of neutral Au-$SeCH_3^-$ complexes. Total energy = Coulomb (electrostatic) interaction + Pauli (exchange) repulsion + Orbital energy + Dispersion.

Reactant	Products		ΔE (kcal mol^{-1})				
			Total	Coulomb	Pauli	Orbital	Dispers
$AuSeCH_3$_NHC1^0	Au_NHC1$^+$	$SeCH_3^-$	-167.6	-244.1	151.8	-74.0	-1.2
$AuSeCH_3$_NHC2^0	Au_NHC2$^+$	$SeCH_3^-$	-164.8	-241.9	152.3	-73.7	-1.5
$AuSeCH_3$_NHC3^0	Au_NHC3$^+$	$SeCH_3^-$	-163.5	-240.8	152.7	-73.7	-1.7
$AuSeCH_3$_NHC4^0	Au_NHC4$^+$	$SeCH_3^-$	-161.6	-238.8	152.3	-73.5	-1.7
$AuSeCH_3$_NHC5^0	Au_NHC5$^+$	$SeCH_3^-$	-162.5	-239.4	154.3	-74.9	-2.5
$AuSeCH_3$_NHC6^0	Au_NHC6$^+$	$SeCH_3^-$	-162.6	-239.7	152.9	-73.6	-2.2
$AuSeCH_3$_NHC7^0	Au_NHC7$^+$	$SeCH_3^-$	-159.8	-236.9	152.3	-73.3	-1.9
$AuSeCH_3$_NHC1b^0	Au_NHC1b$^+$	$SeCH_3^-$	-167.5	-243.3	153.3	-76.1	-1.2
$AuSeCH_3$_NHC2b^0	Au_NHC2b$^+$	$SeCH_3^-$	-165.3	-241.8	154.0	-75.9	-1.5
$AuSeCH_3$_NHC3b^0	Au_NHC3b$^+$	$SeCH_3^-$	-164.2	-240.8	154.2	-75.8	-1.7
$AuSeCH_3$_NHC4b^0	Au_NHC4b$^+$	$SeCH_3^-$	-162.8	-239.5	154.2	-75.8	-1.8
$AuSeCH_3$_NHC5b^0	Au_NHC5b$^+$	$SeCH_3^-$	-162.3	-239.9	156.2	-75.8	-2.8
$AuSeCH_3$_NHC6b^0	Au_NHC6b$^+$	$SeCH_3^-$	-163.6	-240.0	154.5	-75.9	-2.2
$AuSeCH_3$_NHC7b^0	Au_NHC7b$^+$	$SeCH_3^-$	-162.4	-238.5	154.5	-76.0	-2.4
$AuSeCH_3$_Phos1^0	Au_Phos1$^+$	$SeCH_3^-$	-167.4	-243.0	153.8	-76.8	-1.4
$AuSeCH_3$_Phos2^0	Au_Phos2$^+$	$SeCH_3^-$	-163.8	-240.3	155.0	-76.8	-1.7
$AuSeCH_3$_Phos3^0	Au_Phos3$^+$	$SeCH_3^-$	-160.4	-237.6	156.1	-77.0	-1.9
$AuSeCH_3$_Phos4^0	Au_Phos4$^+$	$SeCH_3^-$	-162.1	-237.0	157.4	-80.6	-1.9
$AuSeCH_3$_NHC1^0	$AuSeCH_3^0$	NHC1^0	-61.3	-198.6	199.9	-60.5	-2.1
$AuSeCH_3$_NHC2^0	$AuSeCH_3^0$	NHC2^0	-64.3	-200.4	200.6	-61.2	-3.3
$AuSeCH_3$_NHC3^0	$AuSeCH_3^0$	NHC3^0	-66.9	-203.4	203.2	-62.1	-4.6
$AuSeCH_3$_NHC4^0	$AuSeCH_3^0$	NHC4^0	-66.5	-203.2	203.0	-62.2	-4.1
$AuSeCH_3$_NHC5^0	$AuSeCH_3^0$	NHC5^0	-66.6	-204.2	208.6	-64.7	-6.3
$AuSeCH_3$_NHC6^0	$AuSeCH_3^0$	NHC6^0	-68.2	-202.6	202.8	-62.6	-5.8
$AuSeCH_3$_NHC7^0	$AuSeCH_3^0$	NHC7^0	-67.7	-204.0	203.7	-62.6	-4.7
$AuSeCH_3$_NHC1b^0	$AuSeCH_3^0$	NHC1b^0	-61.0	-200.2	203.6	-62.2	-2.2
$AuSeCH_3$_NHC2b^0	$AuSeCH_3^0$	NHC2b^0	-63.6	-201.8	204.5	-62.9	-3.4
$AuSeCH_3$_NHC3b^0	$AuSeCH_3^0$	NHC3b^0	-65.7	-204.3	206.5	-63.5	-4.4
$AuSeCH_3$_NHC4b^0	$AuSeCH_3^0$	NHC4b^0	-65.3	-204.2	206.9	-63.8	-4.3
$AuSeCH_3$_NHC5b^0	$AuSeCH_3^0$	NHC5b^0	-61.2	-202.7	213.8	-66.1	-6.2
$AuSeCH_3$_NHC6b^0	$AuSeCH_3^0$	NHC6b^0	-67.6	-204.8	207.0	-64.0	-5.8
$AuSeCH_3$_NHC7b^0	$AuSeCH_3^0$	NHC7b^0	-67.2	-204.9	208.5	-64.7	-6.2
$AuSeCH_3$_Phos1^0	$AuSeCH_3^0$	Phos1^0	-54.1	-181.6	188.8	-58.6	-2.7
$AuSeCH_3$_Phos2^0	$AuSeCH_3^0$	Phos2^0	-57.3	-183.2	189.7	-59.6	-4.3
$AuSeCH_3$_Phos3^0	$AuSeCH_3^0$	Phos3^0	-59.5	-184.1	189.4	-59.5	-5.4
$AuSeCH_3$_Phos4^0	$AuSeCH_3^0$	Phos4^0	-53.2	-164.1	176.2	-60.0	-5.2

Stellenbosch University https://scholar.sun.ac.za

Table 8-11: EDA of neutral Au-$SeCF_3^-$ complexes. Total energy = Coulomb (electrostatic) interaction + Pauli (exchange) repulsion + Orbital energy + Dispersion.

Reactant	Products		ΔE (kcal mol^{-1})				
			Total	Coulomb	Pauli	Orbital	Dispers
$AuSeCF_3$_NHC1^0	Au_NHC1$^+$	$SeCF_3^-$	-151.9	-214.1	131.1	-67.5	-1.5
$AuSeCF_3$_NHC2^0	Au_NHC2$^+$	$SeCF_3^-$	-149.4	-212.5	132.0	-67.1	-1.9
$AuSeCF_3$_NHC3^0	Au_NHC3$^+$	$SeCF_3^-$	-148.5	-211.8	132.5	-66.8	-2.3
$AuSeCF_3$_NHC4^0	Au_NHC4$^+$	$SeCF_3^-$	-147.1	-210.4	132.4	-66.7	-2.4
$AuSeCF_3$_NHC5^0	Au_NHC5$^+$	$SeCF_3^-$	-147.6	-209.9	133.5	-68.0	-3.1
$AuSeCF_3$_NHC6^0	Au_NHC6$^+$	$SeCF_3^-$	-147.7	-210.3	132.5	-67.1	-2.9
$AuSeCF_3$_NHC7^0	Au_NHC7$^+$	$SeCF_3^-$	-145.9	-208.6	132.5	-66.7	-3.0
$AuSeCF_3$_NHC1b^0	Au_NHC1b$^+$	$SeCF_3^-$	-151.5	-212.9	132.1	-69.2	-1.5
$AuSeCF_3$_NHC2b^0	Au_NHC2b$^+$	$SeCF_3^-$	-149.6	-211.7	132.9	-68.9	-1.9
$AuSeCF_3$_NHC3b^0	Au_NHC3b$^+$	$SeCF_3^-$	-148.8	-211.2	133.4	-68.7	-2.3
$AuSeCF_3$_NHC4b^0	Au_NHC4b$^+$	$SeCF_3^-$	-147.6	-210.0	133.4	-68.6	-2.3
$AuSeCF_3$_NHC5b^0	Au_NHC5b$^+$	$SeCF_3^-$	-146.9	-210.0	134.9	-68.7	-3.2
$AuSeCF_3$_NHC6b^0	Au_NHC6b$^+$	$SeCF_3^-$	-148.2	-209.6	133.2	-68.8	-2.9
$AuSeCF_3$_NHC7b^0	Au_NHC7b$^+$	$SeCF_3^-$	-147.5	-209.5	134.2	-69.0	-3.3
$AuSeCF_3$_Phos1^0	Au_Phos1$^+$	$SeCF_3^-$	-150.8	-212.7	132.9	-69.4	-1.7
$AuSeCF_3$_Phos2^0	Au_Phos2$^+$	$SeCF_3^-$	-147.4	-210.4	134.2	-69.0	-2.2
$AuSeCF_3$_Phos3^0	Au_Phos3$^+$	$SeCF_3^-$	-144.4	-208.4	135.4	-69.2	-2.3
$AuSeCF_3$_Phos4^0	Au_Phos4$^+$	$SeCF_3^-$	-145.6	-207.8	136.8	-72.3	-2.3
$AuSeCF_3$_NHC1^0	$AuSeCF_3^0$	NHC1^0	-68.4	-201.5	196.6	-61.3	-2.1
$AuSeCF_3$_NHC2^0	$AuSeCF_3^0$	NHC2^0	-72.3	-204.8	198.5	-62.6	-3.4
$AuSeCF_3$_NHC3^0	$AuSeCF_3^0$	NHC3^0	-75.2	-208.0	201.4	-63.6	-5.0
$AuSeCF_3$_NHC4^0	$AuSeCF_3^0$	NHC4^0	-75.5	-208.4	201.8	-64.0	-4.9
$AuSeCF_3$_NHC5^0	$AuSeCF_3^0$	NHC5^0	-75.3	-207.3	204.9	-66.2	-6.7
$AuSeCF_3$_NHC6^0	$AuSeCF_3^0$	NHC6^0	-76.8	-208.6	202.0	-64.2	-6.0
$AuSeCF_3$_NHC7^0	$AuSeCF_3^0$	NHC7^0	-77.4	-209.4	202.6	-64.7	-5.9
$AuSeCF_3$_NHC1b^0	$AuSeCF_3^0$	NHC1b^0	-67.8	-202.1	199.2	-62.7	-2.3
$AuSeCF_3$_NHC2b^0	$AuSeCF_3^0$	NHC2b^0	-71.2	-204.8	200.9	-63.8	-3.5
$AuSeCF_3$_NHC3b^0	$AuSeCF_3^0$	NHC3b^0	-73.6	-207.8	203.7	-64.6	-4.8
$AuSeCF_3$_NHC4b^0	$AuSeCF_3^0$	NHC4b^0	-73.3	-207.7	204.0	-65.0	-4.6
$AuSeCF_3$_NHC5b^0	$AuSeCF_3^0$	NHC5b^0	-69.1	-203.1	207.3	-66.9	-6.4
$AuSeCF_3$_NHC6b^0	$AuSeCF_3^0$	NHC6b^0	-75.4	-207.5	203.0	-65.0	-6.0
$AuSeCF_3$_NHC7b^0	$AuSeCF_3^0$	NHC7b^0	-75.6	-208.1	205.7	-66.4	-6.9
$AuSeCF_3$_Phos1^0	$AuSeCF_3^0$	Phos1^0	-61.1	-183.4	185.1	-60.1	-2.8
$AuSeCF_3$_Phos2^0	$AuSeCF_3^0$	Phos2^0	-64.7	-185.2	186.6	-61.5	-4.5
$AuSeCF_3$_Phos3^0	$AuSeCF_3^0$	Phos3^0	-67.2	-186.5	186.3	-61.5	-5.6
$AuSeCF_3$_Phos4^0	$AuSeCF_3^0$	Phos4^0	-60.4	-165.2	172.3	-62.1	-5.5

Stellenbosch University https://scholar.sun.ac.za

The dispersion contribution to the Au-NHC bond also differs between the neutral and cationic complexes. The higher dispersion stabilisation in the cationic complexes suggests that the interaction of the ligands with each other, as opposed to the metal centre and Cl, make up a large part of this term.

The affinity of Au for S can be observed in the orbital term of the Au-Thio1 energies. Although none of the individual energy terms are similar between Thio1 and Cl, their resulting total energies are comparable.

The orbital energy term for the $SeCH_3^-$ complexes (Table 8-10) is especially stabilising. While it may be tempting to attribute this to the affinity of Au for Se, the same is not observed in the Au-$SeCF_3^-$ complexes (Table 8-11), where the orbital interaction is less substantial. Based on the atomic basin charges of the two Se fragments (Chapter 4), this term might be expected to be higher than 70 kcal mol^{-1} for the TrxR active site Se. The Coulomb term for the $SeCH_3^-$ complexes is more stabilising than for any of the other ligands, suggestive of charge transfer to the Au fragment, and the Pauli term increases proportionately. Both terms are smaller for the $SeCF_3^-$ complexes, and the Au-Se bond in the gas phase is predicted to be slightly weaker than the Au-Cl bond. Similarly to the Au-Cl bond, the Au-Se bond energy decreases slightly as the size of the NHC ligand increases (also via the Coulomb term). There appears to be little difference in the Au-Se bond strength between the NHC and the phosphine complexes. In both the $SeCH_3^-$ and $SeCF_3^-$ complexes the Au-NHC bond appears weaker than in the AuCl complexes, more so in the $SeCH_3^-$ complexes. This is consistent with the greater electron donating power of $SeCH_3^-$. The same is observed for the phosphine complexes with the Se fragments. This indicates that an increase in lability of both NHC and phosphine ligands may occur when a ligand exchange reaction takes places with the TrxR active site Se. As in the cationic and neutral Au-Cl complexes discussed before, the Au-phosphine bond is observed to be weaker than the Au-NHC bond.

8.4 Conclusions

The BDEs indicate that the ease of dissociation of an NHC ligand from an Au complex in solution is not strongly influenced by the N-substituent. This suggests that changing the N-substituent to achieve a desired lipophilicity can be done without fear that the strength of the Au-NHC coordination bond would be adversely affected, and that simply changing between alkyl ligands as N-substituents will not be effective in fine-tuning the bond lability. Exceptions to this are the sterically demanding NHC5 and NHC5b ligands, for which lower bond dissociation energies are observed. The lower BDEs could be related to other signs that

Stellenbosch University https://scholar.sun.ac.za

unfavourable steric interactions take place at the metal centre in complexes bearing these ligands.

The electron donating alkyl phosphine ligands were found to have similar BDEs to the NHC ligands in the Phos-Au-NHC complexes, but the electron withdrawing Phos4 ligand is not as strongly bound. Conversely, the NHC bond to a Phos4-Au complex is especially stable, suggesting that the phosphine ligand would dissociate before the NHC would.

The identity of the NHC ligand in the neutral complexes with Cl was found not to be important in determining the ease of Cl^- dissociation in the solvated phase and little difference was observed in the energy required for NHC dissociation from an AuCl complex. The above also applies to the neutral NHC complexes with the Se ligands. As for the cationic Au-NHC complexes, this suggests that varying the NHC N-substituents may be done to alter the lipophilicity of an Au complex, but a different strategy is called for in tuning the lability of the NHC ligands.

In solution, dissociation of a Cl^- ligand is far less unfavourable than dissociation of an NHC. Cl^- ligands can therefore be expected to dissociate before NHC ligand dissociation.

The alkyl phosphine and NHC ligands were found not to differ significantly in the strength of their bond to an AuSe complex, but Phos4 showed an exceptionally low affinity. At the same time the anionic Se ligand was more strongly bound. This suggests that if a second ligand exchange reaction should occur, the phosphine ligand is more likely to be replaced than the Se ligand. This may be important in designing drugs that can metallate the TrxR active site not only at the Sec position, but also at the neighbouring Cys position.

The reaction free energies reflect the expected order of bond lability Cl^- > phosphine > NHC. For most of the reactions involving NHC dissociation and $SeCH_3^-$ association a positive Gibbs free energy is observed, implying that these reactions should not occur spontaneously. NHC5 and NHC5b are again exceptions, supporting the use of sterically demanding ligands when Au-NHC bond lability is desired. For the ligand exchange reactions involving $SeCF_3^-$ even some of the reactions involving Cl^- dissociation are not predicted to be spontaneous. A possible cause may be the underestimation of the solvent stabilisation undergone by the NHC ligands by the continuum solvation model.

Stellenbosch University https://scholar.sun.ac.za

References

(1) Rubbiani, R.; Can, S.; Kitanovic, I.; Alborzinia, H.; Stefanopoulou, M.; Kokoschka, M.; Mo, S.; Sheldrick, W. S.; Wo, S.; Ott, I. *J. Med. Chem.* **2011**, *54*, 8646–8657.

(2) Rubbiani, R.; Salassa, L.; De Almeida, A.; Casini, A.; Ott, I. *ChemMedChem* **2014**, *9*, 1205–1210.

(3) Jensen, J. H. *Phys. Chem. Chem. Phys.* **2015**, *17*, 12441–12451.

Stellenbosch University https://scholar.sun.ac.za

9 Conclusions and future work

The intent of this study was to compare a series of Au-NHC and -phosphine complexes in terms of their interaction with the Se residing in the active site of the TrxR enzyme, the strength of the Au-ligand bonds, the energetics of ligand exchange reactions, and their lipophilicity. In doing so, we hoped to evaluate the suitability of different NHC ligands in the design of anti-cancer Au prodrugs targeting the mitochondria and TrxR enzyme.

In Chapter 4 the ESP and Se atomic basin charges of the small model compounds, $SeCH_3^-$ and $SeCF_3^-$ were examined and compared to those of the Sec amino acid as well as a dipeptide and tetrapeptide, with the larger compounds presumably bearing a greater resemblance to the Se-containing active site of the TrxR enzyme. The smaller Se fragments were found to exhibit a more negative ESP than the larger molecules, but the atomic basin charges of the small fragments bracketed those of the larger compounds. We reasoned that the smaller fragments would interact more strongly with the cationic Au complexes when forming a vdW complex, but that in terms of coordination bond strength the active site Se would lie between $SeCH_3^-$ and $SeCF_3^-$, hence these were used as model compounds to reduce the complexity of calculations.

Validation of the model chemistry was performed and discussed in Chapter 5. The chosen method (PBE0-D3/TZVP) performed well in terms of reproducing molecular geometries similar to those found in crystal structures of the Au complexes. Variation in the N-C···(Au)···C-N dihedral angle was observed between optimised geometries and crystal structure data, however, the barrier to rotation around this dihedral angle was calculated to be low, hence it was decided that use of this method would not lead to significant errors. The ESP properties of a range of Au complexes were also examined. The ESP distribution of the cationic Au-NHC complexes was found to be very homogenous, similarly to the Au-Phos complexes, another class of delocalised lipophilic cations (DLCs). If electrostatics were driving the formation of a vdW complex combining such an Au complex and an Se fragment, it seems probable that there would be little preference for a specific site on the molecule.

In Chapter 6 the solubility of the Au coordination complexes and ligands was discussed. Determination of the free energy of hydration was performed in order to evaluate the lipophilicity by the octanol/water partition coefficient, and later to calculate free energies of bond dissociation and ligand exchange reactions in water. The cationic Au-NHC and Au-phosphine complexes were found to be similar in terms of lipophilicity, confirming that NHC ligands could be used as a substitute for phosphine ligands in the design of DLCs. A strong correlation between the average ESP and volume of these complexes with their lipophilicity

Stellenbosch University https://scholar.sun.ac.za

was highlighted. The ease of the synthesis of Au-NHC compounds of varying lipophilicities is an advantage that NHC ligands have over phosphine ligands,[1] and has motivated investigation into their use in anti-cancer Au compounds. Our results confirm that varying the N-substituent groups of an NHC ligand can be an effective strategy in designing a drug with a desired lipophilicity, and show that the molecular volume of an Au-NHC complex can be predictive of its lipophilicity *relative to similar complexes.* Further investigation will be necessary to determine whether such a relation exists when the NHC bears non-alkyl N-substituents.

Our investigation into the vdW complexes of several Au-NHC complexes and the model Se compounds was reported in Chapter 7. In the majority of vdW complexes the Au···Se interaction appears to dominate over ancillary electrostatic and dispersion interactions in determining the mode of coordination. This is the case for vdW complexes containing either $SeCH_3^-$ or $SeCF_3^-$, but the Au-NHC species show less affinity for $SeCF_3^-$, in which less electron density is polarised toward the Se atom and stronger electrostatic interactions between the F atoms and Au complex ligands appear to be taking place. We surmise that in a vdW complex formed between an Au complex and the TrxR active site Se, coordination will take place between Au and Se, setting up the adduct for transformation into the three-coordinate transition state.

The Au complexes bearing the larger benzimidazolylidene (NHCxb) ligands were found to establish shorter Au···Se contacts with the Se fragments than those bearing the smaller imidazolylidene (NHCx) ligands. The Au···Se BCPs in the former complexes exhibited higher electron densities, indicative of stronger bonding. A higher energy penalty was also incurred in deforming the Au complexes from their isolated minimum energy structures to those found in the vdW complexes. This may be the result of weaker competing interactions – in the NHCxb complexes, the positive charge is spread over a larger volume, hence electrostatic interactions between Se fragment and the Au-NHCxb complex should be weaker than in the Au-NHCx complexes. This may be beneficial to the formation of a stronger Au···Se intermolecular interaction.

Investigating the free energy of association in water, it was found that few of the gas phase optimised vdW complexes showed negative free energies of association in solution. This implies that association of the monomers will not occur spontaneously, contrary to experimental findings. It was also observed that in many cases the energy requirement for deforming the Au complexes into the geometry they exhibit in their vdW complexes with an Se fragment was substantial. The methodology employed in determining the free energies of association involved gas phase geometry optimisation, hence stronger electrostatic interactions between the oppositely charged monomers were present than would be observed

Stellenbosch University https://scholar.sun.ac.za

in solution. This led to the high deformation energies of the Au complexes and thus an introduction of bias into the free energies of association. Optimisation in a continuum solvent model would most likely result in vdW complexes with larger distances separating the monomers, where less deformation of the Au complexes occurs. The potential effect of performing geometry optimisation in a continuum solvation model on the free energy of association is therefore unclear, and further work is required to gauge the affinity of the Au complexes for the Se fragments in solution.

Relative comparison of the results can provide insight, however. The N-substituent of the NHC ligands was found to have little effect on the Au···Se distances in the vdW complexes, the BCP properties of these intermolecular interactions, or the free energies of association. The sterically congested complexes with the NHC5/NHC5b ligands proved to be the exception. Pauli repulsion was identified as an impediment to vdW complex-formation of the Au_2NHC5 and Au_2NHC5b complexes with the Se fragments. Our results therefore indicate that Au prodrugs bearing sterically demanding NHC ligands, such as Au_2NHC5, will not be as effective as ones bearing NHC ligands of a similar volume, but with less congestion near the metal centre, such as Au_2NHC6. The vdW complexes provide limited insight into what factors may affect the three-coordinate transition state preceding ligand exchange. To estimate the activation energy of a ligand exchange reaction, determination of the structure of the transition state is required, and preferably a search for intermediate products should also be conducted.

The energetics of ligand dissociation and exchange reactions of various Au complexes with the model Se compounds were considered in Chapter 8. The free energies of dissociation in water of NHC ligands from both homo-ligated cationic complexes and neutral complexes bearing an opposing Cl ligand were found to be very similar despite the NHC ligands differing in terms of N-substituent. This suggests that tuning the Au-NHC bond lability cannot be accomplished by varying the N-substituent (at least not when alkyl moieties at the N-substituent position are considered), but that the lipophilicity can be tuned in this manner without affecting the bond strength. The sterically demanding NHC5 and NHC5b ligands do not conform to this statement – these ligands demonstrated relatively lower bond dissociation energies, which was attributed to the relief of Pauli repulsion occurring upon dissociation of these ligands. The use of sterically bulky ligands cannot be recommended, however, as our results indicate that such ligands impede the formation of strong Au···Se intermolecular interactions. In this work, only alkyl fragments at the N-substituent position were considered. Future work should involve a more diverse set of NHC ligands to determine whether the N-substituent can meaningfully affect the Au-carbene bond strength. There is some interest

Stellenbosch University https://scholar.sun.ac.za

in the use of NHCs bearing biocompatible moieties, which would result in lower systemic toxicity of Au prodrugs bearing such ligands.[2,3]

For the phosphine ligands, generally lower bond dissociation energies were observed, in agreement with previously reported findings. Our results therefore suggest that Au complexes bearing an NHC ligand and a phosphine ligand could be used to good effect – the NHC ligand can be adjusted to tune the lipophilicity of the complex, while the more labile phosphine ligand, which also contributes to the lipophilicity of the compound, can dissociate to allow metallation of the enzyme target. In future work, a wider variety of phosphine ligands should be investigated to determine to what extent the Au-P bond strength can be influenced by varying the phosphine substituents.

Overall, NHC ligands appear to be suitable replacements for phosphines in the design of delocalised lipophilic cationic anti-cancer drugs. Due to their ionic nature, and that of their proposed target, the deprotonated Sec moiety of the TrxR active site, solvation effects are difficult to quantify. The effect of solvation may better be taken into account using a mixed implicit/explicit solvation model, as specific solvent-solute interactions are presumed to be important in stabilising dissociating ligands.

References

(1) Lin, I. J. B.; Vasam, C. S. **2005**, *825*, 812–825.

(2) Mercs, L.; Albrecht, M. *Chem. Soc. Rev.* **2010**, *39*, 1903–1912.

(3) Weaver, J.; Gaillard, S.; Toye, C.; MacPherson, S.; Nolan, S. P.; Riches, A. *Chem. - Eur. J.* **2011**, *17*, 6620–6624.

Stellenbosch University https://scholar.sun.ac.za

Appendix – Guide to electronic supplementary information

1 – G09 log files

Log files containing final structures obtained by geometry optimisation. The codes of some of the NHC and phosphine ligands differ between the log files and thesis – these were changed so that the number designations reflect the molecular volume of the species.

Log files	Thesis
NHC3(b)	NHC4(b)
NHC4(b)	NHC3(b)
NHC5(b)	NHC6(b)
NHC6(b)	NHC5(b)
Phos1	Phos2
Phos2	Phos4
Phos3	Phos1
Phos4	Phos3

SeR – Se-containing compounds.

Au-2NHC – cationic Au complexes with two NHC ligands.

Cl-Au-NHC – neutral Au complexes with a Cl and NHC ligand.

Phos-Au-L – Auranofin, Thio1-Au-NHC5, and cationic Au complexes with phosphine and NHC ligands.

SeR-Au-L – neutral Au complexes with $SeCF_3^-$/$SeCH_3^-$ (SeMe) and NHC/phosphine ligands.

Au-L – cationic and neutral mono-ligated Au complexes.

L – neutral and anionic ligands.

Au-2NHC_cp – Au-NHC complexes with NHC ligands in a co-planar arrangement.

Au-2NHC_SeR – vdW complexes of Au-NHC complexes with Se fragments.

2 – data sheets

Excel file containing the following sheets

ESP data – atomic ESP data, atomic basin charges, and volume.

Au_2NHC1_freqs – vibrational/rotational entropy calculation for Au_2NHC1.

Stellenbosch University https://scholar.sun.ac.za

Compound free energies – free energy components of Au complexes and ligands.

vdW complex free energies – free energy components of vdW complexes of Au-NHC species with Se fragments.

BSSE – results of the Counterpoise calculations performed for the vdW complexes.

3 – entropy.py

Python program used to calculate entropies from vibrational modes (the same calculation performed in the Au_2NHC1_freqs Excel sheet.